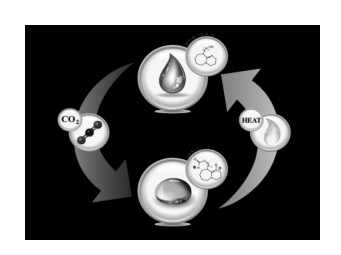
Submitted to: U.S. Department of Energy

Office of Fossil Energy

Award: DE-FE0007466

Project Title: CO₂-Binding Organic Liquids Gas Capture with

Polarity-Swing-Assisted Regeneration



Full Technology Feasibility Study B1 - Solvent-based Systems

Prepared by Battelle, The Fluor Corporation, and Queens University

Principal David Heldebrant

Investigator: <u>david.heldebrant@battelle.org</u>

509/372-6359

Date Submitted: August 31, 2014

Revised May 21, 2015

DUNS Number: 004492575

Recipient Battelle Memorial Institute

Organization: Pacific Northwest Division

P.O. Box 999, MS K6-79

Richland, WA 99352

Project Period: October 1, 2011 through May 30, 2014

Disclaimer

"This report was prepared as an account of work sponsored by an agency of the United States Government. Neither the United States Government nor any agency thereof, nor any of their employees, makes any warranty, express or implied, or assumes any legal liability or responsibility for the accuracy, completeness, or usefulness of any information, apparatus, product, or process disclosed, or represents that its use would not infringe privately owned rights. Reference herein to any specific commercial product, process, or service by trade name, trademark, manufacturer, or otherwise does not necessarily constitute or imply its endorsement, recommendation, or favoring by the United States Government or any agency thereof. The views and opinions of authors expressed herein do not necessarily state or reflect those of the United States Government or any agency thereof."

Abstract

This report outlines the comprehensive bench-scale testing of the CO₂-binding organic liquids (CO₂BOLs) solvent platform and its unique Polarity Swing Assisted Regeneration (PSAR). This study outlines all efforts on a candidate CO₂BOL solvent molecule, including solvent synthesis, material characterization, preliminary toxicology studies, and measurement of all physical, thermodynamic and kinetic data, including bench-scale testing. Equilibrium and kinetic models and analysis were made using Aspen Plus™. Preliminary process configurations, a technoeconomic assessment and solvent performance projections for separating CO₂ from a subcritical coal-fired power plant are compared to the U.S. Department of Energy's Case 10 monoethanolamine baseline.

Contents

- i. Definitions
- ii. Figures
- iii. Tables
 - 1. Synopsis of Results
 - a. Program outcomes
 - b. Key program findings:
 - c. Summary of Power and COE projections
 - d. Conclusions and Recommendations Going Forward
 - 2. Solvent Overview
 - a. Description of CO₂BOLs Chemistry
 - b. Description of Polarity Swing Assisted Regeneration (PSAR)
 - c. Simple Flow Diagram/Schematic(S) Describing Concepts and/or Mechanisms Pertinent to the Process
 - d. Separation Strategies for CO₂BOL and Antisolvent
 - 3. Experimental methods and testing
 - a. PTx cell configuration
 - b. Wetted wall configuration
 - c. Bench cart configuration, packing, circulation rates etc...
 - d. Coalescer Design and separation efficiency
 - e. Antisolvent selection considerations
 - 4. Measured experimental data
 - a. State-Point Data for Solvent-Based Systems
 - b. Viscosity Measurements
 - c. Equilibrium measurements
 - i. Isotherms (PTx method)
 - ii. Antisolvent miscibility and liquid-liquid equilibria
 - d. Kinetic Analysis of CO₂BOLs
 - i. Wetted wall of a first generation CO₂BOL
 - ii. Wetted wall of a second generation CO₂BOL
 - e. Bench scale testing
 - i. Bench scale results of CO₂BOLs thermal case
 - ii. Bench scale results of CO₂BOLs PSAR case
 - iii. Bench scale results of CO₂BOLs PSAR + water case
 - iv. PSAR's impacts on CO₂BOL absorption/regeneration based on bench scale data
 - 1. Absorption performance
 - 2. Stripper performance
 - v. Mass Balance of Cart Data
 - 5. Modeling
 - a. Thermodynamic model
 - b. Transport Properties Model
 - c. Chemical Kinetic Model
 - d. Mass Transfer Correlation
 - e. Wetted Area
 - f. Modeling of Wetted-Wall Data

- g. Modeling of Cart Data
- 6. Techno-Economic Analysis
 - a. Overview
 - b. General Process Flow Diagram
 - c. Flue Gas Conditioning
 - d. CO₂ Absorption
 - e. Absorber
 - f. Solvent Regeneration
 - g. CO₂ Compression
 - h. Material and Energy Balances and Stream Tables
 - i. Cost Estimates Basis
 - j. LCOE Projections
- 7. Estimated useful life of solvent
 - a. Evaporative Losses
 - b. Heat-Stable Salt Formation
 - c. Impact of Hg and Other Impurities
 - i. Impact of Hg
 - ii. Impact of As
 - d. Mechanisms of Degradation of CO₂BOLs
 - i. Thermal
 - ii. Hydrolysis
 - iii. Oxidative Degradation
 - iv. Nitration
 - e. Corrosion potential of CO₂BOLs formulation
 - f. Plastics
- 8. CO₂BOL Formulation Synthesis and Costing
 - a. CO₂BOL Synthesis Strategy
 - b. CO₂BOL Material Costing
- 9. CO₂BOL EH&S Assessment
- 10. Project output
- 11. References

Definitions

Alkylcarbonic acid The acid produced when CO₂ and an alcohol react

BOL CO₂-free Binding Organic Liquid CO₂BOL CO₂-bound Binding Organic Liquid PSAR Polarity Swing Assisted Regeneration

Anti-solvent Nonpolar solvent that decreases the polarity of the CO₂BOL

DBU 1,8-diazabicyclo[5.4.0]undec-7-ene

DOE U.S. Department of Energy EH&S Environment, health and safety

FGD Flue-gas desulfurization

FOA Funding Opportunity Announcement

HSS Heat-stable salts

IL Ionic liquid (a salt at or above it's melting temperature)

MEA Monoethanolamine

MHz Megahertz

MSDS Material Safety Data Sheet MTA Metric Tons Annually

NMR Nuclear magnetic resonance

P* Equilibrium partial pressure of CO₂

PTx Total-pressure testing method, a function of CO₂ at constant

Temperature and known Volume.

ROH Alcohol

STP Standard temperature and pressure (0°C, 1 bar)

VLE Vapor-liquid equilibrium

Zwitterion A molecule with both a + and – charge on it

Zwitterionic liquid An ionic liquid with a + and – charge on the same molecule

Figures

Figure 1. CO ₂ BOLs Absorption and Polarity-Swing-Assisted Regeneration Process	12
Figure 2. Diazabicyclo $[5.4.0]$ -undec-7-ene (DBU) and 1-Hexanol Binding of CO_2 as a CO_2BOL Liquid Alkylcarbonate Salt	13
Figure 3. Candidate Alkanolguanidine (3) with and without CO ₂	14
Figure 4. Reversible uptake of CO ₂ by the Alkanolguanidine (3)	14
Figure 5. Conceptual "Switch" by CO_2 Loading (Polarity Scale Of Nile-Red Indicator dye, μM)	15
Figure 6. Block Flow Diagram for CO₂BOL/PSAR Process	16
Figure 7. Custom made PTx cell assembly.	17
Figure 8. Concentration profile and associated resistances to CO_2 mass transfer in a solvent system (adapted from Dugas 2009)	18
Figure 9. CO ₂ capture materials and processes test carts.	19
Figure 10. CO ₂ Solvent scale-up test cart	20
Figure 11. Solvent cart piping and instrumentation diagram for Dual Bed Absorber/Stripper Configuration.	23
Figure 12. Schematics of the absorber and stripper columns.	24
Figure 13. Representative coalescing tank option ordered from industrial supplier	27
Figure 14. Viscosity Profile of estimated CO ₂ Added to CO ₂ BOL (3) With and Without One Mole Equivalent of Water (40°C) and With Estimated Antisolvent Carryover	
Figure 15. Isotherm of Anhydrous CO ₂ BOL (3)	34
Figure 16. Isotherms of CO₂BOL (3) + 1 Molar Equivalent of Water	35
Figure 17. Isotherms of Anhydrous CO₂BOL (3) Plus 1 Molar Equivalent of Hexadecane Antisolvent	36
Figure 18. Phase Diagram for (in blue) CO_2 -Lean CO_2BOL (3) and Hexadecane and (in red) CO_2 -Lean CO_2BOL (3) and Decane as a Function of Temperature. Areas within the curves represent biphasic behavior.	
Figure 19. Liquid film mass transfer coefficient of DBU-hexanol and 5M MEA	39
Figure 20. Comparison of VLE data measured from WWC plotted VS VLE data from PTx measurements	41
Figure 21. Comparison of K _g ¹ values (3) plotted VS aqueous 5M MEA	42
Figure 22. Measured VLE data of the bench cart (red line) for (3) plotted against VLE data measured from PTx measurements (both at 40 °C).	45
Figure 23. Measured VLE data of the bench cart (red line) for (3) plotted against VLE data measured from PTx measurements (both at 60 °C).	45
Figure 24. CO ₂ capture efficiency of (3) as a function of lean solvent viscosity	46
Figure 25. CO ₂ Absorption rate by (3) as a function of lean solvent viscosity	46
Figure 26. Continuous Bench-Scale Testing (3) on 15% $\rm CO_2$ at 40 $^{\circ}C$ absorption	47
Figure 27. CO_2 capture efficiency plotted against L/G for (3) at two gas inlet concentrations [1: CO_2 (red) and 10% CO_2 (blue)]	
Figure 28. CO ₂ capture efficiency with PSAR, plotted against L/G for (3) at 15% CO ₂	51
Figure 29. Bench-Scale Run Data for CO ₂ BOLs, with and without PSAR	53
Figure 30 Estimated CO ₂ partial pressures in BOL-H ₂ O-C ₁₆ at 100°C. The relative solvent concentrations are equimolar.	56

Figure 31 Fraction of CO ₂ in in BOL-H ₂ O-C ₁₆ at 100°C that is complexed. The relative solvent concentrations are equimolar.	56
Figure 32 Enthalpy of solution of CO ₂ in BOL.	57
Figure 33 Enthalpy of solution of CO ₂ in 1:1 H ₂ O:BOL.	57
Figure 34 Comparison of empirical correlation developed for the CO ₂ -BOLs system with experimental data	58
Figure 35 Estimated effect of water loading on the mixture viscosity at 50°C. The model result and data for the dry system are the same as in Figure 34, and the model results for water loadings of 0.5 and 1.0 are estimated based upon limited data	er
Figure 36 Comparison of CO_2 -BOLs kinetics with that of MEA. For CO_2 -BOLs, the value is take from Eq. 5, while the MEA value has been reported by Versteeg et al. (1996)	
Figure 37 "Effective viscosity" used for Schmidt number in Onda correlation	62
Figure 38 Comparison of K _G calculated by RateSep model to experimental data measured by wetted-wall column.	
Figure 39 Extrapolation of K_G calculations by RateSep to higher CO_2 loadings and the present water	
Figure 40 Parity plot relating the CO_2 recoveries calculated by the model to the experimenta measurements in the bench-scale system (AS = Antisolvent; IAF = Internal Area Factor, of the effective fraction of absorber packing area)	or
Figure 41. Process Flow Diagram – Absorption System	72
Figure 42. Process Flow Diagram – Stripping System	73
Figure 43. Process Flow Diagram – Compression System	74
Figure 44. The proposed reactions of (3), SO ₂ and H ₂ O	83
Figure 45. The proposed reaction of (3) with NO _x and water	84
Figure 46. Proposed Hydrolysis of CO₂BOL by Water at High Temperatures	85
Figure 47. Potential Nitration Mechanism for Alkanolguanidines	86
Figure 48. Visual inspection of bench cart hardware after cleanup	87
Figure 49. Coupons of plastic materials placed in CO_2BOL at room temperature for 7 days	88
Figure 50. One-Step Synthesis of Alkanolguanidine (3)	88
Figure 51. Synthesis of 2-chloro-1,3-dimethylimidazolinium chloride (2)	89
Figure 52. Proposed more economical and less toxic synthesis of Vilsmeier salt 2	89

Tables

Table 1. Summarized LCOE projections for NETL compared to three CO₂BOL/PSAR cases	.10
Table 2. Post-Combustion Gas Composition	.21
Table 3. Absorber/Stripper column specifications.	.24
Table 4. Antisolvent miscibility testing	.29
Table 5. State-Point Data for Solvent Based Systems	.31
Table 6. Saturated Liquid Density for CO ₂ -Free Alkanolguanidine (3)	.33
Table 7. Vapor Pressure Measurements for Alkanolguanidine (3)	.33
Table 8. Upper Critical Solution Temperature of Varied Antisolvents with CO_2 -Lean CO_2BOL	.38
Table 9. WWC data for DBU-hexanol at 35, 45, and 55°C	.40
Table 10. WWC data for 5M MEA 40°C	.40
Table 11.WWC data for (3) at 40, 60, 80, 100 °C	.43
Table 12. Bench scale data for thermal release of (3), no PSAR	.49
Table 13. Bench scale data for <i>PSAR</i> release of (3) in the presence of 5 wt% water	.52
Table 14. Summary of Bench-Scale Run Data for CO₂BOLs, with and without PSAR	.54
Table 15. Process Stream Tables (CO₂BOLs/PSAR case with 356 cP max viscosity)	.75
Table 16. LCOE (fuel) projections for MEA Baselines, and CO₂BOLs/PSAR	.78
Table 17. LCOE (capital & variable) projections for MEA Baselines, and CO₂BOLs/PSAR	.79
Table 18. LCOE (Summary) projections for MEA Baselines, and CO₂BOLs/PSAR	.80
Table 19. Health and Safety and Environmental Impacts of CO₂BOL VS MEA	.90
Table 20. The median lethal concentration (LC50) and 95% confidence limits of the test chemicals for neonates of <i>Daphnia magna</i> and for juvenile rainbow trout. The LC50 was calculated by the moving average angle transformation (Stephan 1989). ²⁴	.94

1. SYNOPSIS OF RESULTS

Overview

PNNL, Fluor Corporation and Queens University (Kingston, ON) successfully completed a three year comprehensive study of the CO_2BOL water-lean solvent platform with Polarity Swing Assisted Regeneration (PSAR). This study encompassed solvent synthesis, characterization, environmental toxicology, physical, thermodynamic and kinetic property measurements, Aspen $Plus^{TM}$ modeling and bench-scale testing of a candidate CO_2BOL solvent molecule.

Key Program Findings

The key program findings are summarized as follows:

PSAR favorably reduced stripper duties and reboiler temperatures. There was also little or no impact to absorption system due to minimal carryover of the anti-solvent into the absorption column. These temperature and reboiler duty reductions translate to significant increases in the power production from a power plant equipped with PSAR as demonstrated from process power plant simulations and shown in Table 1 below.

- >90% CO₂ capture was achievable at reasonable liquid-gas ratios in the absorber
- High RICH solvent viscosities (up to 600 cP) were successfully demonstrated in the bench-scale system. However, the projected impacts of high viscosity to capital cost and operational limits diminished the other levelized cost of electricity benefits.
- Low thermal conductivity of organics significantly increased the required cross exchanger surface area, and potentially other heat exchange surfaces.
- CO₂BOL had low evaporative losses during bench-scale testing
- There was no evidence of foaming during bench scale testing with synthesized flue gas
- Current CO₂BOL formulation costs project to be \$35/kg
- Ecotoxicity (Water Daphnia) was comparable between CO₂BOL and MEA (169.47 versus 103.63 mg/L)
- Full dehydration of the flue gas was determined to not be necessary or economically feasible. However, modest refrigeration power (13 MW for the 550 MW reference system) was determined to be potentially economically feasible, and still produce a water-lean condition for the CO₂BOLs (5 wt% steady-state water loading).
- CO₂BOLs testing with 5 wt% water loading did not compromise anhydrous performance behavior, and showed actual enhancement of CO₂ capture performance.
- Mass transfer of CO₂BOLs was not greatly hindered by the high viscosity but did show increases in the pumping power required.
- CO₂BOL absorbers were sized at 60' in diameter and 177.5' tall to entail a reasonable 2 5 psi pressure drop
- Facile separation of antisolvent from lean CO₂BOL was demonstrated on the bench cart
- No measurable solvent degradation was observed over 4 months of testing even with 5 wt% water present

Through the course of the current project the team has developed and validated the thermodynamic understanding of the $CO_2BOL/PSAR$ system, fully characterized in an electrolyte Aspen $Plus^{\mathsf{TM}}$ model. The unique approach used for the CO_2BOLs thermodynamic characterization is believed to be applicable to other water-lean solvent platforms. Ultimately, the CO_2BOL solvent system was determined to be capable of 90% CO_2 capture with acceptable

liquid-to-gas ratios in the bench-scale absorber system. PSAR was also determined to be feasible in continuous operation, aiding in stripping of CO_2 with minimal impact on absorption performance. The CO_2 BOLs/PSAR system was also determined to have the potential to use infrastructure and hardware similar to aqueous solvents, reducing the need for custom equipment. Energetic projections suggest 8-10% increases in net power from a 550 MW plant, with potential for greater gains with more advanced formulations. While net power increases are significant, the current high viscosity of the loaded CO_2 BOL solvent limits the economic feasibility of its use in a large-scale facility.

Summary of Power and COE projections

Energetic and LCOE projections for several CO₂BOL/PSAR cases are summarized in the table below.

Table 1. Summarized LCOE projections for NETL compared to three CO₂BOL/PSAR cases

	MEA Base	CO₂BOL/PSAR	CO2BOL/PSAR	CO₂BOL/PSAR
	Case	(current	(current	(if 20 cP max
	(recreated	formulation –	formulation –	viscosity
	NETL Case	operated at 356	operated at 578 cP	formulation could
	10)	cP max viscosity)	max viscosity)	be achieved)
RICH solvent				
loading (mol	0.49	0.28	0.34	0.50
CO ₂ /mol solvent)				
Temperature				
Required for	120	104	104	85
Regeneration (°C)				
Estimated Reboiler	1520	1107	965	870
Duty (BTU/lb CO ₂)	1320	1107	903	870
CO ₂ Removed	90%	90%	90%	90%
Increase in Net				
Electric Power over	0%	7%	9%	16%
MEA Recreated	070	/ /0	3/0	10/0
Base Case				
Estimated LCOE	87%	119%	Not Estimated	71%*
Increase	0/70	11970	INOL ESCIIIIALEO	/ 170

* Based on early capital estimates, from initial techno-economic analysis. *Results from this simulation have not been validated experimentally. Furthermore, this case is based on achieving equilibrium conditions.*

The first two $CO_2BOL/PSAR$ cases correspond to projections made using the current solvent formulation and limiting the CO_2 loading of that solvent so that certain viscosity thresholds were not exceeded (356 and 578 cP, respectively). The last $CO_2BOL/PSAR$ case is from the initial technology feasibility study for the project, and assumes that the solvent can be redesigned in the future to not exceed a 20 cP level. The comparison of the $CO_2BOL/PSAR$ cases, suggest that the current viscosity levels of the solvent greatly limit the possible RICH solvent CO_2 loadings, however the performance with a low-viscosity solvent is hypothetical. These limits greatly impact the reboiler duties and solvent recirculation rates. Further, the capital costs associated with high viscosity solvents (356 cP case) was projected to be over 2X that of the MEA base case, which drove most of the associated LCOE increase shown.

Conclusions and Recommendations Going Forward

The project team concludes that CO₂BOLs/PSAR may be a viable technology with further solvent refinement. The current formulation of the CO₂BOL shows promising gains in net power but capital cost impracticality due to high viscosity and low thermal conductivity. ASPEN Plus™ simulations of CO₂BOL energetics project reduced reboiler duty and higher net power output, at the expense of capital costs. For the current formulation, the CO₂BOL cannot be run at its optimal thermodynamic performance range, as the process has to run at a lower lean solvent loading to keep viscosity to a manageable level. This configuration results in a higher solvent circulation rate and higher reboiler temperatures. Furthermore, viscosity limitations for this formulation directly impact capital projections, making the process too costly for commercialization. Therefore, the project team concludes that viscosity reduction is a critical need to reach CO₂BOL performance projections. Fortunately, this formulation was the first to be studied of potentially thousands of CO₂BOL molecules, thus there is potential for many improved formulations to achieve higher performance projections.

The conclusions of this report were made based on the comprehensive data and program findings, which are detailed in the remainder of this document. Herein, lies all program measured data, key findings including all detailed physical and thermodynamic property measurements, ASPEN Plus™ energetic projections, equipment sizing and Environmental health and safety assessment.

2. SOLVENT OVERVIEW

The CO₂-binding organic liquids (CO₂BOLs) solvent platform is a water-lean solvent system that falls under DOE's category of "transformational" solvent systems. The CO₂BOL solvent platform was used in the current solvent study, with the goal of assessing feasibility of this solvent to capture 90% CO₂, and confirming the viability of the solvent's distinctive Polarity-Swing-Assisted Regeneration (PSAR) via continuous flow on the bench scale. Like conventional aqueous based technologies, CO₂BOLs solvents can be regenerated thermally. However, the unique non-aqueous characteristics of CO₂BOLs enable the use of PSAR, which can reduce reboiler temperatures by as much as 70 °C, allowing for improved efficiency gains from the plant's steam cycle. PSAR works by exploiting the fundamental changes in the CO₂BOL's

physical and thermodynamic properties as it converts between a non-polar molecular liquid, to a highly polar ionic liquid as it chemically fixates CO_2 . The PSAR effect simply changes the free energies of solvation of the carbonaceous anions of the solvent, forcing the reaction backwards (CO_2 release).

A high-level schematic of the $CO_2BOLs/PSAR$ process is provided in Figure 1. As with conventional water-based technologies, the incoming flue gas is cooled with a direct contact cooler to remove particulate matter and condense water from the gas. Absorption occurs at $40^{\circ}C$ in a conventional absorber column, after which a non-polar and chemically inert "antisolvent" is co-injected with the RICH CO_2BOL solvent in a static mixer. The biphasic mixture then passes through the cross exchanger and then pumped to a conventional stripper column. Here the PSAR takes effect and CO_2 is released. The lean CO_2BOL anti-solvent mixture is then passed back through the cross exchanger and pumped into a coalescing unit to promote phase separation of the two liquid phases by cooling with cooling water. Next, the lean CO_2BOL and anti-solvent are pumped to the absorber and static mixer respectively.

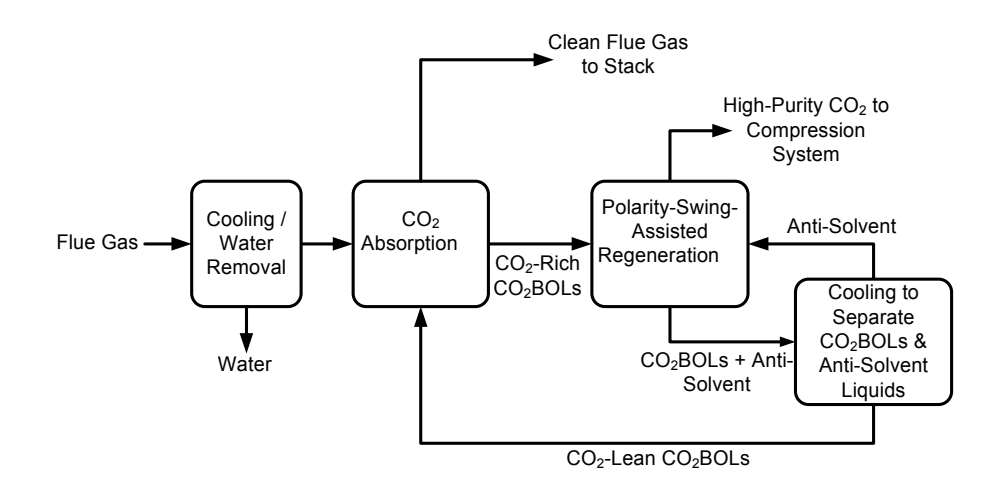


Figure 1. CO₂BOLs Absorption and Polarity-Swing-Assisted Regeneration Process

Description of CO₂BOLs Chemistry

As with any water-lean or concentrated solvent system, one attribute of the CO_2BOLs system is to reduce the amount of water carried by the solvent in order to remove the duty of boiling and condensing as much water in the process. Removing or reducing water allows power plants to exploit the lower specific heats of organics in order to decrease reboiler duty.

The CO_2BOL system was predicated on Philip Jessop's "switchable solvents, with chemical modification of the molecules to reduce volatility and improve chemical durability. 1CO_2BOLs are designed to chemically fixate CO_2 with a carbonaceous alkylcarbonate anion which is conceptually similar to amine based systems which rely on carbamate or bicarbonate carbonaceous anions. The key distinction between CO_2BOLs and amines such as MEA or piperazine is that a non-nucleophilic base is used so that the nitrogen in the molecule cannot react with CO_2 as a carbamate, and in lieu of water, an alcohol is used as the CO_2 carrier. As the base does not chemically react with CO_2 (as is the case with primary and secondary amines forming carbamates), the CO_2 is forced to react with the alcohol moiety first, making an alkylcarbonic acid, which then protonates the base moiety. Once the protonation has occurred, the liquid alkylcarbonate salt is formed. In previous studies at 1 atm CO_2 , some alkylcarbonate

salts have been shown to have CO_2 capacities as high as 20 wt% at 1 atm of CO_2 (Figure 2), however the CO_2 uptake is linked directly to the partial pressure of CO_2 in the gas headspace. The non-nucleophilic (and strong enough) bases that can be used in CO_2 BOLs are amidine or guanidine bases. These bases are characterized by N-allylic systems with strong resonance contributions. The strong bases are needed due to the reduced acidity of alkylcarbonic acids compared to carbonic and carbamic acids utilized in 3° amines and 1° and 2° amines respectively. As with any conventional chemically selective CO_2 solvent, the CO_2 can be stripped from the CO_2 RICH ionic liquid thermally.

$$CO_2$$
 O

Figure 2. Diazabicyclo[5.4.0]-undec-7-ene (DBU) and 1-Hexanol Binding of CO₂ as a CO₂BOL Liquid Alkylcarbonate Salt

The first-generation CO₂BOLs (designed by Jessop) were a dual component mixture of a base and an alcohol, and were quickly proven impractical due to high evaporative losses. Efforts were made to reduce the volatility by conjoining the alcohol and base together into a single molecule, similarly to alkanolamines (which have the -OH group to improve water solubility and to reduce vapor pressure). The conjoining in what we call a second generation CO₂BOL solvent achieved greatly reduced volatility. ^{2,3} Thermodynamically speaking, the weaker amidine bases have a heat of reaction ~60 kJ/mol but are barely capable of 90% CO₂ capture. For this reason, stronger guanidine based systems were focused on as they have a higher CO₂ capture efficiency (up to 99%) with a ~85 kJ/mol heat of reaction, which is comparable to MEA (85 kJ/mol). In alkanolguanidine systems CO₂ reacts with the alcohol and base moieties on the molecule forming zwitterionic liquids upon carboxylation. While volatility was greatly reduced, these materials were inherently viscous prior to CO₂ uptake, and several iterations of molecules were designed and synthesized until a low-viscosity alkanolguanidine was made. The best-case compound used in this study is an alkanolguanidine based on a cyclic guanidine core derived from 1,3-dimethylimidazolidine (3) and a secondary amino alcohol (Figure 3). CO₂ release is performed by thermal heating (Figure 4).

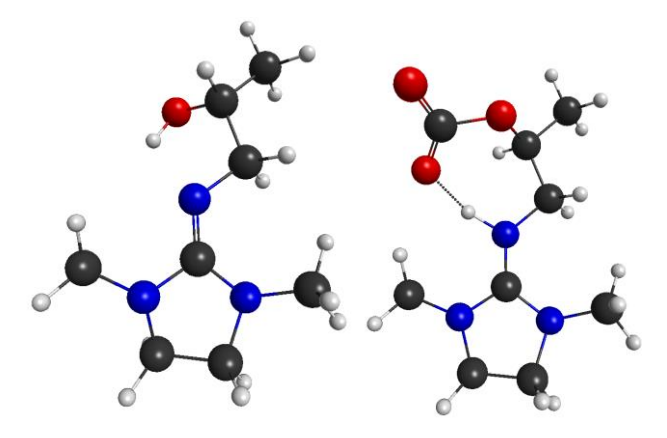


Figure 3. Candidate Alkanolguanidine (3) with and without CO₂

Figure 4. Reversible uptake of CO₂ by the Alkanolguanidine (3)

The absorption of CO_2 by the alkanolguanidine is proposed to begin with diffusion of $CO_{2(g)}$ into the BOL (Equation 2.1). The now dissolved $CO_{2(d)}$ inserts into the O-H bond of the alcohol moiety, which then produces an alkylcarbonic acid BOL-OCO₂H (Equation 2.2). This alkylcarbonic acid is now acidic enough to transfer its proton either inter- or intra-molecularly to the guanidine moiety, which then forms the zwitterionic CO_2BOL (Equation 2.3). The CO_2 is released (decarboxylated) thermally (Equation 2.4), producing the CO_2 -free BOL and dissolved CO_2 . The dissolved CO_2 diffuses out of solution into the gas phase (reverse of Equation 2.1) to complete the cycle.

$$CO_{2(g)} \leftrightarrow CO_{2(d)}$$
 (2.1)

$$CO_{2(d)} + BOL \leftrightarrow BOL - OCO_2H$$
 (2.2)

$$BOL-OCO_2H \leftrightarrow CO_2BOL$$
 (2.3)

$$CO_2BOL \rightarrow BOL + CO_{2(d)}$$
 (2.4)

Description of Polarity Swing Assisted Regeneration (PSAR)

The distinctive polarity change of switchable ionic liquids such as CO_2BOLs provides a unique material property to exploit for CO_2 release.⁵ The reversible conversion of a non-polar molecular (CO_2 lean) form of the CO_2BOL into a highly polar ionic (CO_2 RICH) form is controlled by the degree of CO_2 loading. Conventional solvent systems with co-solvents such as water are used in excess to dissolve the CO_2 carrier, thus no transformation in polarity is observed. This is also true for functionalized ionic liquids or technologies that use organic co-solvents. The unique changes in polarity as a function of CO_2 loading are conceptually shown in Figure 5.²⁻⁴ Here a solvatochromatic scale is shown that links the polarity using a dye that changes its wavelength as a function of a solvent's dielectric constant. The scale is representative of how

far the polarity can change for some switchable ionic liquids such as CO_2BOLs . This degree of polarity change is dictated by the amount of CO_2 absorbed, which is influenced by temperature and the partial pressure of CO_2 over the liquid. Alternatively, CO_2 loading can be controlled by polarity simply by adding a non-polar chemically inert additive called an "anti-solvent."

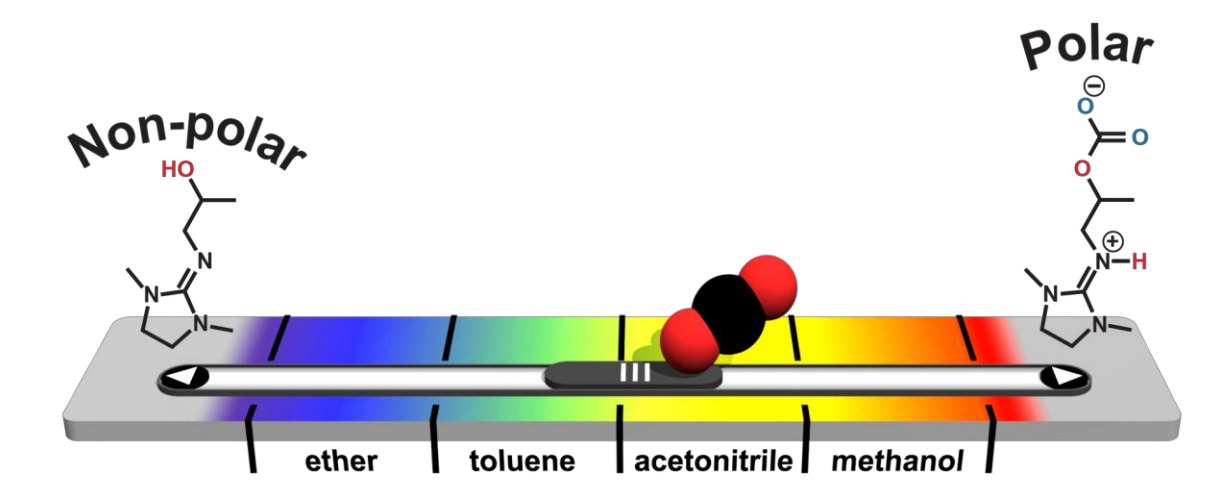


Figure 5. Conceptual "Switch" by CO_2 Loading (Polarity Scale Of Nile-Red Indicator dye, μM)

The PSAR works by the addition of a non-polar anti-solvent that decreases the dielectric constant of the now CO₂BOL/anti-solvent mixture, which in turn reverses the CO₂ absorption and favors CO₂ release.⁵ The miscibility of the anti-solvent and BOL is directly linked to CO₂ loading and temperature as both control the miscibility of the antisolvent and CO₂BOL.⁵ A more detailed description is provided vide infra. Conceptually the PSAR is self-accelerating; mild heating induces partial CO₂ release from the CO₂BOL, which then makes the CO₂BOL less polar, which then allows higher miscibility of the anti-solvent, as more anti-solvent dissolves in, the less stable the CO₂ containing anions in the solution become, forcing more CO₂ release. One can envision the nonpolar antisolvent destabilizing the ionic form of a CO₂BOL (the alkylcarbonate) and shifting the equilibrium to the left (Figure 5) by a process of changing the Gibb's free energy of solvation of the CO₂ containing ions in the solvent. Essentially, polar ions are stabilized in polar solvents but are unstable in non-coordinating (less polar solvents). This in turn aids in the release of CO₂ at a given temperature. It should be noted that when antisolvent is present and miscible in the CO₂BOL, the CO₂ release is still equilibrium controlled at a given temperature, but the equilibrium favors a lower CO₂ loading than the CO₂BOL would have in the absence of antisolvent. The PSAR is also controllable by the amount of antisolvent added. Antisolvent loadings anywhere from 0.5-3 molar equivalents to CO₂BOL have been shown to decrease regeneration temperatures by as much as 73 °C, with a theoretical lowest regeneration temperature of 65 °C if enough antisolvent is added.

Simple Flow Diagram/Schematic(S) Describing Concepts and/or Mechanisms Pertinent to the Process

Taking the high level overview flow sheet in **Figure 1** as an outline, one can expand the level of detail to see the nuances of the CO₂BOL/PSAR process in **Figure 6**. This flow sheet is representative of the mechanisms and concepts in the CO₂BOL & PSAR processes, but formal process flow diagrams are provided and discussed in detail in Section 6.

After analyzing process performance and confirming compatibility of the CO_2BOL with currently available infrastructure, the $CO_2BOL/PSAR$ process is projected to run in analogy to NETL Case 10 (MEA capture) process arrangement albeit with the addition of the PSAR antisolvent circulation loop, pumps and coalescing system. Another deviation from Case 10 is the addition of a small 13 MW unit after the direct contact cooler. This unit aids in additional dehumidification of the incoming flue gas to lower the accumulation in the solvent to a 5wt% steady-state level. Further dehumidification was deemed uneconomical due to extreme refrigeration requirements.

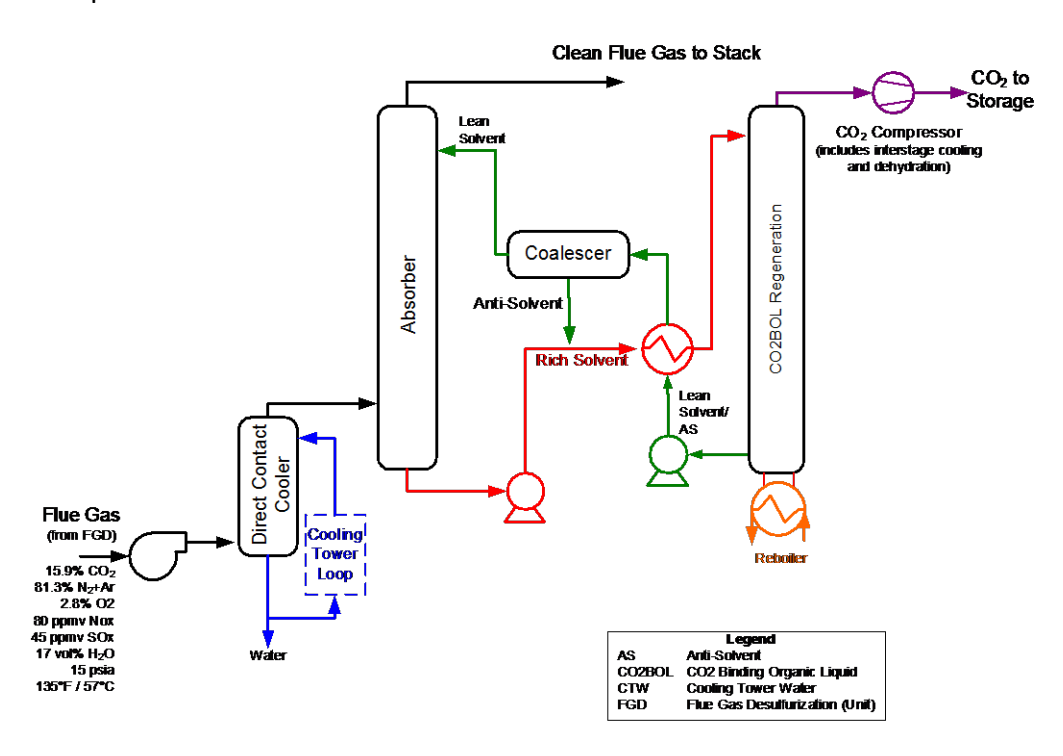


Figure 6. Block Flow Diagram for CO₂BOL/PSAR Process

3. EXPERIMENTAL METHODS AND TESTING

This section details the experimental methodologies and equipment configurations used to measure the key data for the program. Provided are detailed descriptions of equilibrium, kinetic and bench carts cells and other key instruments used in this study. Also provided are key assumptions used for data analysis.

PTx cell configuration

All equilibrium measurements for PTx data were obtained using a custom-made 430 cm³ internal volume windowed stainless steel cell autoclave with a chamber diameter of 5.08 cm Figure 7. The cell was fitted with two opposing sight windows made of borosilicate glass to allow for visual observation of the liquid level, stirring and phase behavior of the liquid during testing. Temperature control of the cell was achieved by submerging it inside in a temperature regulated silicone oil bath. Placing a large cross-shaped magnetic stir bar inside the cell and placing the entire cell and bath assembly over a magnetic stir plate achieved mixing inside the cell. A top flange was fitted with three connection ports, one for a liquid injection port, and another for gas injection, and a vacuum assembly to pressure regulation and cell drying. The

injection port was comprised of a gas-tight syringe with pressure transducers and thermocouple at the syringe and the manifold. An additional third pressure transducer and thermocouple was installed on the cell main chamber.

All vapor liquid equilibrium (VLE) measurements were performed under isothermal conditions. The cell was cleaned and dried and preheated inside the bath to reach the desired temperature. Then the cells were loaded through the injection port with a measured quantity of solvent sample between 20 and 50 mL. The cell was then placed under vacuum to off-gas any residual absorbed gas and potentially volatile vapor. Once the pressure and temperature stabilized the injections were performed. Routine gas injections through the gas inlet port were performed, with each injection being between 0.1 and 10 milimoles of supercritical grade CO₂ provided from Praxair. Real time recording of all temperature and pressures from a custom made computer program in LabVIEW allowed for real-time analysis of pressure in the cell. Operators watched the cell pressure and temperature reach a steady state before recording the equilibrium pressure at that given temperature. After steady state, new injections were performed. Solvent loading was calculated assuming ideal behavior, while gas phase compositions were calculated from pure component vapor pressures using Raoult's law. The CO₂ concentration in the liquid phase could then be calculated using the mass balance of material inside the cell.

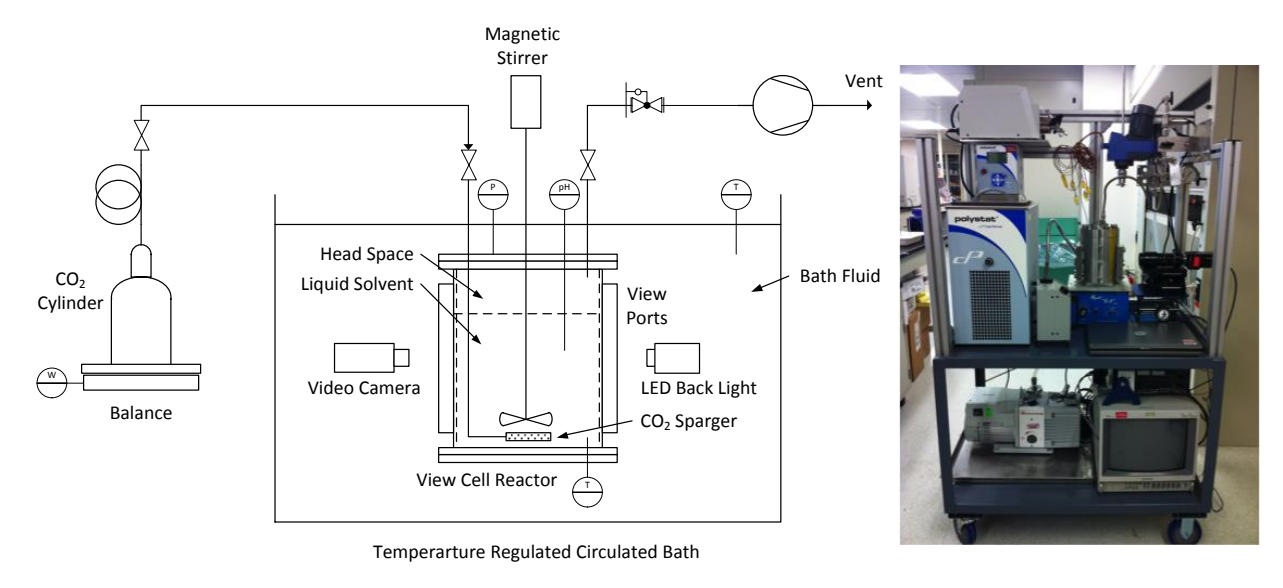


Figure 7. Custom made PTx cell assembly.

Wetted wall configuration

CO₂ absorption kinetic behavior was measured using PNNL's in house wetted-wall column. Wetted wall columns (WWC) have been used widely for gas-liquid absorption kinetics measurements. In a WWC contactor, the gas-liquid interface is provided by a fall film of liquid over a column of known height and diameter and thus the contact area is known. From the gas side concentration change and flow rate, the flux across the gas-liquid interface can then be calculated. By making a series of flux measurements at various CO₂ partial pressures at gas inlet, it is possible to determine the equilibrium CO₂ partial pressure at a projected zero flux point and to simultaneously determine an overall mass transfer coefficient from the changes in flux as a function of departure from equilibrium.

The overall mass transfer coefficient K_G as well as the gas and liquid film mass transfer coefficients k_g and k'_g , as shown in the diagram in Figure 8, are defined by the following relationship:

$$N_{CO2} = K_G(P_{CO2} - P^*_{CO2}) = k_g(P_{CO2} - P_{CO2,i}) = k_g'(P_{CO2,i} - P^*_{CO2})$$

Where N_{CO2} is the CO₂ flux through the gas, P_{CO2} is the partial pressure of CO₂ in the bulk gas phase, $P_{CO2,i}$ is the partial pressure of CO₂ at the gas-liquid interface, and P^*_{CO2} is the partial pressure of CO₂ at equilibrium with the bulk liquid phase.

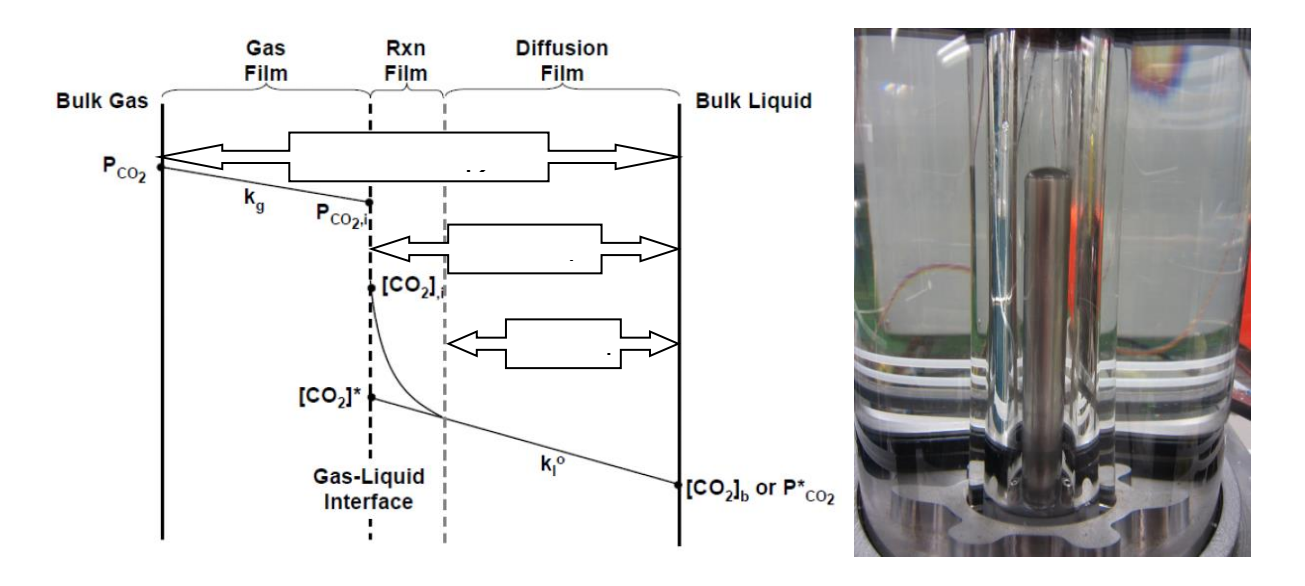


Figure 8. Concentration profile and associated resistances to CO₂ mass transfer in a solvent system (adapted from Dugas 2009)

The overall resistance to mass transfer can be expressed as a sum of the resistance terms for the gas and the liquid phases:

$$\frac{1}{K_G} = \frac{1}{k_g} + \frac{1}{k_g'}$$

If the gas film mass transfer coefficient k_g is known, then the liquid film mass transfer coefficient k'_g can be determined from the measured K_G values. Note that k'_g combines the effects of gas-liquid reaction kinetics and liquid film mass transfer resistance. For a given gas-liquid contactor, k_g depends on specific geometry of the contactor, gas and liquid physical properties, and gas flow rate. Correlations for k_g were obtained for the Battelle WWC using 2M piperazine (a fast reacting solvent) and assuming equivalence of the measured overall mass transfer coefficient.

Bench cart configuration, packing, circulation rates etc...

The bench-scale testing system is a mobile test apparatus for evaluating CO_2 capture performance of absorbent liquid materials both in the laboratory and in the field. The data generated by the system includes bed effluent concentration and flow rate, pressure drop, and temperature profile for both the absorber and the stripper columns. The CO_2 concentration in the solvent both at the absorber and stripper will also be measured periodically. These data

were fitted to suitable absorption/desorption models. The absorption model parameters are inputs to a process simulation model that is used to evaluate the economics of specific CO_2 capture solvents and absorption processes. The solvent testing system is on separate "cart" comparted to the supporting infrastructure, which enables new cart-based technologies to be rapidly constructed and tested. The relationship of the solvent bench-scale cart to other test carts is illustrated in Figure 9. The utility cart supplies feed and purge gases, electrical power, heat exchange fluids, and data acquisition functions. Gas stream sampling is handled by a separated cart-based mass spectrometer.

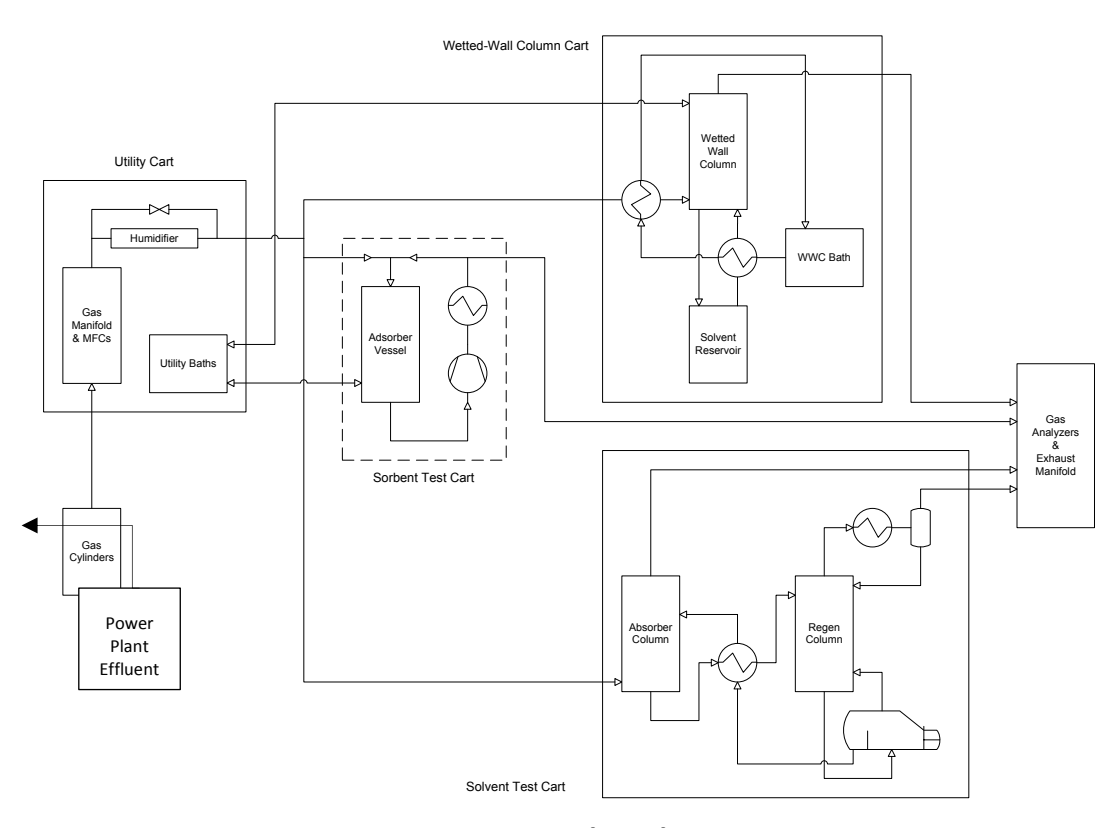


Figure 9. CO₂ capture materials and processes test carts.

The solvent testing system nominally holds 1-2 liters of liquid solvent. The maximum feed gas flow rate is 30 standard liters per minute (slpm), which corresponds to about 0.5 kg/hr CO_2 under with typical flue gas compositions. Feed gas pressures can be set up to 60 psig. The feed gas used in the laboratory is blended from bottled sources and can be saturated with water vapor. The operating temperature of the stripper is up to 200°C. A picture of the solvent testing system is shown in Figure 10.

.



Figure 10. CO₂ Solvent scale-up test cart.

The solvent testing system consists of an absorber bed and a stripper bed that can be set up as an absorption system only (with recirculating solvent), a stripping system only, or an integrated unit that both absorbs CO_2 and strips out CO_2 from the selected solvent. Single bed operations with the absorber column are useful to study sorbent kinetics at a range of solvent lean and RICH loadings. Flow rates of the gas and liquid can be varied to evaluate the mass transfer (both liquid and gas phase) and reaction kinetics of a particular solvent. Single bed operations with the stripper column are useful to study CO_2 desorption as a function of reboiler heat duty, pressure, and solvent flow. By combining the two columns together their interactions can be studied and such things as optimum lean/RICH loading, thermal and oxidative degradation, foaming, and solids formation can be evaluated.

In the single bed operation for the absorber column, a carboy of solvent mixture at a given concentration is pumped at a measured flow, through the heat exchanger, and down flow through the absorber column. As the solvent is flowing down the column, a given gas feed flow rate can be fed up flow into the absorber column. The concentration of the gas effluent is continuously measured. Based on the change in CO_2 concentration in the gas stream from inlet to outlet and its flow rate, the solvent loading and CO_2 removal efficiency can then be calculated. Periodic sampling of the liquid can be used to verify the expected liquid CO_2 loading.

During initial testing, liquid and gas flow rates can be varied initially with water and air to determine expected flooding points. Future tests with solvent and flue gas surrogate can then be maintained within these limits. With the solvent and flue gas surrogate, the mass transfer, kinetics, and solvent capacity can be determined for various solvent and gas concentrations.

In the single bed operation for the stripper column, solvent previously loaded with CO_2 is effectively studied for stripping characteristics. The CO_2 loading of the solvent can be performed in the skid's absorber column or outside of the system with a bubbler. The loaded solvent is placed in a carboy outside the system. Once the reboiler, condenser, and solvent

preheater heat exchangers have reached their steady state temperatures, the solvent can be pumped at a measured flow rate down through the column. The flow rate and CO₂ concentration of the effluent gas is to determine the change in solvent loading. Periodic sampling of the liquid can be used to verify the expected liquid CO₂ loading. The system provides an excellent method to quantify the stripping system.

In the dual bed operation, a measured quantity of the solvent mixture at a given concentration is placed into the stripper feed tank. Heat exchangers are allowed to reach their set point temperature prior to initiation of flow. The flue gas surrogate flow is initiated as the solvent is pumped from the stripper feed tank, through the absorber column and collected in the absorber feed tank. The solvent that has been loaded to a known level with CO_2 is then heated through the stripper preheater and is flowed down through the stripper column. As the CO_2 is released, it returns to the stripper feed tank. Flow rate and concentration measurements are made periodically on both gas effluents. Flow rates of the two pumps must be adjusted to maintain the levels in both feed tanks. Periodic samples of both lean and RICH streams can be taken.

The utility cart provided a humidified simulated 'wet' flue gas feed. For the purposes of this procedure, the target composition of the stream is the post combustion. The maximum flow rate is 30 slpm and the nominal stream composition is shown in Table 2.

Gas Constituent	Volume Percentage
N ₂	73%
H₂O	8.7%
CO ₂	15%
O ₂	2.5%
Ar	0.9%
SO ₂	0.2%

Table 2. Post-Combustion Gas Composition

Both the absorber and the stripper columns are identical except for length. A schematic of the absorber and stripper column design is shown in Figure 12. The temperature and pressure ratings and other specifications of the column are listed in Table 3. Both the absorber and stripper systems consist of a column, a feed tank, a pump, flow meter, level sensor, liquid preheat exchanger, and a gas effluent conditioner.

The columns are 1-3/8" diameter stainless steel tubes with Type EX Sulzer Laboratory Packing. Packing heights differ between the absorber and stripper columns. Eleven thermocouple ports are attached evenly down the length of the tube. Liquid enters and exits through ¼" tubes attached to the top and bottom flanges, respectively. The gas enters through a ¾" tube attached 2-3/4" from the bottom of the tube. This ¾" tube extends inside the column and is designed to allow gas flow downward but preclude entry of liquid from above. The gas exits through a ¾" tube that sits approximately ½" above the liquid feed tube at the top of the column. This design once again is to preclude liquid entry into the gas line. The pressure

drop across the column is measured through ¼" tubes at the same level as the gas lines. In the absorber, liquid level sensors are provided at three points at the top of the column. The purpose of these level sensors is to indicate when flooding of the column is occurring. In the stripper, liquid level sensors are provided at three points at the bottom of the column. These verify that the reboiler is working properly. Both columns have a pressure relief valve set to 60 psig. Detailed flow sheets of piping and instrumentation of the cart is provided in Figure 11. Temperature limitations on the reboiler required the use of nitrogen stripping gas. It should be noted that such a configuration couldn't be used in a functioning plant.

All viscosity (and some density) measurements were performed using a flow-through piston—style VISCOPRO 2000 System purchased from Cambridge Viscosity, Inc. This unit utilized a SPC-372 Sensor, with the optional Density measuring Software D2.11. This viscometer was chosen for the ability to continuously flow sample through it at a range of flows and temperatures while reading both viscosity and density of the CO₂BOL during absorption and desorption conditions. The viscometer was fitted with three interchangeable piston heads to measure three ranges of viscosity. Gear pumps (Cole-Palmer brand) were used to deliver a controlled liquid flow rate ranging from 60 mL/min to 1L/min. In some measurements, the viscometer was used to measure hot-lean solvent, and others it was used to measure cold-RICH solvent

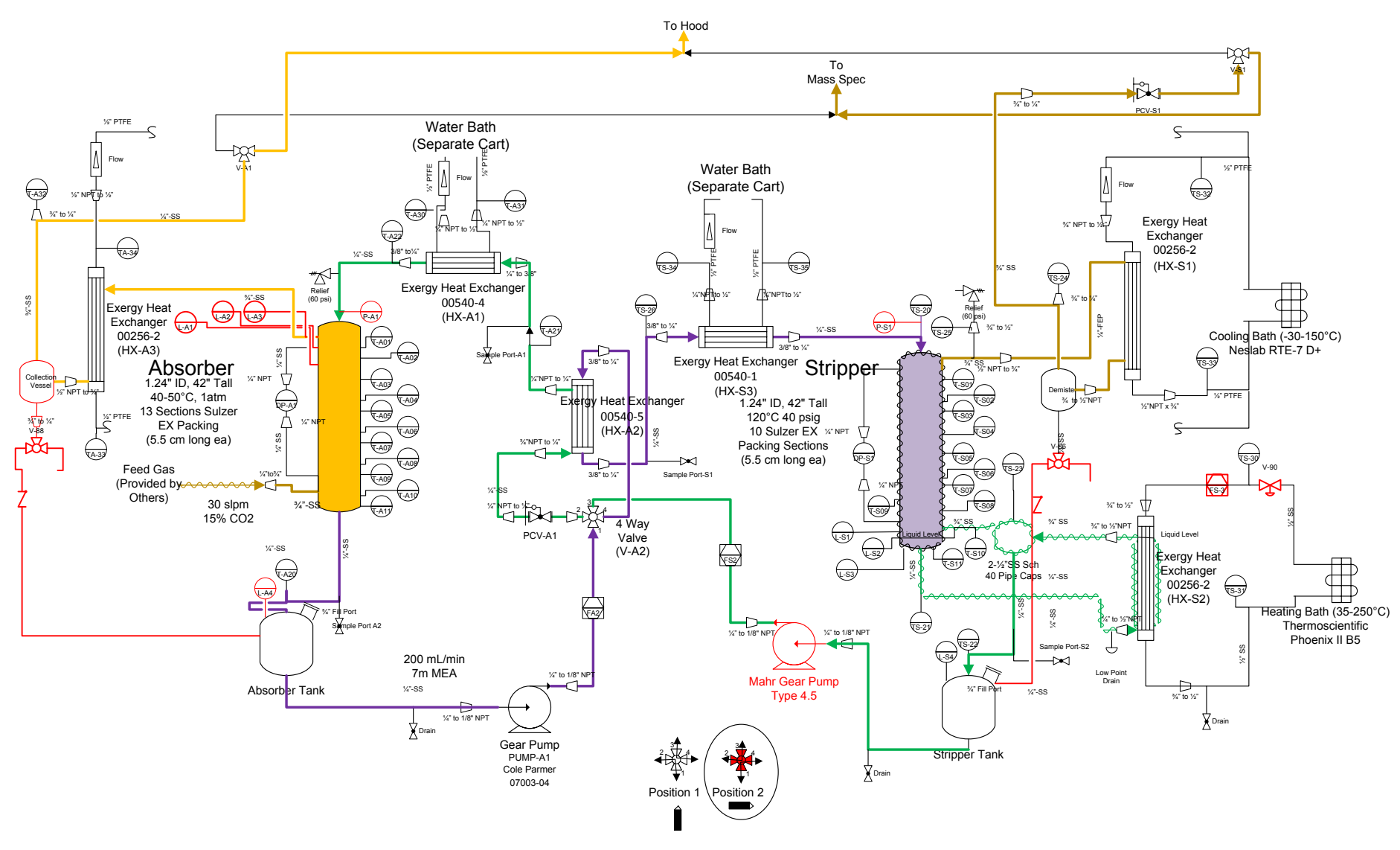


Figure 11. Solvent cart piping and instrumentation diagram for Dual Bed Absorber/Stripper Configuration.

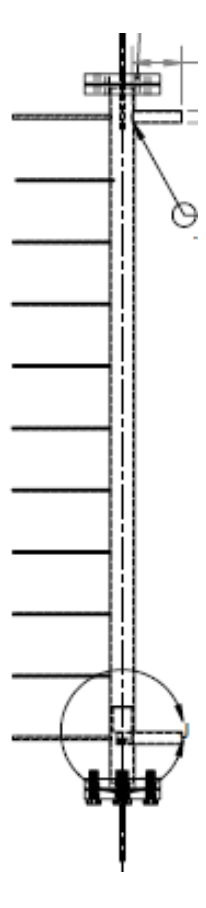


Figure 12. Schematics of the absorber and stripper columns. Horizontal lines are thermocouple inputs inside the column.

Table 3. Absorber/Stripper column specifications.

Max Allowable Working Temperature	200°C		
Max Allowable Working Pressure	60 psig		
Shell Outside Diameter	1.37"		
Shell Thickness	0.065"		
Shell Material	316 Stainless Steel		
Wetted Materials	316 SS, Teflon		
Packing Material	Sulzer Laboratory Packing Type EX		
Bed Height	42.57"		
Packing Height Absorber/Stripper	28.1"/21.6"		
Packing Shelf	1-1/4"		
Flange Connections	1" ANSI B16.5 Blind Flange, modified		
Gasket	Expandable PTFE Insertable		
Solvent Connection Ports	Ф0.25"×0.028" tube		
Gas Connection Port	Ф0.75"x0.035" tube		

The feed tanks are 4" schedule 40 pipes with pipe caps. Level is measured using a capacitance level probe. Prior to operation, the tank volume was calibrated with this level. The feed tanks can be filled through a ¾" fill port and can be drained following testing at a low point drain valve. The absorber tank feeds a Cole Parmer gear pump with a digital drive with a flow rate between 5 mL/min and 330 mL/min. Nominal liquid flow rate is 150-200 mL/min. The stripper tank feeds a Mahr gear pump with a variable speed three-phase motor whose speed is controlled by a 4-20 mA signal. This pump has a flow range of between 22 and 220 mL/min.

The flow rate can be measured using an oval gear flow meter. Calibration of the flow will be required prior to operations. Pressure is also measured with a 0-100 psi pressure transducer. Prior to entering the columns, the liquid passes through two Exergy heat exchangers. The first provides recuperation between the hot stripper effluent liquid and the cold absorber feed liquid. The second heat exchangers are heated each with a water bath found on the utility cart. These heat exchangers are meant to shim up the temperature of the solvent to its appropriate level before it enters the column. All water baths have inlet and outlet temperature measurements and rotameters to measure coolant/heating fluid flow rates.

The gas effluents for both the absorber and stripper are cooled in Exergy heat exchangers to approximately 4°C. This low temperature allows the water to condense and collect in the demister, thus providing a reasonably dry product gas to the mass spectrometer for analysis. In both cases water is collected and can be either transferred back into its appropriate feed tank or removed from the system and disposed of. The gas effluent from the absorber and stripper columns can either be vented or sent to the mass spectrometer for analysis.

As mentioned previously, both the absorber column and the stripper column have the above-mentioned components. The stripper column has an additional heat exchanger that acts as a reboiler. Solvent passing through the column is collected in an Exergy heat exchanger where it is heated to its boiling point. A mixture of gas and liquid flows into the phase separator where the gases flow back up the column (a mixture of steam and CO₂ stripped from the liquid) while the lean liquid drains back into the stripper feed tank. While normal operations for the absorber should be close to atmospheric pressure, the stripper may have pressures up to 30 psig to increase the boiling point of the stripping section above 100°C. The maximum operating temperature of the stripper is 150°C. Temperatures above this value can be prevented by properly setting the excess temperature protection on the reboiler circulator bath. This circulator bath has a flow meter and a control valve to allow the flow to the reboiler heat exchanger be set to a specific value.

The 4-way valve V-A2 has two positions. In position 1, the absorber and stripper are operated independently. Liquid from the absorber feed tank flows though the absorber pump and back into absorber column. Liquid from the stripper feed tank flows through the stripper pump and back into the stripper column. In position 2, the CO_2 -RICH solvent from the absorber feed tank flows into the stripper column and then into the stripper feed tank. The stripper feed pump then transfers the hot CO_2 -lean solvent through a cross exchanger to reduce its temperature, then through a shim heat exchanger and into the absorber column.

Operation of the column can be performed manually or automatically. Continuous operator monitoring is not required when operating in a single column mode. Continuous operator

monitoring may be required with dual bed operation. The data acquisition and control system can be set to prevent an imbalance in pump flow rates that could result in one of the pumps running dry. If this feature is operational, the operator may be absent for long periods of time. If this feature is not enabled, the operator may be absent under these conditions for no more than 10 minutes at a time and this absence should occur only if the system flows have stabilized. Valve operation and liquid sampling are the responsibility of the operator and are not automated.

Data logging of the temperatures and pressures are performed using a control/data acquisition system installed on the utility cart. The pumps and baths can be controlled manually or using the data acquisition system. The system is based on a National Instruments Compact RIO hardware platform and custom-built LabVIEW software. Process alarms such as temperature and pressure limits are implemented through the control/data acquisition system. When an abnormal event is detected the control system software will open the main power contactors of the utility cart to power down all electrical equipment such as baths and pumps. An operator can also initiate such emergency shutdown manually by either sending a software command or pressing the off-button on the utility cart control panel. The system also allows access by an operator from a remote computer to monitor process status and to intervene if needed. The test runs are generally expected to last less than one day.

The project team redesigned the absorber column due to a flooding issue for the structured packing. Significant amount of time has been applied to recalculating dimensions that can account for our estimated viscosity for our CO₂BOL molecules. Basic process design and operating assumptions are listed as follows:

- (1) Feed gas composition: 15.9% CO₂ and balance N₂ (dry flue gas)
- (2) CO₂ capture efficiency is 90%.
- (3) Absorption conditions: 40°C and 1 bar
- (4) Test scale is 0.2 to 0.5 kg/hr captured CO₂
- (5) Lean solvent loading is 5 wt% (g-CO₂/g-free solvent)
- (6) Absorber L/G, or liquid to gas mass velocity ratio, is from 4 to 10

Assumptions (1) and (2) are driven by project deliverables. The flue gas composition implies a post-FGD stream of an Illinois No. 6 coal-fired power plant with minor flue gas components neglected. By choosing an absorption temperature of 40°C in assumption (3), we recognize that refrigeration or cooling duty of flue gas pre-conditioning will be significant at a lower absorption temperature. We also have the most extensive VLE and physical property data available at 40°C for DAP solvent. The test scale assumption (4) is mainly driven by the size of the existing test cart and the desire to avoid substantial upgrade or downsize of balance of the plant equipment. Assumptions (5) and (6) reflect the most favorable operation conditions identified by previous ASPEN-Plus based technology feasibility study.

Packing Selection

The absorber column is packed with Sulzer EX laboratory packing. It is a gauze type structured packing with high efficiency and low-pressure drop but a capacity lower than what the target test scale requires (0.2 to 0.5 kg/hr captured CO_2). Gauze type packing is still preferred

because the high number of theoretical stages per height helps to keep the mobile test cart height low enough to fit within a standard walk-in fume hood. The relatively insensitivity of effective surface area to liquid load of a gauze packing also simplifies design and operations. Commercial gauze structured packing materials are also available in size up to several meters and have been successfully used for industrial distillation and absorption for decades. Commercially available structured gauze packing materials having a larger capacity than the Sulzer EX packing include Sulzer BX, Koch-Glitsch, ACS (now under AMACS), etc. PRO-PAK packing was selected due to its high-efficiency in small diameter columns. A 2" diameter column was determined to be suitable for the PRO-PAK packing to enable a 14% vapor loading capacity.

Coalescer Design and separation efficiency

The coalescing unit was designed and ordered from an industrial supplier (Figure 13). The unit is a horizontal tube fitted with internal fans to promote mixing, and a boot to collect the denser CO_2BOL . The flow of LEAN CO_2BOL and decane are delivered through port 1 on while the CO_2BOL is pumped out through the boot in port 2 and decane is decanted from the top in port 3. The top of the unit was fitted with a 1/8" diptube to decant the decane layer. The diptube was connected to a gear pump, which pumped decane through a static mixer (mixing with RICH CO_2BOL) upstream of the stripper pre-heater.

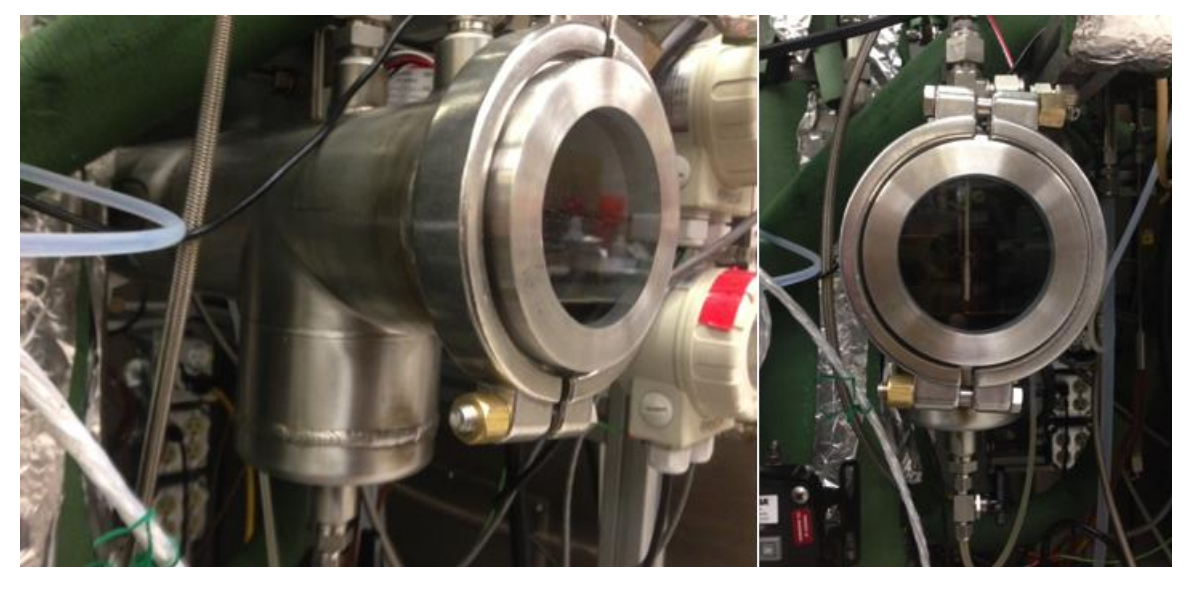


Figure 13. Coalescing tank option ordered from industrial supplier.

Continuous operation of the decanter showed facile continuous separation of CO_2BOL and antisolvent (decane). The calculated resonance time for the CO_2BOL and decane in the coalescing tank was three minutes. Visual observations of the two separate flows showed single phase fluids from the coalescing tank, with the decane layer being clear and colorless and non-viscous, with the CO_2BOL layer being yellow/orange and slightly viscous. Samples of the CO_2BOL and Decane layers were subjected to ^{13}C NMR to determine their compositions. The NMR spectra matched the measured LLE data of decane and BOL shown in Figure 18.

Antisolvent selection considerations

For antisolvent selection, a non-polar, non-toxic non-volatile material is desired. Screened candidates included alkanes, fatty acids, fatty acid methyl esters, fatty alcohols, geurbet alcohols, siloxanes, cyclosiloxanes. Candidate materials were tested for miscibility with the BOL as a function of temperature and as a function of CO_2 loading. Table 4 lists a few of the tested candidate antisolvents.

The majority of antisolvents were either miscible or completely immiscible with the BOL in the CO_2 -free form at any temperature or CO_2 loading. For the sake of time and budget, the team focused on using decane and hexadecane as antisolvents to complete the testing, with the former used in the bench cart testing, and the latter for modeling of the process at scale. It is recommended that a more thorough antisolvent screen will need to be performed to maximize antisolvent performance in the PSAR process.

Table 4. Antisolvent miscibility testing

	nm	Antißolvent Name	nm	MW	Formula	DBU/Hexanol	CO2-2.5%	CO2-2.5%	Compound	T°C
1	489	Hexamethyldisiloxane	488.5	162.38	C ₆ H ₁₈ OSi ₂	Miscible, TRT	Miscible, 🖫 T	Miscible	immisc.IRT	51
2	490	Octamethyltrisiloxane	489.5	236.53	C ₈ H ₂₄ O ₂ Si ₃	Miscible, TRT	Miscible, 🖫 T	Miscible	immisc.IRT	~64
3	491	Decamethyltetrasiloxane	490.5	310.69	C ₁₀ H ₃₀ O ₃ Si ₄	Miscible, TRT	Miscible, TRT	Immiscible	immisc.IRT	80-812
4	491	Octamethylcyclotetrasiloxane	490.5	296.62	C8H24O4Si4	Miscible, TRT	Miscible, IRT	Miscible	immisc.IRT	55
12	496	α-Pinene	495.5	136.23	C10H16	NotItested	Notatested	Notatested	Miscible, TRT	
13	498.0	11 imonene	498.0	136.23	C10H16	NotItested	Notatested	Notatested	Miscible, TRT	
14	520	1,833Cineol	519.5	154.25	C10H18O	NotItested	Notatested	Notatested	Miscible, TRT	
15	521.0	Methyl ® Laurate	521.0	214.35	C13H26O2	NotItested	Notatested	Notatested	Miscible, TRT	
8	525.0	2-Octyl-1-dodecanol	525.0	298.56	C20H42O	Miscible, TRT	Not⊡tested	Not@tested	Miscible, TRT	
16	527.0	Tributyrin	527.0	302.37	C15H26O6	Not tested	Not I tested	Not tested	Miscible, TRT	
10	530.0	Caprylicacida(Octanoic)	530.0	144.21	C8H16O2	Miscible, TRT				
6	533	Oleyli ????? Alcohol	532.5	268.48	C18H36O	Miscible, TRT	Not⊡tested	Not@tested	Miscible, TRT	
7	535.0	2-Butyl-1-octanol	535.0	186.34	C12H26O	Miscible, TRT	Not I tested	Not tested	Miscible, TRT	
	543.5	CO2BOLī(3)	543.5	171						
5	N/A ₃ S	hexamethylcyclotrisiloxane	N/ABSolid	222.46	©C6H18O3Si3	Miscible, TRT	Miscible, TRT	Miscible	Solid, TRT	55
11	N/A∄S	Capric⊞cid	N/ABSolid	172.26	C10H20O2	Miscible, ∄ T				
9	NRDIN	Silicon®Dil	NRD@Not@disso	162.37	C6H18OSi2	Miscible, PRT	Not ested	Not tested	immisc.@RT	121
	λmaxဩ	w/Nile®red	λmax®v/Nile®	ed			DBU/Hexanol	DBU/Hexanol		Heat,miscible
								on⊡ce		Compound

4. MEASURED EXPERIMENTAL DATA

The physical and thermodynamic properties of solvent systems are vital to projecting acceptable performance of a solvent for CO_2 separations. All physical and thermodynamic properties of (3) were measured for anhydrous and water-saturated conditions to study the impacts of water on the CO_2BOL solvent properties. All key physical properties of (3) are outlined in the state-point data table. The properties are listed as CO_2 lean and CO_2 RICH (3) to mimic absorber and desorber conditions. Viscosity studies were measured as a function of CO_2 loading for anhydrous and hydrated conditions to project the viscosity gradient of the solvent between lean and RICH loadings in the process. VLE curves were measured for (3) as a function of CO_2 partial pressure in anhydrous conditions with and without antisolvent, and hydrated without antisolvent. Liquid film mass transfer coefficients were measured for DBU-1-hexanol (as a representative first generation CO_2BOL) and (3) as a function of loading and temperature. Lastly, continuous bench scale testing was performed on anhydrous (3), (3) with decane antisolvent for PSAR testing, and (3) with 5 wt% water with decane antisolvent on a saturated inlet gas stream. Each bench scale condition was run at four different L/G ratios at 5, 10 and 15% CO_2 inlet concentrations.

State-Point Data for Solvent-Based Systems

All physical property data were measured for (3) using in house equipment or contract testing from external vendors. The material properties measured are used to project all performance metrics of the (3). Key physical and thermodynamic properties tested included specific heat, thermal conductance, vapor pressure, boiling point, and decomposition point, in addition to viscosity and density measurements as a function of CO₂ loading at varied temperatures. All measured data were placed into the State-Point Data Table (Table 5) (which was taken from the Funding Opportunity Announcement (FOA) (DE-FOA-0000403). The measured density of (3) in the absence of CO₂ was 1.03 g/mL. 10 wt% CO₂ loading on (3) exhibited a density of 0.97 g/mL. The viscosity of (3) was measured at 40°C to be 1.9 cP, which increased to over 3,000 cP with 0.5 molar equivalents of water at 10 wt% CO₂. This viscosity of (3) at 10 wt% CO₂ was two orders of magnitude lower than the previous generation CO₂BOLs, however refined measurements with accurate molar loadings showed viscosities up to 3,000 cP under what was initially the RICH loading projection of 10 wt%. A more detailed discussion of viscosity measurements is provided in the next section. The thermal conductance and vapor pressure of (3) were both measured as a function of temperature by subcontracted vendors. The vapor pressure can be considered negligible at 40°C and is on the order of 1.21 mm Hg at 100°C. The low vapor pressure confirms non-volatility of (3), and fugitive emissions are projected to be low.

Table 5. State-Point Data for Solvent Based Systems

	Units	Measured/Estimated Performance	Projected Performance
Pure Solvent		CO ₂ BOL (3)	CO ₂ BOL (3)
Molecular Weight	mol ⁻¹	171.14	171.14
Normal Boiling Point	°C	262 (decomposes >200)	262 (decomposes >200)
Normal Freezing Point	°C	< 0	< 0
Vapor Pressure @ 15°C	bar	0.179 (37°C) (DBU) 0.001 (100°C)	0.001
Working Solution			
Concentration	kg/kg	1 (anhydrous) 0.91 (hydrated)	1 (anhydrous) 0.91 (hydrated)
Specific Gravity (15°C/15°C)	-	1.03	1.03
Specific Heat Capacity @ STP	kJ/kg-K	1.9	1.9
Viscosity @ STP	сР	1.9 (CO ₂ -free solvent) 50 (lean solvent)	1.9 (CO ₂ -free solvent) 11 (lean solvent)
Surface Tension @ STP	dyn/cm	Not measured	Unknown
Absorption			
Pressure	bar	1 (near atmospheric, 0.15 bar CO $_2$ partial pressure)	1 (near atmospheric, 0.15 bar CO₂ partial pressure)
Temperature	°C	40	40
Equilibrium CO ₂ Loading	mol/mol	0.5 (at 0.15 bar CO_2 partial pressure)	0.5 (at 0.15 bar CO ₂ partial pressure)
Heat of Absorption	kJ/mol CO ₂	-80 (anhydrous) -90 (hydrated)	-80 (anhydrous) -90 (hydrated)
Solution Viscosity	сР	356 (hydrated 40°C)	< 356 (hydrated)
Desorption			
Pressure	bar	2	2
Temperature	°C	103.8 °C	103.8 °C
Equilibrium CO₂ Loading	mol/mol	0.25 ^c	0.25
Heat of Desorption	kJ/mol CO ₂	-80 (anhydrous) -90 (hydrated)	-80 (anhydrous) -90 (hydrated)

Viscosity Measurements

The viscosity Increase as a function of increased CO_2 loading significantly impacts the process, thus a quantification of viscosity in the RICH and LEAN solvents was needed as a function of temperature. Viscosities were measured for (3) as a function of CO_2 loadings at varied temperatures, however 40 °C data is the most vital as RICH solvent leaving the absorber will be the most viscous due to a combination of lower temperature and highest CO_2 loading. Further, the impacts of water and any potential antisolvent carried over into the absorber also needed study, for this reason, viscosity was also measured with water and antisolvent present. Loadings of water

and hexadecane were limited to 1 molar equivalent, as any higher loading would make the CO₂BOL a solute rather than the solvent.

The three viscosity profiles are shown in Figure 14. As expected, the viscosity of the solvent increases with CO₂ loading. Unexpectedly, the addition of water did not precipitate out bicarbonate salts as other CO₂BOL derivatives previously had, indicating this formulation has a significant tolerance to water. Further, the viscosity with antisolvent showed evidence of gelling at higher loadings. This gelling accounts for the higher deviation seen in the green triangles. For this reason, hexadecane was not used in bench scale testing, though hexadecane's miscibility temperature and physical properties were used for the modeling construction, as VLE data was available. A viscosity model was made from the measured data viscosities to account for this behavior and make formal projections of viscosity of RICH and LEAN solutions. A more detailed discussion of the viscosity modeling can be found below in the Modeling Section (5).

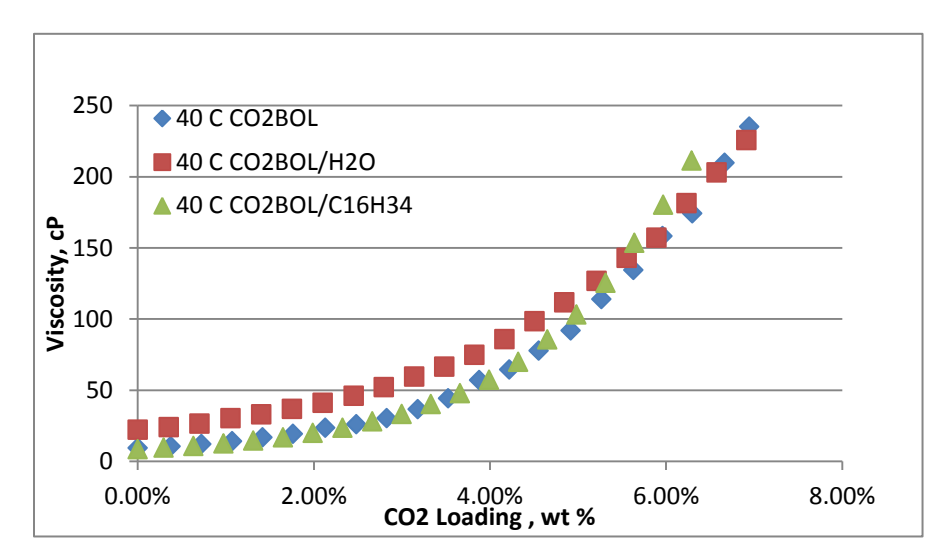


Figure 14. Viscosity Profile of estimated CO₂ Added to CO₂BOL (3) With and Without One Molar Equivalent of Water (40°C) and With Estimated Antisolvent Carryover

(NMR) measurements were made to confirm the impact of water on CO_2BOL chemistry and the speciation of CO_2 in solution. A solution of (3) was loaded with 10 wt % water and CO_2 , and a neat ^{13}C nuclear magnetic resonance spectrum was taken at 40 °C of the homogeneous solution. The spectrum showed that half of the CO_2 in solution was the desired alkylcarbonate, while half of the CO_2 was bound as a bicarbonate salt. The speciation study of CO_2 showed that water could chemically react with CO_2 and the CO_2BOL to form a bicarbonate salt, or water can solvate bicarbonate or alkylcarbonate salts in solution. In either case, water stabilizes CO_2 in solution more strongly than the anhydrous CO_2BOL , aiding in CO_2 capture, without drastically impacting viscosity. A thermodynamic model detailing the speciation of CO_2 and water was constructed in order to express the impacts of water in solvent chemistry. A more detailed discussion of this model can be found in the Modeling Section (4).

The density of (3) was measured in the absence of CO_2 as a function of temperature, covering the range of temperatures of absorption and desorption. The data are provided in Table 6. The density of the solvent was found to decrease with increases in temperature (20°C to 80°C).

Table 6. Saturated Liquid Density for CO₂-Free Alkanolguanidine (3)

Temperature °C	Measured Density g/cc	Correlated Density g/cc	% Deviation
20	1.0295	1.0294	0.02
40	1.0120	1.0121	-0.01
60	0.9944	0.9946	-0.02
80	0.9769	0.9768	0.02

Volatility of (3) was measured to project evaporative losses in the stripper. Saturated vapor pressure measurements were performed at 100-200°C, and the data are tabulated in Table 7, wherein the Antoine equation was used to correlate the measured data. (3) was found to be nonvolatile, with a vapor pressure of 1.21 mm Hg at 100°C, gradually increasing to 152.67 mm Hg at 200°C. With reboiler temperatures below 160°C, the team concludes that evaporative losses will be minimal for (3).

Table 7. Vapor Pressure Measurements for Alkanolguanidine (3)

Temperature °C	Measured	Correlated	Deviation %
102.00	1.21	1.29	-2.80%
108.58	2.07	2.05	0.37%
113.97	3.06	2.93	1.87%
118.41	4.10	3.88	2.41%
125.15	5.75	5.81	-0.48%
128.51	7.32	7.05	1.65%
139.96	12.67	13.00	-1.13%
140.01	13.17	13.03	0.46%
150.00	20.82	21.19	-0.78%
150.00	20.61	21.19	-1.22%
160.00	32.12	33.18	-1.40%
169.99	50.12	50.16	-0.04%
170.00	50.28	50.18	0.09%
179.89	73.43	73.29	0.08%
180.05	73.21	73.75	-0.32%
189.97	103.99	104.96	-0.40%
190.07	104.95	105.32	-0.15%
200.03	152.67	146.50	1.79%

Equilibrium Measurements

Isotherms (PTx method)

CO₂ Isotherms (no water present)

 CO_2 /liquid isotherms for (3) were measured for anhydrous conditions, with antisolvent and with water using the PTx method inside the custom made cell (*vide supra*). The anhydrous data are presented in Figure 15 (the P* of CO_2 over the CO_2BOL) that is plotted against the CO_2 loading of the CO_2BOL on the x-axis. Here, isotherms were run in duplicate at 40, 60, 80 and $100^{\circ}C$ to cover the range of absorption and desorption conditions. The heat of solution calculated from the anhydrous VLE data is -80 kJ/mol of CO_2 . As expected, there is a noticeable temperature dependence on the CO_2 uptake compared to aqueous systems. The higher temperature sensitivity is linked to the lack of co-solvent stabilization of the CO_2 containing anion. In the case of a CO_2BOL or other concentrated solvent, the solvent's CO_2 -RICH and CO_2 -LEAN forms are responsible for self-solvation and stabilization of charge. This sensitivity is smaller in aqueous systems due to the strong hydrogen bonding and solvation from the solvent (water) that stabilizes the CO_2 carrier.

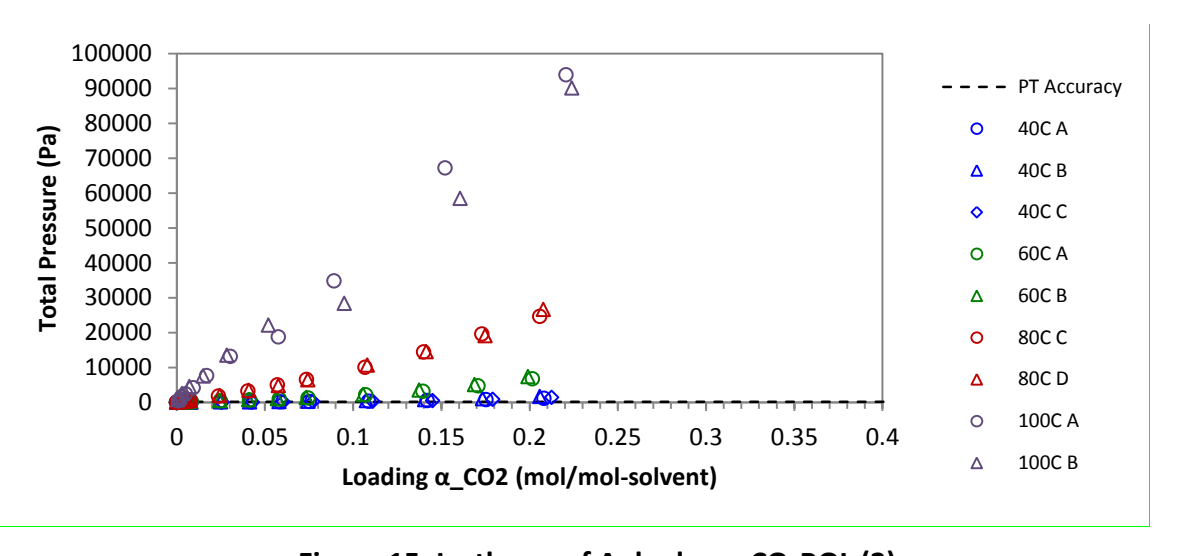


Figure 15. Isotherm of Anhydrous CO₂BOL (3)

CO₂ Isotherms (with added water)

To show the impacts of water on CO_2 uptake and release, isotherms were also run in the presence of one molar equivalent of water, or 10 wt% (Figure 16). The resulting total pressure is higher than the anhydrous measurements due to the high vapor pressure of water compared to the CO_2BOL , indicating that not all of the water is complexed to the CO_2 . Low complexation was confirmed using NMR. In the VLE curves, the total pressure is reported as a combination of the partial pressures of both water and CO_2 . Thus, P^* had to be extrapolated from the data as it could not be directly measured.

The total pressure drop concomitant with increasing CO₂ loading corresponds to the consumption of water either chemically, forming a bicarbonate salt (similar to aqueous amine systems) or simply solvating the CO₂BOL's alkylcarbonate. The calculated heat of solution in the hydrated case was -90 kJ/mol of CO₂. The higher heat of solution is expected, as reactions with

water either by solvation or chemical fixation are stronger than that of the alkylcarbonate itself. Visual inspection of the cell showed no solid precipitation or phase separation of the layers, indicating this formulation of CO_2BOL has a high water tolerance and testing with water may be performed in the bench cart. This observation was the initial indication that full dehumidification upstream might not be required in the $CO_2BOL/PSAR$ process.

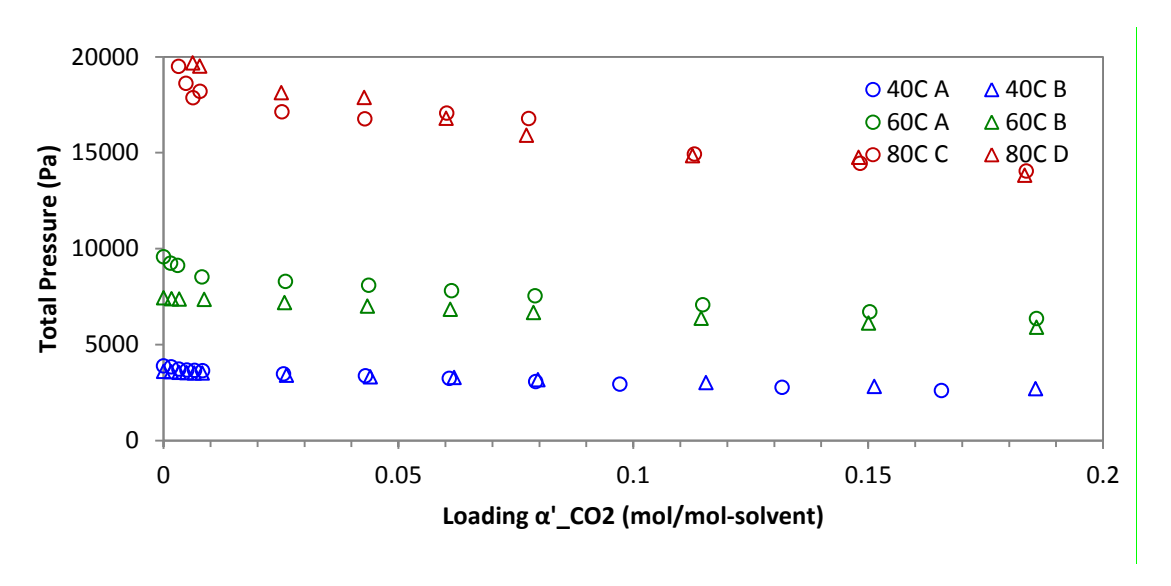


Figure 16. Isotherms of CO₂BOL (3) + 1 Molar Equivalent of Water

CO₂ Isotherms (with antisolvent present)

Measured vapor-liquid equilibrium (VLE) curves with the CO₂BOL and a molar equivalent of hexadecane antisolvent were next measured (Figure 17). Hexadecane was used due to its availability, low cost, and insignificant vapor pressure. The isotherm measurements show no observed PSAR effect at temperatures up to 60 °C, as expected, but an observed effect at 80 and 100 °C. Visual inspections of the cell confirmed a biphasic liquid system at 40 and 60 °C, indicating no mixing between the fluids had occurred. Without miscibility between the two phases, there is not enough antisolvent in solution to impact polarity. Conversely, at higher temperatures a single liquid phase was observed, indicating enough antisolvent was mixed with the CO₂BOL, promoting a polarity change. Phase separation between the hexadecane and the CO₂BOL was repeatedly observed by cooling to 40°C, indicating that separation of the antisolvent and CO₂BOL can be done by cooling the mixture to absorption temperatures. These observations are advantageous because they suggest that the PSAR process can be promoted in the stripper but avoided in the absorber. More specifically, the antisolvent has minimal impact on CO₂ loading under conditions in the absorber, but has a noticeable effect on stripping. The notable increase in P* over the anhydrous VLE curves at 80°C and 100°C show that the PSAR can release more CO₂ at a given temperature, or alternatively, a lower temperature could be used to release the same amount of CO₂. The former configuration of PSAR may be applicable to promote a higher thermal compression of CO₂ to save on mechanical compression, and the latter would drop the reboiler temperature to provide efficiency gains in the steam cycle, vide infra.

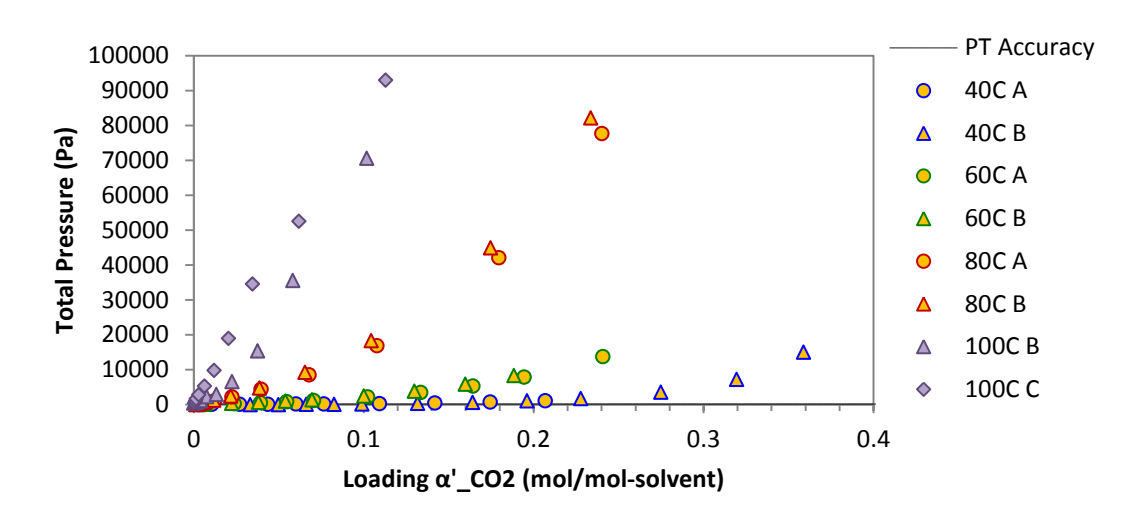


Figure 17. Isotherms of Anhydrous CO₂BOL (3) Plus 1 Molar Equivalent of Hexadecane Antisolvent

Antisolvent miscibility and liquid-liquid equilibria

As the PSAR effect was quantified in the VLE curves, studies were needed to show how to control the miscibility of the CO₂BOL and candidate antisolvents as a function of *both* CO₂ loading and temperature. Exploration of the phase behavior of CO₂BOLs and candidate antisolvents showed that the BOL in a completely CO₂-free loading could phase separate from antisolvents by cooling below a miscibility point. The phase diagram below (Figure 18) shows the phase diagram for hexadecane and CO₂BOL (3) in blue. The diagram indicates complete miscibility of the hexadecane and (3) above 62°C, and spontaneous separation of the mixture into two liquid phases below that temperature. For example, if the CO₂BOL/hexadecane mixture, after CO₂ has been removed, is cooled to 40°C, the CO₂BOL-RICH phase (at left in the diagram) will contain 92 wt% CO₂BOL and 8 wt% hexadecane. The antisolvent-RICH phase (to the right in the diagram) would contain 22 wt% CO₂BOL and 78 wt% hexadecane antisolvent. Cooling to 20°C instead of 40°C ensures that more CO₂BOL is recovered, but does not cause much of a decrease in the carryover of antisolvent in the recovered CO₂BOL stream (6 wt% hexadecane instead of 8%). Process simulations take into consideration the estimated carryover of 5-8 wt% of antisolvent into the absorber.

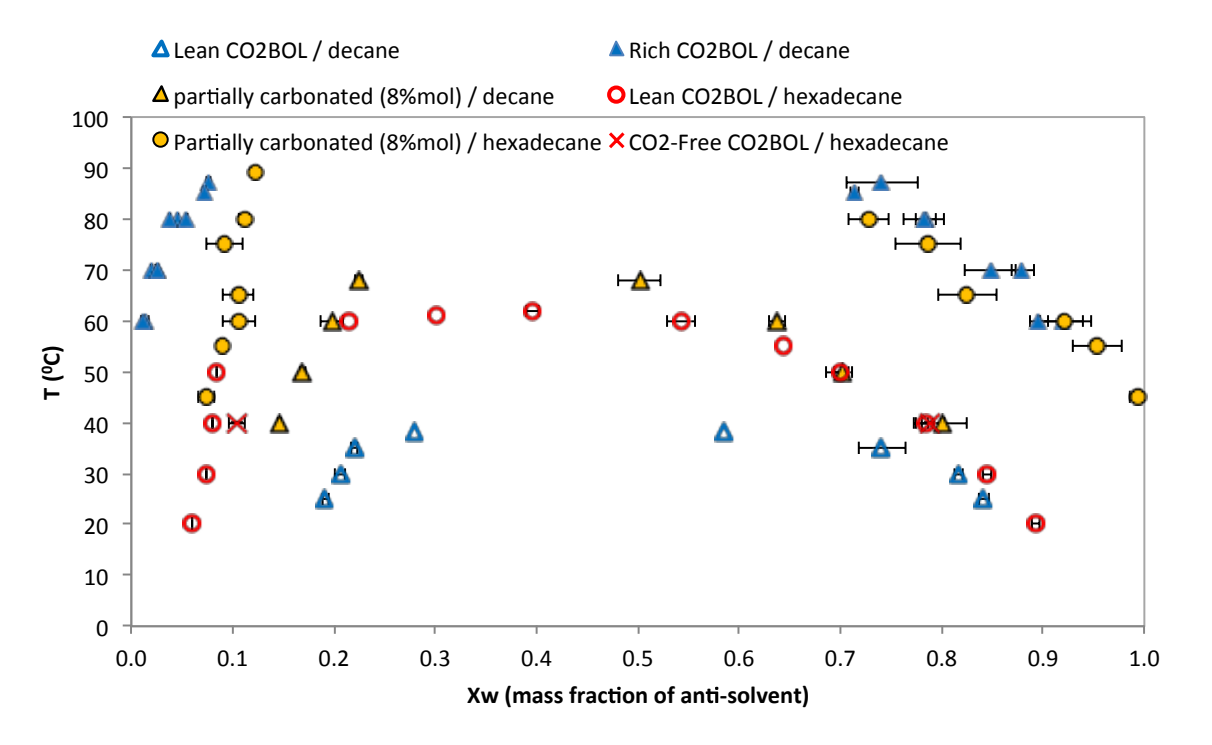


Figure 18. Phase Diagram for (in blue) CO₂-LEAN CO₂BOL (3) and Hexadecane and (in red) CO₂-LEAN CO₂BOL (3) and Decane as a Function of Temperature. Areas within the curves represent biphasic behavior.

Similar tests were performed with decane as the antisolvent. The mixture of CO_2 -LEAN CO_2 BOL and decane is miscible in all proportions above 40°C, but if the system is cooled to 25°C then it splits into a CO_2 BOL-RICH phase (81% CO_2 BOL and 19% decane) and an antisolvent-RICH phase (16% CO_2 BOL and 84% CO_2 BOL). Therefore, choosing decane as the antisolvent causes there to be more antisolvent carryover in the recovered CO_2 BOL.

When CO_2 is added to the CO_2BOL /antisolvent mixture, the phase behavior changes dramatically. CO_2 -RICH CO_2BOL is much less miscible with hexadecane. Two phases are observed even at 86°C, but *only for some concentrations*. For other concentrations, the CO_2BOL /hexadecane mixture is a single phase. Unfortunately the mixtures are viscous, which is causing technical problems during the acquisition of phase behavior data for these mixtures. At lower temperatures, the addition of CO_2 to the CO_2BOL /hexadecane mixture causes the expansion of the two-phase region of the phase diagram, so that the hexadecane carryover in the CO_2BOL -RICH phase is as low as 4%, although the exact value depends strongly on the CO_2 content. The very high viscosity and the two-phase behavior at high temperatures are only observed at CO_2 saturation (estimated stripper conditions). Complete miscibility between decane and the CO_2 -RICH CO_2BOL occurs at 92°C, indicating strippers need to operate at or above 92°C for the full antisolvent effect if decane is used as an antisolvent with (3).

Having some antisolvent carryover in the recovered CO_2BOL should be considered a good thing, because that antisolvent content will help to lower the viscosity of the CO_2 -RICH CO_2BOL . The amount of antisolvent content that is needed to sufficiently lower the viscosity is not yet known but it should not be difficult to tune the process to ensure that amount is carried over. The above

results demonstrate that we can tune the amount of antisolvent carryover by adjusting the temperature of the CO₂BOL-antisolvent separation step and by changing the choice of antisolvent.

Thus, the phase behavior indicates that separation can occur spontaneously by cooling the mixture of BOL (3) and antisolvent to the absorption temperature. Multiple antisolvents were tested for their miscibility temperature, formally called the upper critical solution temperature (Table 8), and it was found to be linked to the chain length of antisolvent, i.e., shorter chains had lower miscibility temperatures. This valuable finding allows us to select candidate antisolvents that will promote phase separation upon cooling to projected temperatures of operation. For the initial VLE and LLE measurements, hexadecane was chosen as the most viable antisolvent due to its cost and low vapor pressure, however decane was chosen for the bench scale testing due to its lower miscibility temperature.

Table 8. Upper Critical Solution Temperature of Varied Antisolvents with CO₂-LEAN CO₂BOL

Antisolvent	Chain Length	T _{miscibility} (°C)	Vp (mm Hg)	USD (\$)/kg
Heptane	7	> 30	58.1	1.40
Decane	10	38	3.20	1.40
Dodecane	12	39.3	0.414	1.10
Hexadecane	16	62	0.0497	1.00

a) Vapor pressure reported at miscibility temperature.

Kinetic Analysis of CO2BOLs

This section discusses the CO_2 flux measurements of Gen 1 and Gen 2 CO_2 BOLs using our in house wetted wall apparatus. The wetted wall apparatus needed validation prior to running CO_2 BOL solvents by performing a validation against an MEA standard. There is a great deal of published values of liquid film mass transfer coefficients for MEA, notably the CO_2 equilibrium pressure and liquid film mass transfer coefficient data for 5M MEA from Rochelle's group. 6 5M MEA was run on our wetted wall column (WWC) at 40° C, and the data were compared with the literature data, confirming agreement between both P^* and k'_g values.

Wetted wall of a first generation CO₂BOL

To our knowledge a non-aqueous solvent system has never been tested in a wetted wall apparatus. Rather than risk any loss of degradation of custom made solvent, a first-generation CO_2BOL comprised of a 1:1 by mole DBU-hexanol mixture was used for the kinetic evaluation. The DBU-hexanol selection was also chosen due to both reagents being commercially available at liter quantities needed for the WWC measurements. The data collected from this generation-1 CO_2BOL chemistry would be used as guide to dial in conditions and operating parameters needed for the CO_2BOL (3).

Measurements were made at 35, 45, and 55° C each at three CO_2 loading levels of 0.5, 1.0, and 4.4 wt%. The loading is presented as grams of CO_2 per gram of unloaded solvent. The molar loadings of CO_2 are 4.5, 9.7, and 43%. All tests were performed at near atmospheric pressure.

Exposure to air would introduce water and subsequently bicarbonate salts which would precipitate out of solution and complicate the measurement's accuracy and precision. Thus, loading solvents inside sealed 3L glass flasks minimized exposure to air. CO_2 was delivered as dry ice primarily to ensure accuracy as accurate masses could be recorded of solid CO_2 rather than sparging. After loading, the solvent was pumped into the WWC for testing.

The WWC data are presented in Table 9 and Table 10. Data at low loadings (< 0.5 wt%) were gathered but not presented due to a large degree of scatter, which is attributed to large error bars in collecting an accurate LEAN loading of CO_2 . In these measurements the solvent loading is considered constant as the amount of CO_2 exchange between the gas and liquid phases is considered negligible to the amount of CO_2 initially loaded to the solvent. At very low CO_2 loadings the exchange amount may no longer be negligible.

The DBU-hexanol at the same molar solvent loading as 5M MEA at 40°C and 60°C, shows a larger equilibrium CO_2 pressure P* and lower liquid film mass transfer coefficient (k'_g). At a 9.72% molar loading level the k'_g value for DBU-hexanol at 40°C is estimated to be 2.45×10⁻⁶ mol/s/m²/Pa by interpolation, which is approximately one third of the k'_g value of 7.64×10⁻⁶ mol/s/m²/Pa for 5M MEA at the same temperature. Interestingly, the k'_g values are comparable when plotted as a function of driving force (Figure 19).

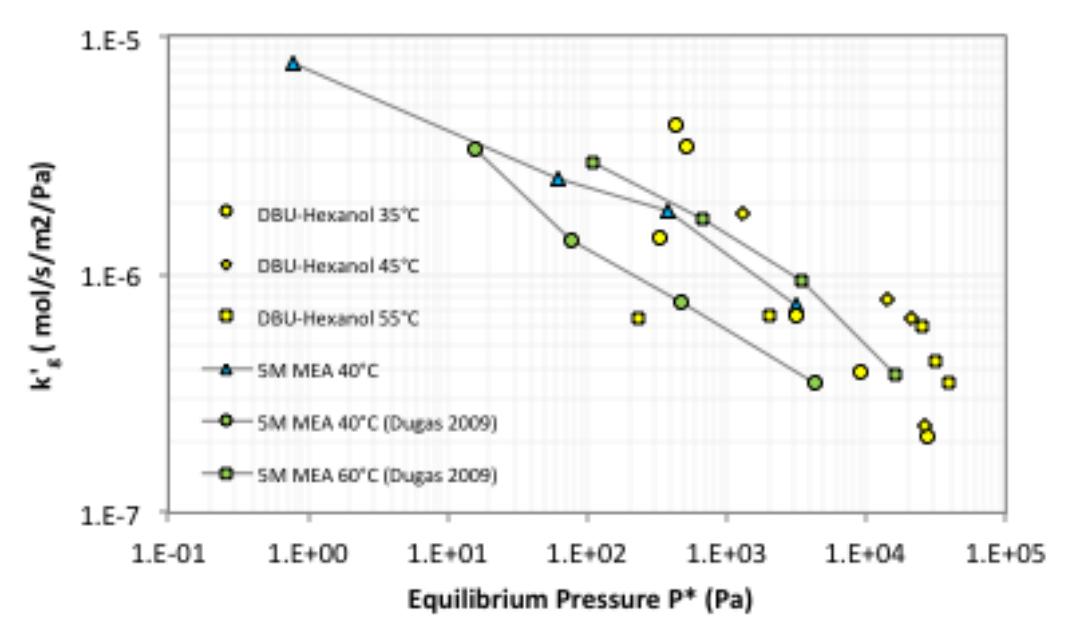


Figure 19. Liquid film mass transfer coefficient of DBU-hexanol and 5M MEA

Table 9. WWC data for DBU-hexanol at 35, 45, and 55°C $\,$

Data Set	Temperature	CO21Loading	CO21Loading	P*	K _G	kg	kg'
	[P C P]	[2g-CO2/g-solvent]	[Imol-CO2/mol-solvent] 2	[3 Pa 2]	[mols̄ -1m-2Pa-1]	[mols -1m-2Pa-1]	[mols -1 m -2 Pa -1]
2012-09-24a	35	0.50%	0.0291	431.2	3.52E-06	2.20E-05	4.19E-06
2012-09-25c	35	1.00%	0.0582	505.3	2.94E-06	2.20E-05	3.40E-06
2012-09-26a	35	4.44%	0.2574	3130.2	6.50E-07	2.20E-05	6.70E-07
2012-09-25d	45	1.00%	0.0582	1282.8	1.64E-06	2.20E-05	1.77E-06
2012-09-26b	45	4.44%	0.2574	14031.9	7.63E-07	2.20E-05	7.91E-07
2012-09-25e	55	1.00%	0.0582	2003.0	6.51E-07	2.20E-05	6.71E-07
2012-09-26c	55	4.44%	0.2574	25338.3	5.92E-07	2.20E-05	6.08E-07

Table 10. WWC data for 5M MEA 40°C

Data Set	Temperature	CO21Loading	CO21Loading	P*	K _G	kg	kg'
[ユyyyy-mm-ddxi]	[P C P]	[द्य-CO2/g-solvent]	[amol-CO2/mol-solvental22	[P a !]	[mols̄-¹m-²Pa-¹]	[mol͡s -1m-2Pa-1]	[mols -1 m -2 Pa -1]
2012-09-18a	40	2.04%	0.0912	0.8	5.67E-06	2.20E-05	7.64E-06
2012-09-19a	40	5.64%	0.2614	61.4	2.27E-06	2.20E-05	2.53E-06
2012-09-20a	40	7.76%	0.3597	383.5	1.70E-06	2.20E-05	1.84E-06
2012-09-20b	40	10.76%	0.4988	3095.0	7.19E-07	2.20E-05	7.43E-07

Wetted wall of a second generation CO₂BOL

Once meaningful data was collected from the first generation tests, the team completed the kinetic analysis of the (3) CO_2BOL using the wetted wall column apparatus. The equilibrium data collected at 40, 60, 80 and 100 °C from this test agreed with the equilibrium data from the PTx testing (Figure 20). The data also provided validation that the solvent was the same compound that was tested for the equilibrium data.

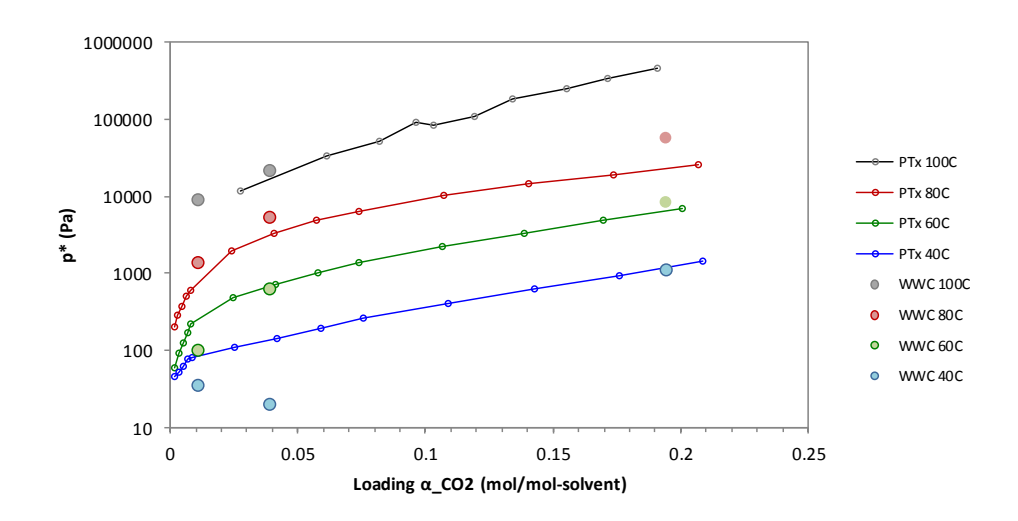


Figure 20. Comparison of VLE data measured from WWC plotted VS VLE data from PTx measurements

The liquid film mass transfer coefficients (Kg¹) were measured at 40, 60, 80 and 100 °C on the wetted wall column and plotted as a function of driving force (Figure 21). Three loadings (0.25, 1, and 5 wt%) were tested. The loading is plotted at grams of CO₂ per gram of unloaded solvent. All tests were performed at near atmospheric pressure, and CO₂ was measured gravimetrically using massed dry ice additions. As Figure 21 shows, there is similar kinetic behavior of the (3) when compared to DBU-1-hexanol. The Kg¹ values were in the same range as aqueous solvents such as MEA at comparable loadings. Further, inverse temperature dependence was also observed; *i.e.* the solvent's Kg¹ gets larger with a decrease in temperature. The implications of this test confirm comparable kinetic performance of (3) to aqueous systems, albeit at a far higher viscosity. Most organic or water-LEAN systems are hypothesized to exhibit similar behavior, though the project team cautions that these observations are the first of their kind and require more studies and validation prior to being universally embraced.

The WWC data measured for (3) are presented in Table 11. (3) Exhibits a larger equilibrium CO_2 pressure P* at all temperatures, and comparable liquid film mass transfer coefficient (k'_g) at the same molar solvent loading as 5M MEA at 40°C and 60°C, but lower k'_g at 80 and 100 °C. (3) Shows lower P* yet higher k'_g values than DBU-hexanol, which is expected as (3) has a stronger absorption of CO_2 and a higher viscosity.

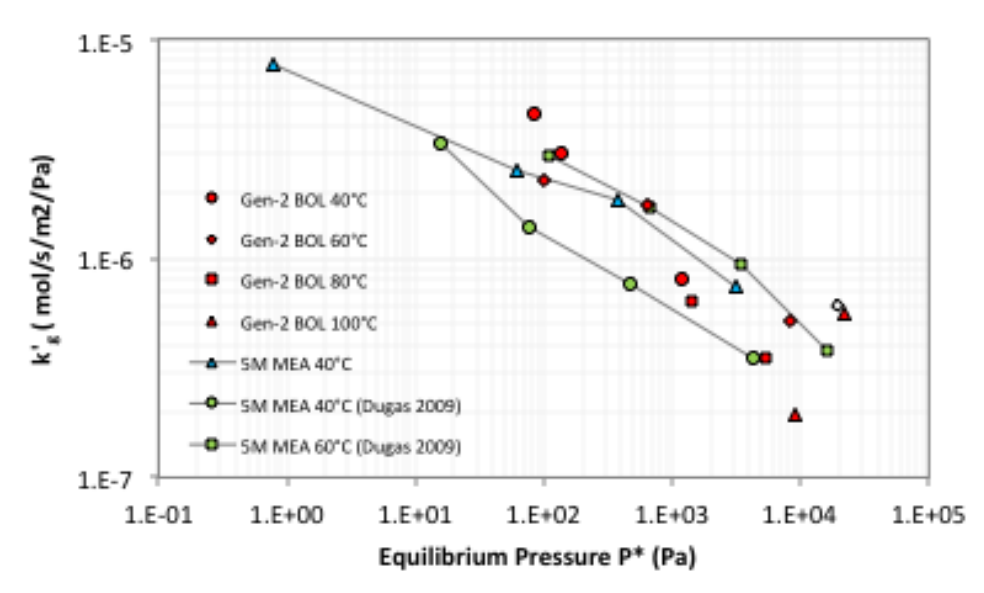


Figure 21. Comparison of ${\rm K_g}^1$ values (3) plotted VS aqueous 5M MEA

Table 11.WWC data for (3) at 40, 60, 80, 100 $^{\circ}\text{C}$

Data 5 et2	Temperature ?	CO21Loading?	CO21Loading 2	P* ?	K _G ⊡	k _g ?	k _g '⊡
?	[PC]?	[曖-CO2/g- solvent頃②	[ªmol-CO2/mol- solvent₫②	[P a i]2	[mol͡s-¹m ⁻ ²Pa ⁻¹]፻	[mol͡s ¹m ²Pa ¹]፻	[mol͡s-¹m ⁻ ²Pa ⁻¹]②
2013-10- 10a2	40.27	0.27%₪	1.06%?	34.8?	3.75E-062	2.20E-05?	4.52E-062
2013-10- 14a2	40.52	1.00%₪	3.88%?	19.72	2.67E-062	2.20E-05?	3.04E-062
2013-10- 15a2	40.52	4.99%2	19.43%2	1111.9?	7.66E-07?	2.20E-052	7.94E-07?
2013-10- 09a2	59.82	0.27%2	1.06%?	99.42	2.03E-062	2.20E-052	2.24E-062
2013-10- 11a2	59.82	1.00%2	3.88%?	635.12	1.61E-062	2.20E-052	1.74E-062
2013-10- 15b2	60.12	4.99%₪	19.4%?	8312.62	5.03E-072	2.20E-05?	5.15E-072
2013-10- 09b2	79.02	0.27%2	1.06%3	1400.22	6.21E-072	2.20E-05?	6.40E-072
2013-10- 11b2	80.32	1.00%2	3.9%?	5461.82	3.41E-07?	2.20E-05?	3.47E-072
2013-10- 09c2	99.92	0.27%2	1.06%?	8922.62	1.93E-072	2.20E-05?	1.95E-072
2013-10- 11c?	99.52	1.00%2	3.88%?	21806.72	5.47E-07?	2.20E-05?	5.61E-072

Figure 21 shows the mass transfer data for the Gen 2 CO_2BOLs being equal to or higher than the MEA reference values, despite known viscosity increases at the higher CO_2 loadings. One possible explanation of the k'_g values being higher than expected may be enhanced physical solubility of CO_2 in organic liquids. The solubility of CO_2 in water is considered negligible, but can be an order of magnitude higher in organics. It is known that CO_2 solubility has an inverse temperature dependence, as CO_2 can be readily dissolved in concentrations of up to 0.05 mol fraction in an organic liquid such as alcohols.⁷ A higher $[CO_2]_d$ in solution physically may be driving the liquid phase kinetics of absorption, thus enhancing the Kg^1 . This would also account for the inverse temperature dependence where the solvent is *faster* at lower temperatures. As temperature increases, the CO_2 solubility *decreases*, thus ending what we would call a rate "enhancement" by physically dissolved CO_2 as the rate "enhancement" is lost at about 55 °C, not surprisingly where CO_2 physical solubility in organics becomes negligible at atmospheric pressure. If this hypothesis were to be validated, enhanced absorption kinetics may be achieved at lower absorption temperatures.

A second area of focus for future analysis would be to investigate the differences in film thickness and composition of aqueous versus organic films. The Wilcox group at Stanford recently proposed such a hypothesis in a recent publication. Organic films may be not have the same ordering of reactive then diffusion barriers as their aqueous counterparts, thus new film theories may be needed to accurately measure and predict solvent performance. The team recommends future studies in both areas to gain a more complete understanding of mass transfer in organic systems.

Bench Scale Parametric Testing

Bench-Scale Batch-Wise Absorption Testing and PT_x Validation of Column Performance Using a Second-Generation CO₂BOL (no antisolvent or water added)

In order to begin bench-scale system testing three liters of Gen-2 CO_2BOL (3) were loaded and subjected to batch-wise absorption measurements using the absorber side of the cart only. The solvent was pumped into the bench cart under a nitrogen atmosphere. Two batch-wise absorption tests were performed (40 °C and 60 °C) to compare the equilibrium CO_2 uptake by the (3) to measured VLE data. The measured absorption data from the cart at 40 °C (Figure 22) and 60 °C (Figure 23) (based on mass balance calculations) correspond with measured equilibrium data from the PTx cells.

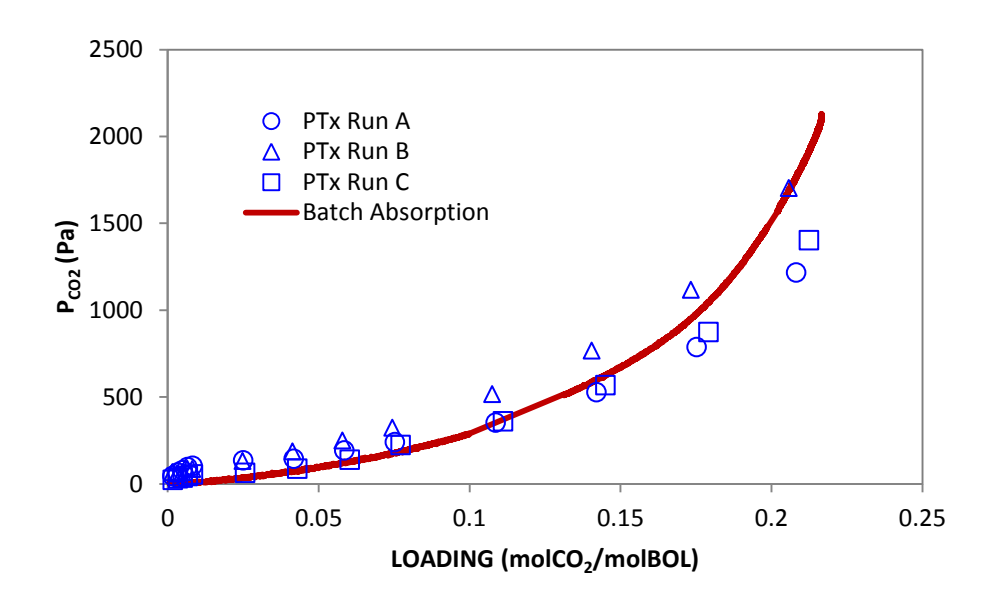


Figure 22. Measured VLE data of the bench cart (red line) for (3) plotted against VLE data measured from PTx measurements (both at 40 °C).

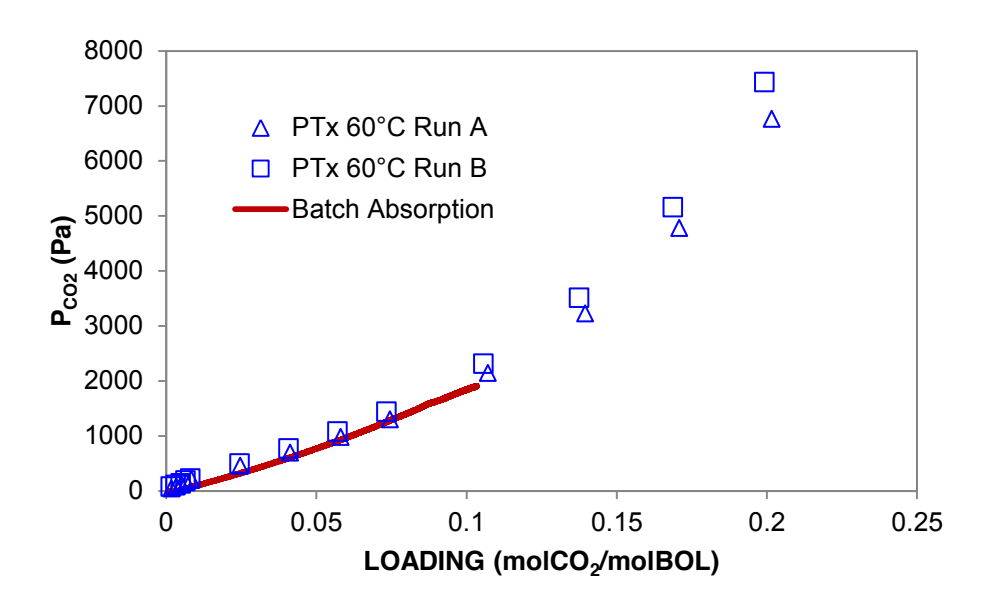


Figure 23. Measured VLE data of the bench cart (red line) for (3) plotted against VLE data measured from PTx measurements (both at 60 °C).

Establishment of equilibrium loading of (3) allowed for CO_2 uptake behavior of to be calculated from test conditions. Continuous flow testing of (3) was performed using the bench cart under a variety of conditions. Testing conditions included 15% and 10% CO_2 streams, 40 °C absorption, and varied LEAN solvent viscosities. Special attention was focused on the viscosity of the LEAN BOL, as this viscosity can be directly linked to the LEAN loading of the BOL, and thus the absorption capacity of the BOL. Viscosities were measured at 31.5 °C because the lines to the viscometer were

not insulated. Under initial testing conditions, (3) was able to capture over 90% CO_2 regardless of the LEAN BOL viscosity (Figure 24) and the CO_2 absorption rate was also independent of LEAN solvent viscosity (Figure 25).

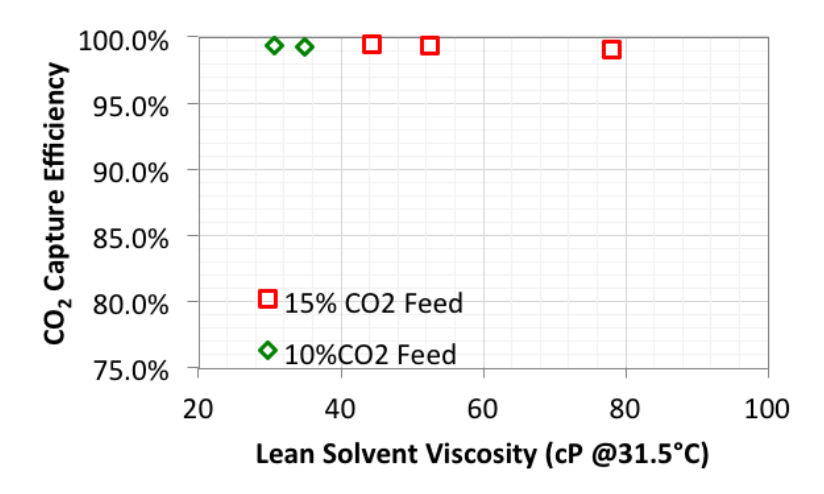


Figure 24. CO₂ capture efficiency of (3) as a function of LEAN solvent viscosity

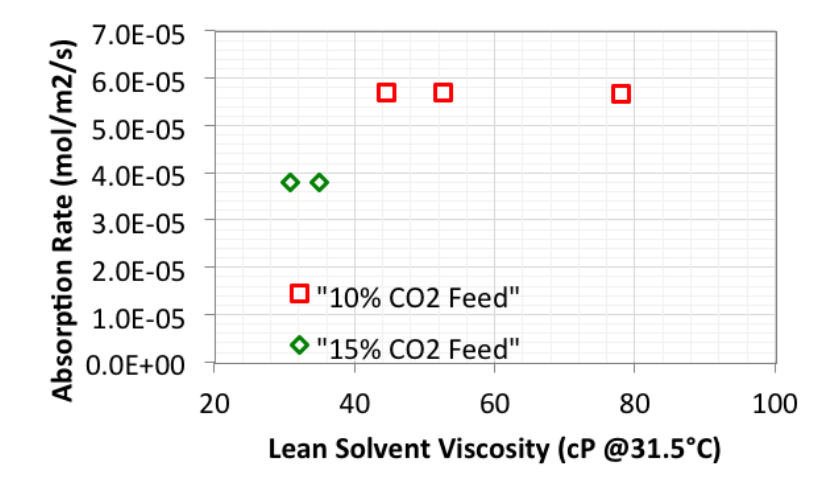


Figure 25. CO₂ Absorption rate by (3) as a function of LEAN solvent viscosity

After analyzing the data in Figures 1 and 2, the high capture rates were attributed to the residence time of the BOL inside the absorber column. Specifically, with the high surface area packing and viscous fluid, drainage was slow. This extended residence time allowed the BOL to achieve equilibrium loading of CO₂ rather than being kinetically limited. Initial attempts to slow down the absorption rate were unsuccessful, as the viscosity of the RICH solvent would continuously increase, effectively slowing down the drainage of the RICH-BOL out of the column and equilibrium-loading conditions were always reached. A continuous test under these conditions showed 48 hours of CO₂ capture of >98% was achieved in this configuration with no observed loss in activity or selectivity (Figure 26).

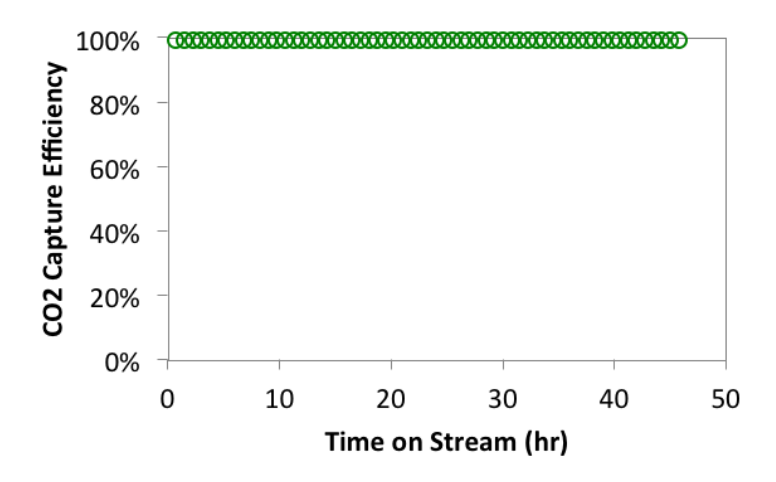


Figure 26. Continuous Bench-Scale Testing (3) on 15% CO₂ at 40 °C absorption

To avoid equilibrium loading conditions, the absorber column and stripper columns were reversed. In the original configuration, the absorber was twice the size of the stripper, as we had originally believed the CO₂ uptake would be slow and a larger column would be needed. By switching the columns, the residence time of the BOL in the absorber could be cut in half and potential kinetic loading could be observed.

Once the columns were swapped, the CO_2 absorption followed kinetic loading profiles. Here the viscometer was kept in its original location where it now was measuring the hot LEAN solvent coming out of the stripper (~75 °C). Testing conditions included varied L/G ratios, varied stripping gas flows and solvent circulation at two inlet concentrations of CO_2 (10 and 15%). All data are plotted in Figure 27 and tabulated in Table 12. Similarly to DBU-1-hexanol, (3) showed decreasing CO_2 capture with increases L/G (Figure 27). The thermal baseline testing was performed at four L/G ratios, with varied stripping gas flows and solvent circulation at two inlet concentrations of CO_2 (10 and 15%). T_{stripper} varied between 75-82 °C and N_2 strip was varied between 2 and 6 slm to keep the viscosity of the cold LEAN solvent to below 100 cP. For the 15% gas inlet concentration, (3) captures 90% CO_2 at an L/G slightly above 2 and for 10% inlet, 90 % capture is achieved at an L/G close to 3. There was no evidence of foaming or 'misting' of (3) during the testing, indicating superior performance for (3) than DBU-1-hexanol. Ultimately, the parametric studies confirm that (3) is capable of the required DOE target 90% capture at reasonable L/G's.

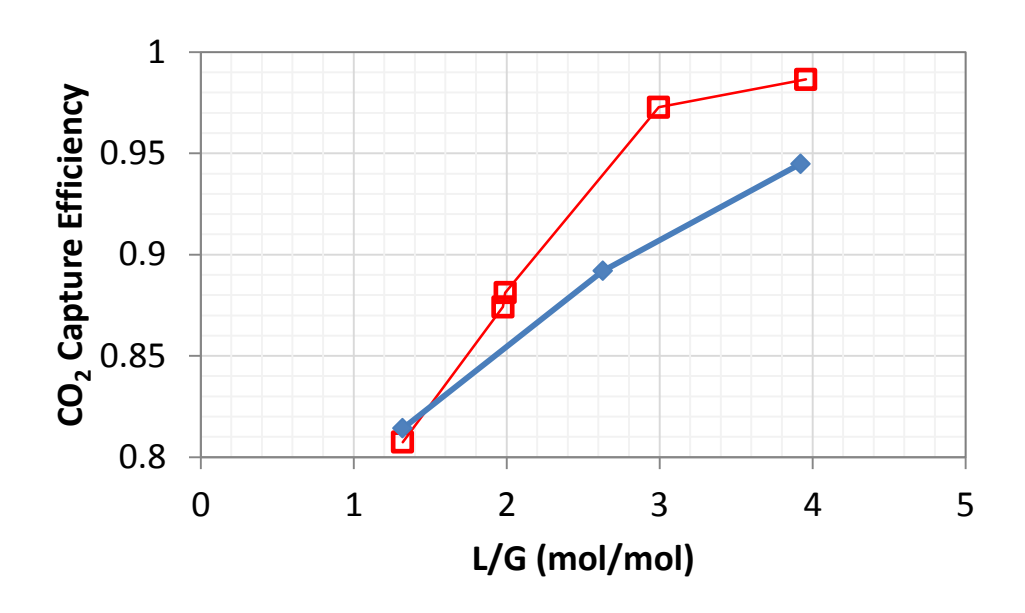


Figure 27. CO_2 capture efficiency plotted against L/G for (3) at two gas inlet concentrations [15% CO_2 (red) and 10% CO_2 (blue)]

.

Table 12. Bench scale data for thermal release of (3), no PSAR.

T _A	Ts	Q _{S,N2}	capture	N _{CO2,Abs}	L/G_abs			T_VISC
[°C]	[°C]	[slm21.1°C]		[mol/m2/s]	[mol/mol]	[cP]	[g/cc]	[°C]
37.3	77.9	2.074	0.0%	0.00E+00	2.01	25.23	0.897	32.5
36.3	81.5	3.059	99.4%	3.83E-05	3.95	34.89	0.928	31.1
36.4	80.9	5.654	99.4%	3.83E-05	3.94	30.72	0.923	31.0
36.5	80.5	3.561	99.5%	5.72E-05	3.95	52.54	0.939	31.4
38.0	75.1	2.244	99.1%	5.70E-05	3.95	77.96	0.953	32.6
36.4	80.8	3.459	99.5%	5.72E-05	3.94	44.31	0.938	31.2
43.2	75.4	5.063	98.6%	1.34E-04	3.96	8.30	1.094	73.6
44.4	76.4	5.061	97.3%	1.76E-04	2.99	10.38	1.058	73.5
46.0	75.3	5.061	83.7%	2.27E-04	1.99	17.66	0.928	72.2
45.1	75.9	7.060	87.4%	2.37E-04	1.98	12.24	0.917	72.7
49.3	76.8	6.065	80.7%	3.28E-04	1.32	17.67	0.878	72.0
45.2	76.1	6.070	94.5%	1.29E-04	3.92	17.31	0.902	67.9
46.6	74.8	6.066	81.4%	2.21E-04	1.32	21.73	0.911	66.5

Key: T_A = Absorber temp, T_S = Stripper temp, Q_S = stripper feed gas, η = % CO_2 captured, L/G = liquid/gas ratio, μ = viscosity, ρ = density, T_{Visc} = Temperature of viscosity measurement.

Continuous Bench-Scale Testing of (3) With Added PSAR Regeneration Cycle

The PSAR hardware (coalescing tank, static mixer and circulation pump) was next added to the system to enable antisolvent additions. 5L of decane antisolvent was added to the system. Decane was chosen for the testing rather than hexadecane for two reasons; prevention of gelling, and the lower T_{miscibility} with the BOL (as the cart could only heat the stripper to ~100 °C). In all PSAR testing, the decane circulation loop was set to one molar equivalent (80 cc/min. PSAR testing was run under similar testing conditions as the thermal case albeit with the decane circulation. During PSAR testing, the viscometer was placed in line to measure the RICH solvent coming out of the absorber column (~ 40 °C). PSAR was tested at three L/G ratios, varied stripping gas flows and solvent circulation at two inlet concentrations of CO₂ (10 and 15%). T_{stripper} was 75 °C and N₂ strip was varied between 4.5 and 6 slm to keep the viscosity of the cold LEAN solvent to at or below 25 cP. All experiments are run for one-hour steady state with no observed foaming or biphasic behavior in the absorber. The PSAR data are plotted in Figure 29 and tabulated in . PSAR regeneration of (3) showed decreasing CO₂ capture with increases L/G as seen in the thermal regeneration. For the 15% gas inlet concentration, (3) captures 90% CO₂ at an L/G of 4 and for 10% inlet, 95 % capture is achieved at an L/G close to 4.8. Here it is seen that PSAR addition still allows for 90 % capture at reasonable L/G's, albeit higher than the thermal regeneration case. It should be noted that a precise measured delivery rate of (3) to the absorber could not be measured, and was thus estimated based on mass balance data.

Parametric runs of PSAR were kept at steady state for no more than one hour due safety concerns due to high evaporative losses of decane antisolvent out of the absorber and stripper columns. The liquid condensers needed routine draining and recharging of decane in the coalescing tank to keep the liquid levels high enough for circulation through the decane dip-tube. A less-volatile antisolvent would prevent this limitation. The conditions of CO₂ the PSAR runs are plotted in Table 14.

Continuous Bench-Scale Testing of (3) With PSAR Regeneration Cycle With 5 wt% Water Loading

The final bench scale testing was performed with the previously described PSAR hardware with the addition of gas humidifiers for both the stripper and absorber sides of the cart, in addition to gravimetric loading of 5 wt% of water loading to (3). The humidifiers were filled with deionized water and connected upstream of the cart columns to humidify the gas streams at the respective temperatures of absorption (40 °C) and stripping (75 °C). Deionized water was also gravimetrically added to (3) in the cart. As with prior PSAR testing, the decane circulation loop was set to 1 molar equivalent (80 cc/min). PSAR/water testing was run using similar conditions as the PSAR case with the exception of the gas delivery to the absorber and stripper columns being saturated with water.

PSAR with water was tested at two L/G ratios (3 &4), at 6 slm of stripping gas flow at an inlet concentrations of CO_2 of 15%. In all tests, the viscosity of the cold LEAN solvent was kept at or below 25 cP, and each data point corresponds to a one-hour steady state. Figure 28 shows the PSAR/water data, which is also tabulated in Table 13. The PSAR was found to work in the presence of water, with no observable foaming or biphasic behavior in the absorber. Here, the data showed enhanced CO_2 capture, which is attributed to water making (3) a better solvent due to bicarbonate formation or hydration of the CO_2 -RICH species. Here 90% capture is achieved at an L/G of 3, instead of an L/G of 4 in the absence of water. Again, parametric runs were kept at steady state no longer than one hour to keep evaporative losses of decane to an appreciable level.

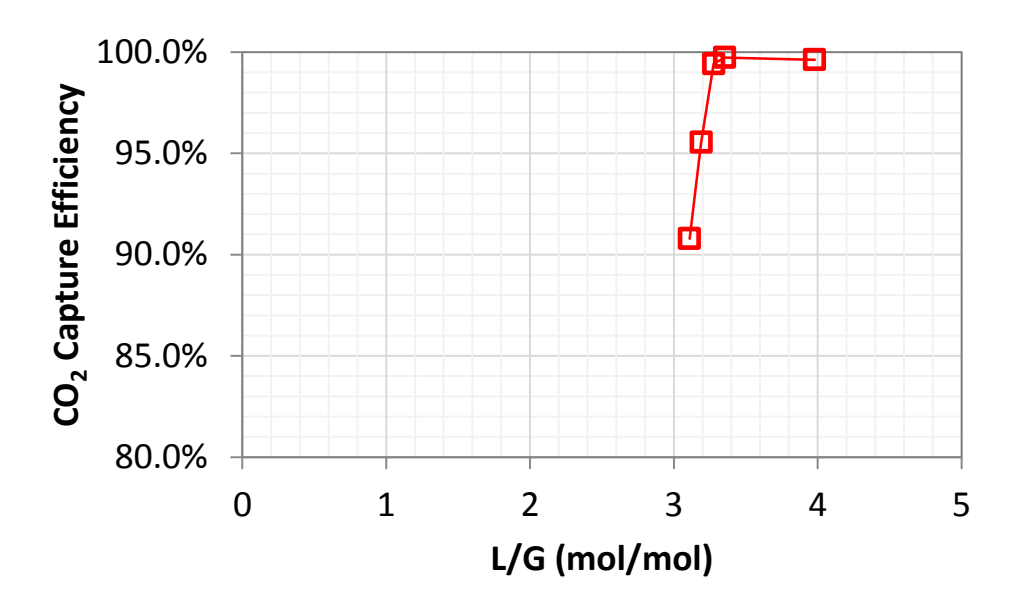


Figure 28. CO₂ capture efficiency with PSAR, plotted against L/G for (3) at 15% CO₂

Table 13. Bench scale data for *PSAR* release of (3) in the presence of 5 wt% water.

T _A	Ts	Q _{S,N2}	capture	N _{CO2,Abs}	L/G_abs			T_VISC
[°C]	[°C]	[slm21.1°C]	[3:3]	[mol/m2/s]	[mol/mol]	[cP]	[g/cc]	[°C]
40.2	76.1	6.062	99.6%	4.61E-05	3.98	24.89	0.909	43.0
40.5	76.0	6.062	99.7%	6.84E-05	3.35	24.10	0.912	42.3
40.9	75.5	6.057	99.4%	9.07E-05	3.28	25.47	0.912	41.9
41.8	75.0	6.055	95.5%	1.09E-04	3.19	26.27	0.912	41.9
42.8	74.5	6.056	90.8%	1.24E-04	3.11	26.26	0.911	43.3

Key: T_A = Absorber temp, T_S = Stripper temp, Q_S = stripper feed gas, η = % CO_2 captured, L/G = liquid/gas ratio, μ = viscosity, ρ = density, T_{Visc} = Temperature of viscosity measurement.

PSAR'S IMPACTS ON CO₂BOL ABSORPTION/REGENERATION BASED ON BENCH SCALE DATA

An additional, more detailed analysis of the bench data for the thermal and PSAR cases was performed to determine the PSAR impacts on absorber performance. Absorber performance was estimated by plotting the CO_2 capture against the L/G for both cases. The data are plotted in Figure 29 and tabulated in Table 14. As indicated in the plot, the PSAR shows minimal impact at L/G's at 2.7 and 3.8, but has a small dip in capture efficiency at an L/G of 1.8 which may be due to experimental error or incorrect assumptions of antisolvent carryover into the absorber which would impact the BOL delivery to the absorber. That being said, a reasonable projection of comparable absorber performance with and without PSAR can be made.

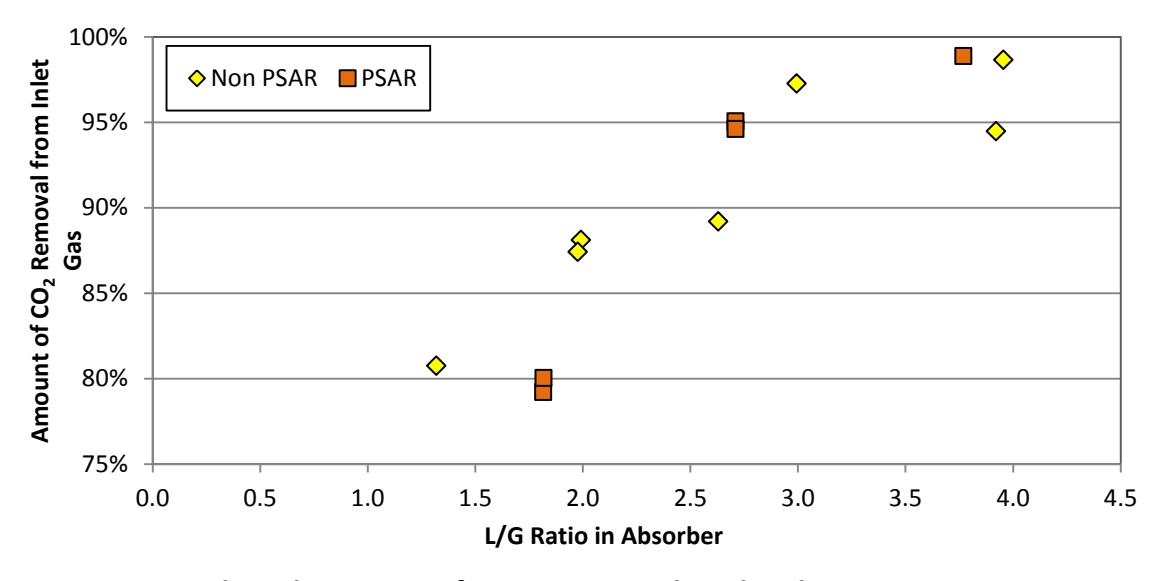


Figure 29. Bench-Scale Run Data for CO₂BOLs, with and without PSAR

Table 14. Summary of Bench-Scale Run Data for CO₂BOLs, with and without PSAR

		Total 3Gas 2	Molar2	Molar2	Average 2			Rich2	Lean S olvent2	Solvent2	Nitrogen	Molar2	Average ?
Condition	Run∄D	Flowanto⊡	Fraction 3 of 2	Fraction3of2	Absorber	L/G∄n2	Capture 2	Solvent2	Loading,ano?	Viscosity 2	Flowinto	Fraction 2	Stripper2
Condition	Kullad	Absorber ²	CO2iiniGasi	CO2iniGasi	Temp2	Absorber	Efficiency	Loading 2	antisolvent 2	(cP) 	Stripper2	of CO2 In 2	Temp2
		(mol/s)	Entering?	Exiting?	(°C)			(molacO2/a	(mol3CO2/2	[Temp(°C)]	(mol/s)	Stripper2	(°C)
No⊡PSAR	20140304A	0.00140	0.1491	0.0024	43.2	3.96	98.6%	0.11	0.07	8.3474]	0.00349	0.055	75.4
No⊡PSAR	20140304A	0.00185	0.1502	0.0048	44.4	2.99	97.3%	0.13	0.09	10.4474]	0.00349	0.093	76.4
No ® PSAR	20140305A	0.00278	0.1495	0.0205	46.0	1.99	88.1%	0.15	0.08	12.3473]	0.00349	0.108	75.9
No⊡PSAR	20140310A	0.00278	0.1495	0.0216	45.1	1.98	87.4%	0.15	0.08	12.2473]	0.00487	0.073	75.9
No⊡PSAR	20140311A	0.00416	0.1496	0.0328	49.3	1.32	80.7%	0.18	0.09	17.7月72]	0.00419	0.109	76.8
No⊡PSAR	20140314A	0.00140	0.1490	0.0096	45.2	3.92	94.5%	0.16	0.13	17.3468]	0.00419	0.050	76.1
No⊡PSAR	20140314A	0.00209	0.1494	0.0186	46.7	2.63	89.2%	0.19	0.14	23.8467]	0.00419	0.060	76.0
PSAR	20140507A	0.00101	0.0769	0.0009	40.4	3.77	98.9%	0.10	0.08	16.745]	0.00322	0.025	74.1
PSAR	20140509A	0.00209	0.1493	0.0352	42.6	1.82	79.1%	0.16	0.11	23.843]	0.00418	0.059	72.5
PSAR	20140510A	0.00209	0.1493	0.0338	42.8	1.82	80.0%	0.16	0.11	23.844]	0.00349	0.067	74.0
PSAR	20140512A	0.00140	0.1489	0.0086	40.1	2.71	95.1%	0.14	0.10	22.841]	0.00419	0.049	74.4
PSAR	20140512A	0.00140	0.1490	0.0094	40.1	2.71	94.6%	0.14	0.10	23.841]	0.00349	0.059	74.2

The gas measurements in **Table 14** were used to confirm whether a reasonable mass balance was realized between CO_2 absorbed and CO_2 stripped. In each case the CO_2 balance was within 16%, except for 20140304A, which had a 33% difference between outlet and inlet CO_2 mass.

5. MODELING

Thermodynamic model

A thermodynamic model was developed based upon consideration of the solution chemistry and used four types of PTx data:

- 1. Absorption of CO₂ on the neat BOL.
- 2. Effect of water on the absorption of CO₂ on BOL.
- 3. Effect of the anti-solvent on the absorption of CO₂ on BOL. It should be noted that the BOLS-anti-solvent system has a region of liquid-liquid immiscibility that is affected by the addition of CO₂.
- 4. Quaternary data with all four principal components (BOL, CO₂, water and anti-solvent) present.

Special attention was devoted to ensuring that the thermodynamic model captured the key effects of the solvent system (BOL, water and antisolvent; the antisolvent here is hexadecane, C_{16}). The first effect is the complexation of CO_2 and BOL, which is enhanced by the addition of water and diminished when the anti-solvent is added. Due to the thermodynamic non-ideality of the system, the ElecNRTL-RK model in Aspen Plus was chosen, together with the chemistry capability. The chemistry capability enables the effect of chemical reactions (chemical complexation) to be captured in the thermodynamic model.

The chemistry model for the CO₂BOL-PSAR system is based upon the understanding of the fundamental chemistry, as well as practical experience with electrolyte process simulation. Two complexes are postulated, which results in the following two chemical-equilibrium equations:

$$2 CO_2 + 2 BOL \leftrightarrow BOLCO_2^+ + BOLCO_2^-$$
 (1)

$$H_2O + BOL + CO_2 \leftrightarrow BOLH^+ + HCO_3^-$$
 (2)

Breaking out separate charges for the CO₂BOL-CO₂ ionic species (BOLCO₂, BOLCO₂, and BOLH) allowed for Aspen Plus to enable the Born term, which accounts for the effect of the ionic strength and the solvent dielectric constant. This term is vital in predicting the effect of the low-dielectric-constant anti-solvent to reduce the tendency of the mixed solvent to complex CO₂.

The resulting model quantitatively describes the data, and captures the relative solubility of CO_2 in the system as the composition of the BOL- H_2O - C_{16} solvent changes. Figure 30 presents the CO_2 partial pressure at 100 °C for four representative solvent compositions. The composition on the x-axis is the CO_2 loading with respect to BOL. Figure 30 shows that adding 1 mole of H_2O to 1 mole of BOL significantly reduces the CO_2 partial pressure, while adding 1 mole of C_{16} to 1 mole of BOL

sharply increases the CO_2 partial pressure. The 1:1:1 BOL- H_2O - C_{16} solvent has an absorption strength between neat BOL and 1:1 H_2O :BOL. Figure 31, which presents the fraction of CO_2 that is complexed, provides an explanation of the results in Figure 30. The lowering of the CO_2 partial pressure is caused by increased complexation of the CO_2 .

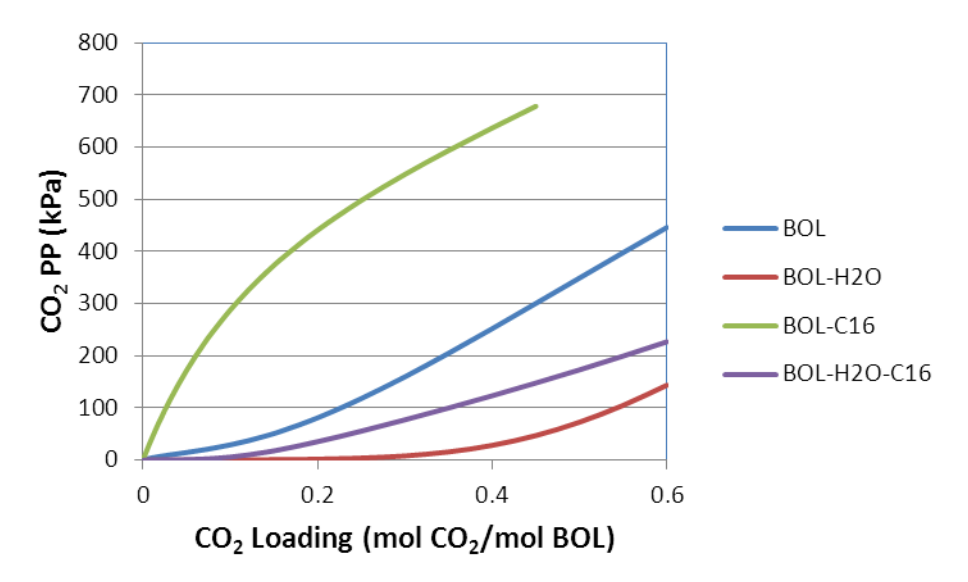


Figure 30 Estimated CO₂ partial pressures in BOL-H₂O-C₁₆ at 100°C. The relative solvent concentrations are equimolar.

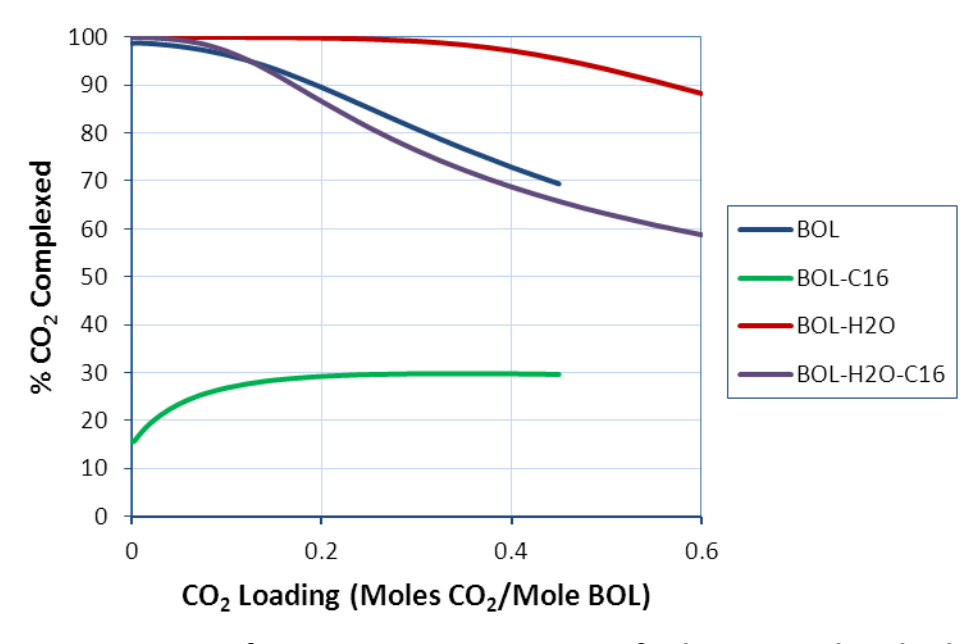


Figure 31 Fraction of CO_2 in in BOL- H_2O - C_{16} at 100°C that is complexed. The relative solvent concentrations are equimolar.

The enthalpy of solution of CO₂ in the solvent is extremely important because the paramount goal of CO₂ capture processes is to reduce the energy cost of CO₂ capture and this energy cost is

directly related to the enthalpy of solution. The enthalpy of solution of most interest is that with BOL- H_2O mixtures as the solvent and this is because the solvent used for absorption has low concentrations of C_{16} , and these are presented next. Figure 32 shows the enthalpy of solution of CO_2 in BOL as a function of temperature and CO_2 loading. At a temperature of $40^{\circ}C$ (typical absorber temperature), the enthalpy of solution is about -82 kJ/mol at low CO_2 loadings and then decreases in magnitude with CO_2 loading. As the temperature increases, the magnitude of the enthalpy of solution decreases, and also the CO_2 loading at which the value drops decreases. This is expected behavior.

Figure 33 presents the calculated CO_2 enthalpy of solution in the 1:1 H_2O :BOL solvent. The difference here is that the enthalpy of solution first increases with CO_2 loading, and may decrease in magnitude if the temperature is sufficiently high (say, $\geq 80^{\circ}C$).

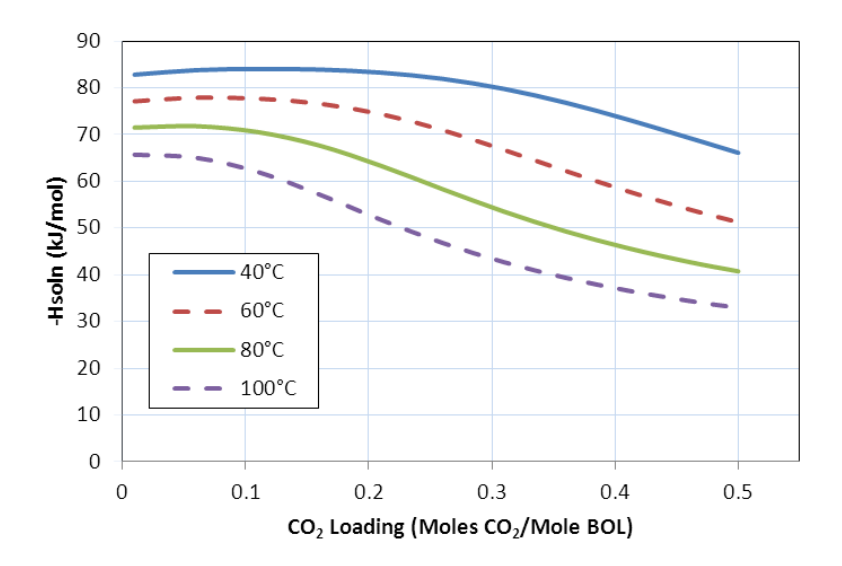


Figure 32 Enthalpy of solution of CO₂ in BOL.

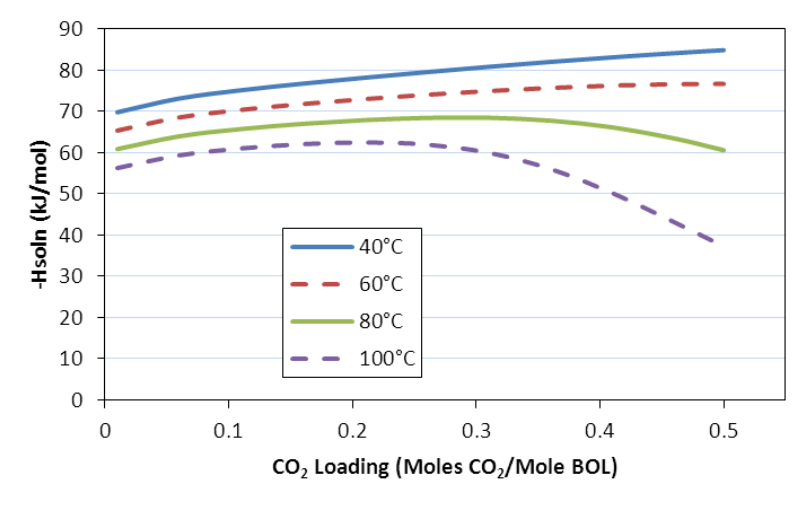


Figure 33 Enthalpy of solution of CO₂ in 1:1 H₂O:BOL.

Transport Properties Model

The only special model developed for transport properties is for viscosity, and here a user model was implemented in Aspen Plus. Figure 34 compares model calculations and data for the dry CO₂-BOLs system, and indicates that the model provides a quantitative description of the data. Figure 35 shows the effect of water on the mixture viscosity at a representative temperature of 50°C. The addition of water causes an increase in viscosity. The model is based upon severely limited data, but is expected to provide a semi-quantitative estimation of the effect of water on the mixture viscosity. Review of Figure 34 and Figure 35 clearly indicates that the viscosity of the RICH solvent can be quite high. The viscosity model together with the kinetic model discussed next has been used to identify optimum conditions for the CO₂ capture process.

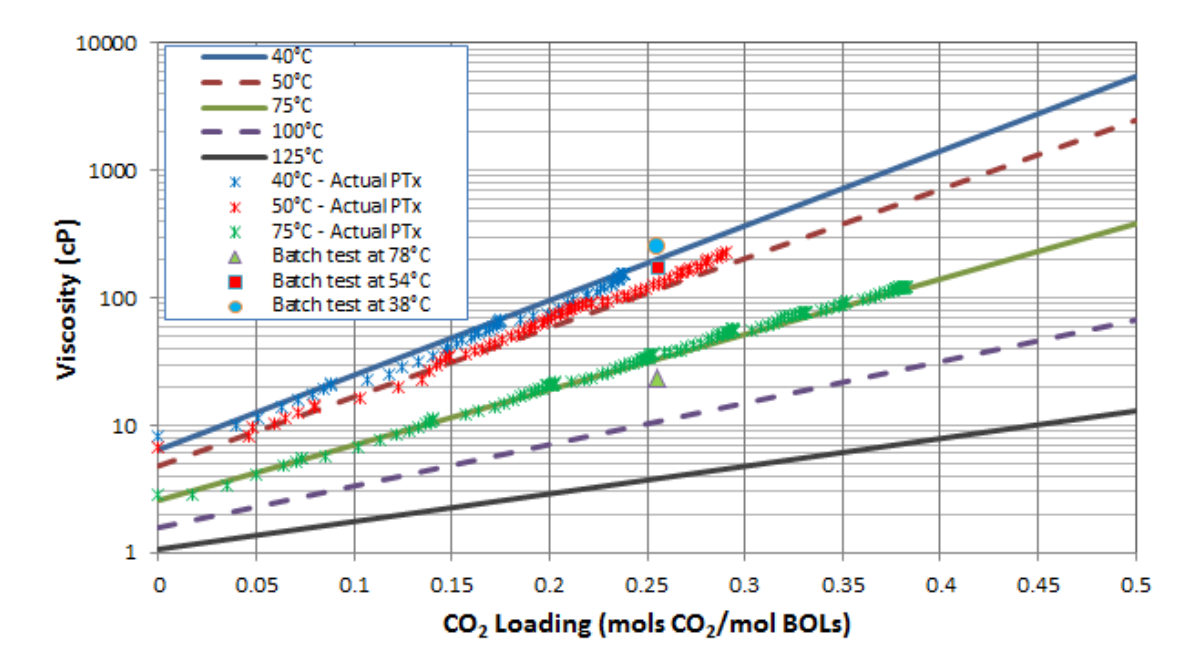


Figure 34 Comparison of empirical correlation developed for the CO₂-BOLs system with experimental data.

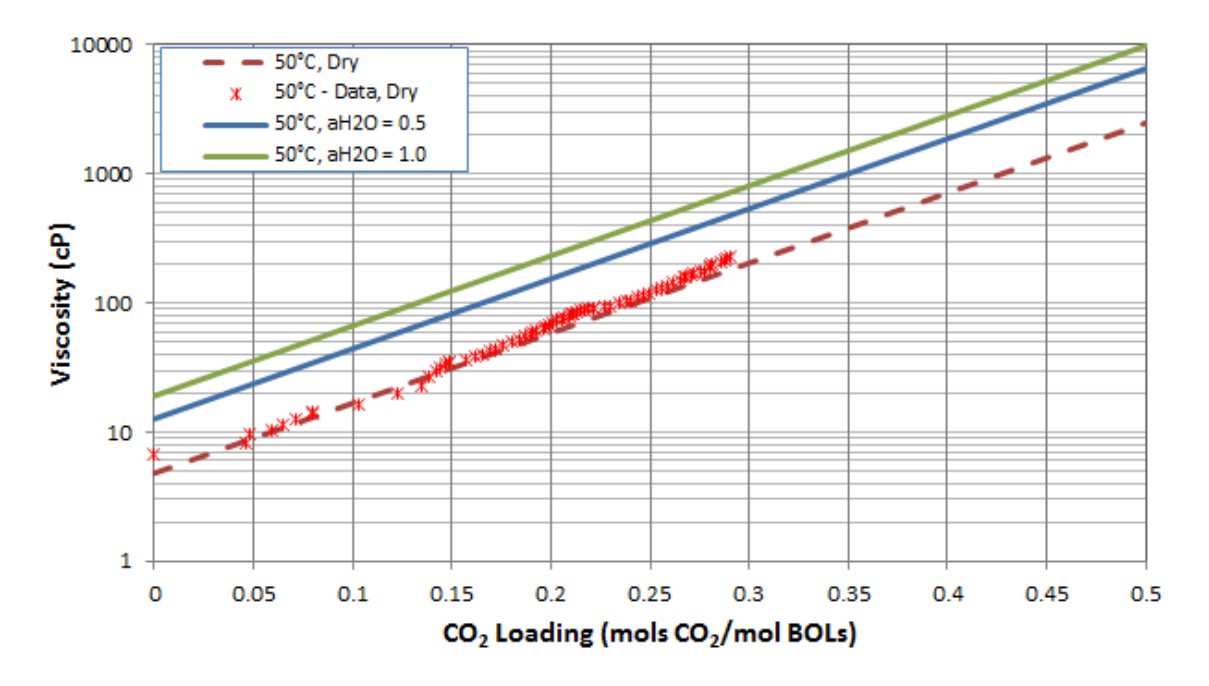


Figure 35 Estimated effect of water loading on the mixture viscosity at 50°C. The model results and data for the dry system are the same as in Figure 34, and the model results for water loadings of 0.5 and 1.0 are estimated based upon limited data.

Chemical Kinetic Model

The kinetic model used here is based upon power-law kinetics for the forward reaction, and with the kinetics for the reverse reaction devised such that the chemical equilibrium limit is obeyed.

$$R_1 = k_1 C_{Tot}^2 a_{CO2} a_{BOL} \left(1 - \frac{a_{BOLCO2} + a_{BOLCO2} -}{a_{CO2} a_{BOL} K_1} \right)$$
 (3)

$$R_2 = k_2 C_{Tot}^2 a_{CO2} a_{BOL} a_{H2O} \left(1 - \frac{a_{BOLH} + a_{HCO3} -}{K_2} \right)$$
 (4)

In equations 3 and 4, R_1 and R_2 are the reaction rates in kmol/m³.s, k_1 and k_2 are the temperature-dependent rate constants, C_{Tot} is the solution molarity in kmol/m³, K_1 and K_2 are the chemical-equilibrium constants, and α is the component activity defined as the product of the mole fraction and the activity coefficient. k_1 and k_2 are defined by the usual Arrhenius equation.

$$k_1 = k_{10} exp \left\{ -\frac{E_1}{R} \left(\frac{1}{T} - \frac{1}{313.15} \right) \right\}$$
 (5)

$$k_2 = k_{20} exp\left\{-\frac{E_2}{R}\left(\frac{1}{T} - \frac{1}{313.15}\right)\right\}$$
 (6)

The parameters in equations 5 and 6 have been adjusted to provide a best representation of the wetted-wall and cart data. The comparisons with the data are presented later.

$$k_{10} = 1,500 \frac{m^3}{kmol.s}$$

$$k_{20} = 1,500 \frac{m^3}{kmol.s}$$

$$E_1 = 25 \frac{kJ}{mol}$$

$$E_2 = 25 \frac{kJ}{mol}$$

As can be seen, only rough values of the kinetic parameters have been chosen at the present time. The kinetic model developed here has been compared to the data reported by Versteeg et al.⁹ in Figure 36. At a representative temperature of 60°C, CO₂BOLs kinetics is slower than that of MEA by close to an order of magnitude. k_{10} and E_1 are based upon experimental data, while k_{20} and E_2 have been estimated.

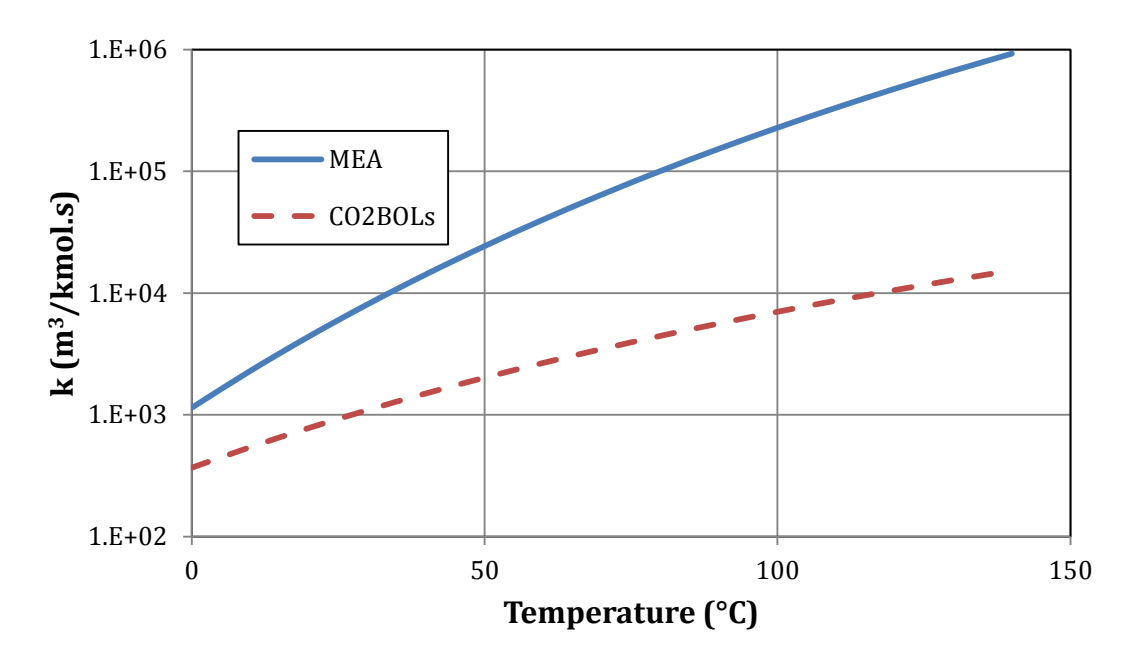


Figure 36 Comparison of CO₂-BOLs kinetics with that of MEA. For CO₂-BOLs, the value is taken from Eq. 5, while the MEA value has been reported by Versteeg et al. (1996).

Mass Transfer Correlation

The mass-transfer model is based upon the work of Onda-1968.¹⁰ The Onda correlation was developed using data at relatively low viscosities (generally around 1 cP), and it was found that the decrease in the mass-transfer coefficient with rising viscosity was too strong in comparison with the wetted-wall and cart data. Hence the Onda-1968 correlation has been empirically modified for high-viscosity systems. The nomenclature used here is the same as in Onda's paper.

$$\kappa_{i,k,j}^{L} = 0.0051(Re_{Lj}^{\prime})^{0.667}(Sc_{Li,k,j})^{-0.5}(a_{pj}d_{pj})^{0.4}(\mu_{j}^{L}g/\rho_{tj}^{L})^{0.333}$$
(7)

$$Re'_{Lj} = \frac{\rho_{tj}^L u_{sj}^L}{\mu_j^L a_{wj}} \tag{8}$$

$$Sc_{Li,k,j} = \frac{\mu_j^{L'}}{\rho_{i_j}^L D_{i,k,j}^L}$$
 (9)

$$u_{sj}^L = L_j / c_{tj}^L A_{tj}$$

$$\tag{10}$$

In the Schmidt number definition (Eq. 9) $\mu_j^{L'}$ is an "effective" viscosity, which is modified for viscosities greater than 10 cP as shown below.

If
$$\left[\mu_{i}^{L} \le 10 \ cP\right], \ \mu_{i}^{L'} = \mu_{i}^{L}$$
 (11)

If
$$\left[\mu_j^L > 10 \ cP\right]$$
, $\mu_j^{L'} = 10 \left(\frac{\mu_j^L}{10}\right)^{0.5}$ (12)

In effect, the exponent on the Schmidt number is 0.25 rather than 0.5 when the mixture viscosity exceeds 10 cP. Figure 37 provides a graphical depiction of the "effective viscosity" used for the Schmidt number in the Onda correlation.

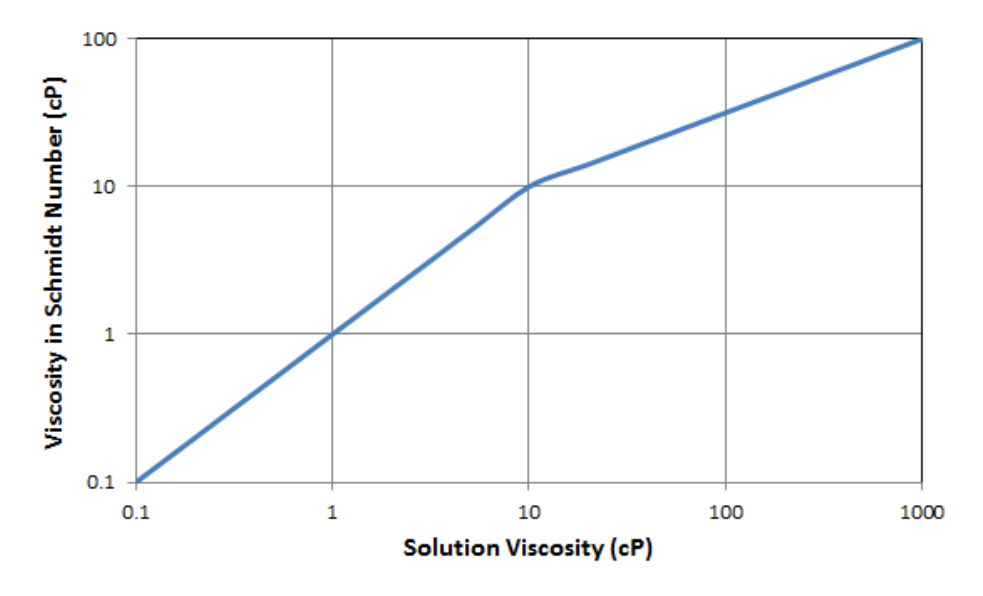


Figure 37 "Effective viscosity" used for Schmidt number in Onda correlation.

Wetted Area

Packing models usually include a correlation that relates the wetted area to the dry area. In the present case, due to limited data available, the two values are assumed to be the same.

$$\frac{a_e}{a_p} \equiv 1 \tag{13}$$

Modeling of Wetted-Wall Data

The correlations described above have been used to model the wetted wall data. The model specifications are as follows:

- The Aspen Plus RateSep model has been used such that the column, which is 1.26 cm in diameter and 9 cm high, has been modeled as a packed column with total area of 0.003562 m³, which is equal to the surface area of the wetted-wall column.
 - The column pressure is fixed at 1 atm.
 - Gas and liquid flow rates are fixed at 3.3 l/min and 1.5 l/min, respectively.
- CO₂ composition in the gas phase is varied starting at a mole fraction of 0.15 and then reduced until the driving force for absorption is small.
- K_G is calculated as the flux calculated by RateSep divided by the pressure driving force $(P_{CO2}^{Vapor} P_{CO2}^*)$.

Figure 38 compares K_G values calculated by the model to the experimental data measured by the wetted-wall column. The model captures both the values and the trends of the data. The wetted-wall data did not study CO_2 loadings above 0.2 and also limited the data to dry systems. Figure 39 provides model extrapolations into compositions not covered by data. While the model extrapolations in Figure 39 are reasonable, it should be noted that they are uncertain due to lack of supporting experimental data.

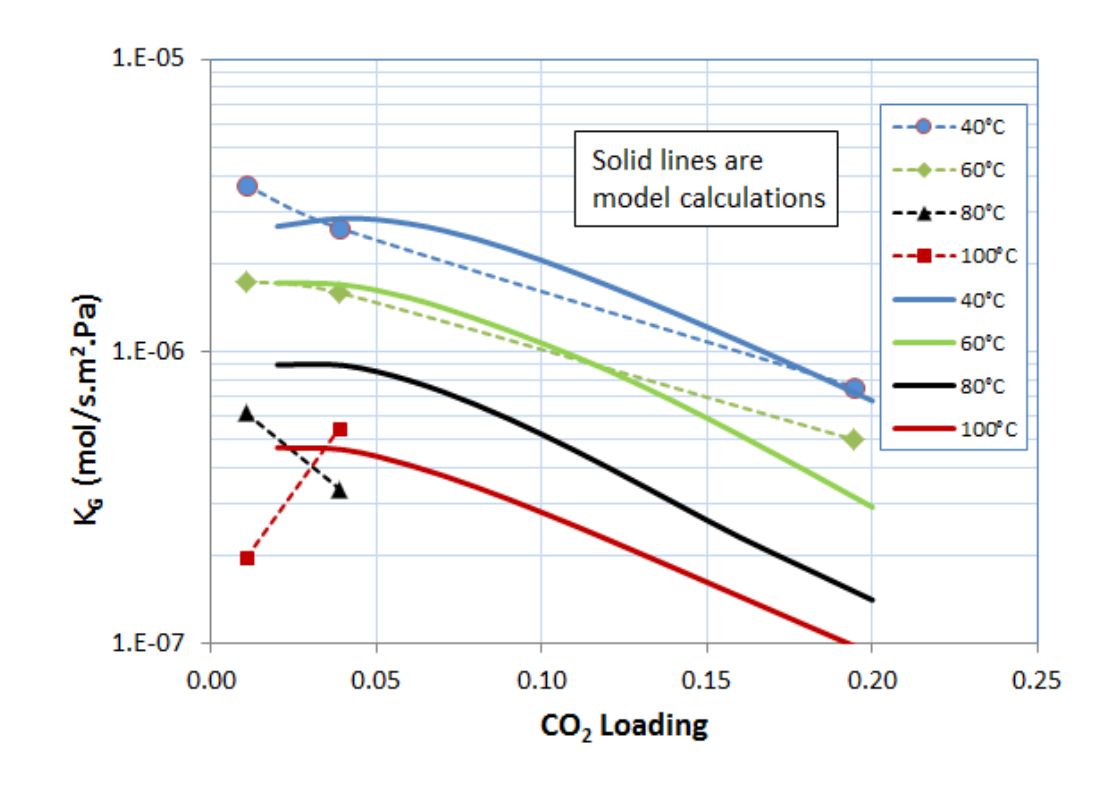


Figure 38 Comparison of K_{G} calculated by RateSep model to experimental data measured by wetted-wall column.

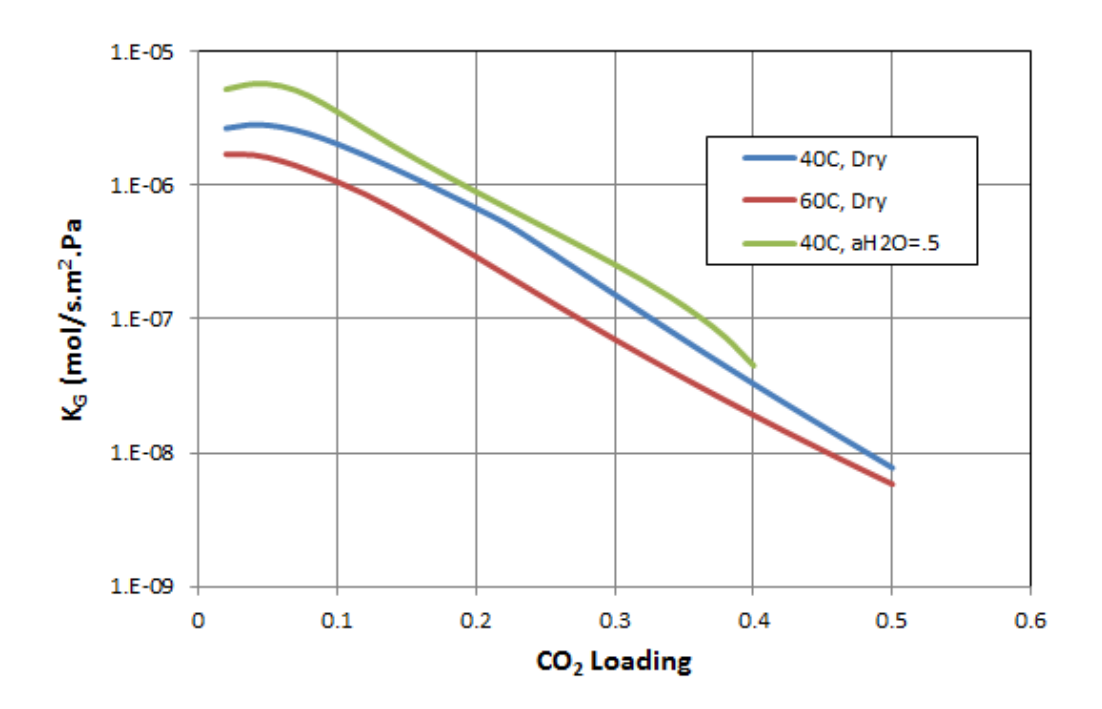


Figure 39 Extrapolation of K_G calculations by RateSep to higher CO₂ loadings and the presence of water.

Modeling of Cart Data

The RateSep model in Aspen Plus has been applied to modeling of the cart data. The focus has been on the absorption data, which has been modeled as follows:

- The absorber dimensions are D = 0.072 m and H = 0.316 m.
- The interfacial area of the packing has been specified as 12.336 cm²/cm³.
- The thermodynamic model, and kinetic and transport-property correlations are the same as used for the wetted-wall modeling.
- In addition, the calculated interfacial area has been adjusted by changing the Interfacial Area Factor (IAF) in Aspen Plus.
 - The gas and liquid flow rates for each point are as measured in the experiment.

Figure 40 compares CO_2 recoveries calculated by the model to the experimental values measured in the cart. In the case of the data without antisolvent (denoted as "NO AS"), the model calculations with IAF = 1 indicate higher recoveries than the measurements, while setting IAF = 0.61 provides an adequate average description of the data. In the case of cart runs with antisolvent (denoted as "AS"), the value of IAF that best fits the data is slightly lower, i.e., IAF = 0.51. In conclusion, an IAF value between 0.5 and 0.6 is expected to provide a good description of absorption columns.

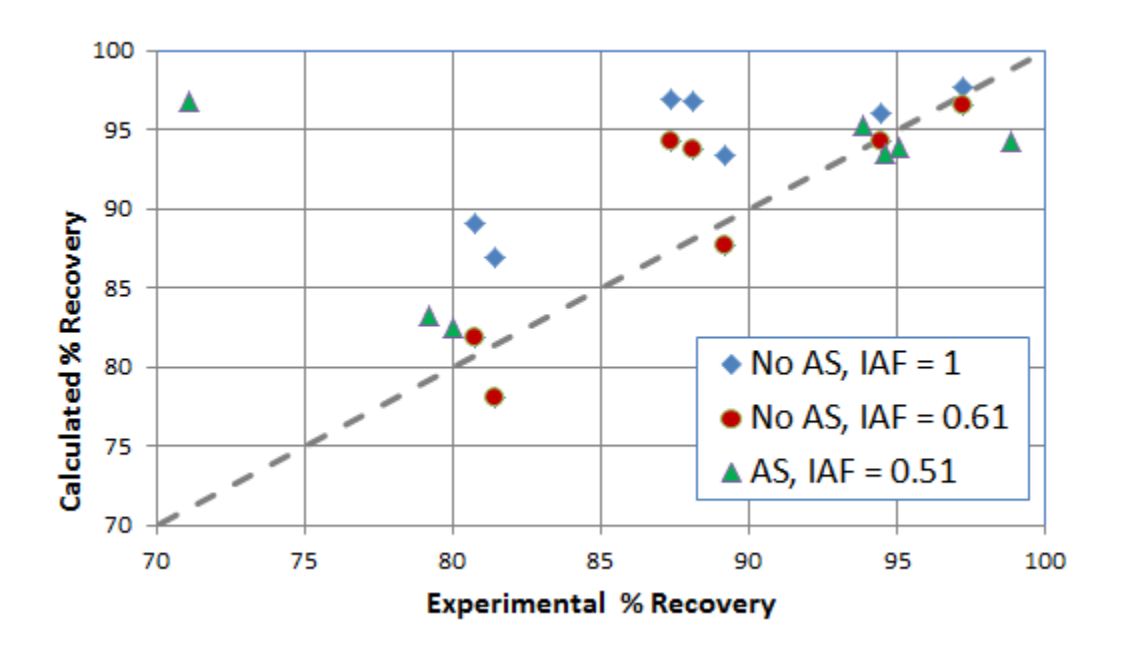


Figure 40 Parity plot relating the CO₂ recoveries calculated by the model to the experimental measurements in the bench-scale system. (AS = Antisolvent; IAF = Internal Area Factor, or the effective fraction of absorber packing area)

6. TECHNO-ECONOMIC ANALYSIS

Overview

The benchmark for comparison of the CO₂BOLs technology is Case 10 of National Energy Technology Laboratory's (NETL) Cost and Performance Baseline for Fossil Energy Plants, Volume 1: Bituminous Coal and Natural Gas to Electricity (NETL Report No. DOE/NETL-2007/1281, August 2007). The report was updated to Revision 2 in November of 2010: DOE/NETL-2010/1397.¹¹ In both revisions of the document, Case 10 represents a Subcritical Pulverized Coal (PC) power plant with carbon capture (CC). Case 9 represents the same power plant with no carbon capture, but scaled to the same net electric power output (550 MWe).

The techno-economic analysis described herein is for the candidate CO_2BOL (3) using the unique polarity-swing assisted regeneration cycle described in the previous sections. In this case, the CO_2BOL process is operated in a system similar to the MEA-based Case 10 system, albeit with an antisolvent (hexadecane assumed) injected to the RICH CO_2BOL solvent prior to stripping, followed by separation of the antisolvent from the LEAN- CO_2BOL prior to absorption. This process infrastructure for a commercial-scale version of the $CO_2BOL/PSAR$ process is largely available, including the absorber, stripper, cross exchanger, and coalescing unit. Thus in this analysis, the $CO_2BOL/PSAR$ system was directly compared to the NETL Case 10 baseline.

The initial feasibility study for CO₂BOLs/PSAR (2012) was based on the assumption that a version of CO₂BOLs solvent could be developed with a maximum loaded viscosity of 20 cP, and for this hypothetical case near-equilibrium performance was assumed. This viscosity limit was based

on industrial heuristics of maximum viscosities that would enable the use of conventional pumps and absorber and stripper columns. Subsequent wetted-wall and bench-scale testing during Phase 2 of the project showed that the CO₂BOLs/PSAR system could viably operate at viscosities greater than 20 cP, with operations as high as 500 cP, but with known impacts on scaled-up equipment sizing and associated high capital costs. Nevertheless, the higher viscosity ranges were used in the current TEA to represent the current state of the solvent development, understanding the future reductions in loaded CO₂BOLs solvent viscosities could enable system cost and performance more in line with the earlier projections. A more detailed discussion on viscosity reduction strategies is provided in Section 7.

Simulations were performed using Aspen Plus. The simulations were used to project the sizing of process equipment and energy needs (such as, but not limited to, pumping costs, refrigeration requirements, reboiler duty). Sub models for the CO2BOLs/PSAR specific properties were developed and used to support the larger simulation. These include thermodynamic transport, and kinetic models.

There were few notable differences in the sizing of equipment for the 356 cP CO_2BOL case compared to the recreated Case 10 baseline, specifically the absorber, which Aspen Plus had sized to maintain a reasonable 2-2.5 psi pressure drop with a viscous solvent. The absorber for CO_2BOL 356 cP case was sized at 60' in diameter and 177.5' tall, while the stripper was 47.5' in diameter and 143.5' tall compared to the NETL Case 10 absorber at 44' in diameter and 171 ' tall, and stripper at 23' diameter and 107' tall. No formal sizing was made for the other cases at this time, as the 20 cP target is merely a projection of potential performance and the 578 cP is too costly for commercialization. The formal cost breakdown of the larger equipment are reflected in Table 17.

General Process Description

The CO₂BOLs/PSAR system was designed to recover 90% of the CO₂ contained in the flue gas coming from the 550 MWe subcritical pulverized coal power plant. The product CO₂ is delivered to the plant battery limits at 2,215 psia. Due to the large CO₂ capture capacity required, the carbon-capture system was designed with a two-train configuration (2 x 50% units). The flue gas feed to the system was split evenly and directed towards two identical parallel trains. The following sections provide descriptions of the major components of the CO₂BOLs/PSAR process, written for Train 1. The descriptions for analogous equipment and units of Train 2 are identical.

The following sections describe the primary components of the carbon capture system that were modeled. Referenced equipment numbers correspond to the process flow diagram in **Figure 41**, Figure 42, and Figure 43.

With respect to pumping for the entire process flow diagrams, good design practice necessitates that pump discharge pressures are sufficiently high to provide enough static head and frictional pressure drop with additional allowances for control devices necessary to operate the process and it is believed that the design provided here meets those objectives. However, it is observed that the pumping power for the 356 cp viscosity CO₂BOL case is more than 3 times the pumping power for the NETL Case 10 reference case and the hypothetical 20 cp CO₂BOL case. To speculate whether this pumping power could be reduced, the Aspen Plus process simulation was used with specified (0.73) pump efficiency, specified column heights and an assumed 1 bar control

valve allowance to examine the potential to reduce the pumping power. The analysis also made a configurational change where the RICH pump and decanter antisolvent were supplied to the pump suction of a stripper feed pump that delivered the mixture to the stripper. This analysis indicated potential for 6 MW of pumping power reduction with this change, though the formal costing analysis is based on the initial pumping power.

Flue Gas Conditioning

The flue gas feed to the carbon capture system comes from the Flue Gas Desulfurization unit (FGD) in the power plant where the majority of the sulfur contained in the flue gas has been removed. The flue gas stream is first routed to the 3-Stage Direct Contact Cooler (DCC) (C-101). The 3-Stage DCC is comprised of three separate packed sections. There are two sections for cooling the flue gas and one section for trim sulfur dioxide (SO_2) removal. The first cooling section removes water from the flue gas using the normal supply of cooling water. The second cooling section, or the trim cooling section, further removes water from the flue gas using chilled water. The main objective of the second cooling section is to maintain an optimum level of water in the SO_2 Polar-based SO_2 removal process.

The flue gas entering the carbon capture plant is first cooled in the bulk cooling section (bottom packed bed) of the 3-Stage DCC by a circulating water stream. The circulating water enters the column at the top of the bulk cooling section and contacts the flue gas over a bed of packing. The circulating water is heated by the cooling and condensing of water vapor in the flue gas. The water is collected in the DCC boot and circulated through the DCC Bulk Cooler (E-101 A/B/C) by the DCC Bulk Cooler Pumps (P-101 A/B/C). The cooled circulating water stream exiting the DCC Bulk Cooler is returned to the top of the DCC bulk cooling section. Heat is removed from the circulating water stream by cooling water in the DCC Bulk Cooler.

A continuous slip stream is diverted from the circulating water downstream of the DCC Bulk Cooler Pumps to the DCC Water Filter (F-101) to remove particulate matter. The filtered water is returned to the liquid surge volume in the boot of the DCC.

In order to minimize degradation of the CO_2 solvent, the final traces of SO_2 in the flue gas are removed in the middle section of the 3-Stage DCC. In this section, the flue gas, which has been cooled to $90^{\circ}F$ in the bottom packed bed, is contacted with a circulating scrubbing solution which absorbs most of the residual SO_2 in the flue gas. The scrubbing solution is extracted from the column below the trim SO_2 Removal Section and it is sent back to the middle of the column by the DCC Scrubbing Solution Pumps (P-108 A/B/C). The pH of the circulating scrubbing solution is maintained by injecting sodium hydroxide (NaOH) supplied by NaOH Injection Package (PK-101) into the circulating scrubbing solution loop as needed. A blowdown is required from this circulating loop in order to maintain the salt concentration of the circulating scrubbing solution and to remove the absorbed sulfur species.

Flue gas leaving the SO_2 removal section of the DCC is further cooled to $47^{\circ}F$ in the trim cooling section (top packed bed) against a second chilled circulating water stream. The objective of the trim cooling section is to maintain the water balance at an optimum level in the plant. The circulating water enters the column at the top of the trim cooling section and contacts the flue gas

coming from the middle section of the column over a bed of packing. It is heated by the cooling and condensing of water vapor in the flue gas and removed from the column at the bottom of the trim cooling section. The water is circulated through the Refrigeration Plant (PK-102) by the DCC Trim Cooler Pumps (P-102 A/B/C) and returned back to the top of the trim cooling section. Heat is removed from the secondary circulating water stream in the Refrigeration Plant (PK-102). Water that is condensed out of the flue gas in both the bulk and trim cooling sections of the DCC must be removed from the system to prevent accumulation of water in the DCC.

CO₂ Absorption

The Blower is located in the flue gas path between the DCC and Absorber. The Blower is used to overcome approximately 2-2.5 psi of flue gas pressure drop through the CCC Plant (DCC, Absorber, and ducting). The flue gas discharged from the Blower enters the bottom of the Absorber and flows upward through the packed column where it reacts with the CO_2BOL solvent to remove 90% of the carbon dioxide contained in the flue gas.

Semi-RICH solvent loaded with CO_2 is extracted at an optimized point in the column and sent by the Absorber Intercooler Pumps (P-103 A/B/C) through the Absorber Intercooler (E-103 A/B). The solvent is cooled against cooling water and returned to the Absorber below the extraction point for intercooling.

Treated gas from the absorption section enters the condensing section of the Absorber where vapor phase solvent is cooled and condensed by a circulating cooling water stream in the Absorber Condenser (E-106), which is built into the column. The captured solvent is collected below the Absorber Condenser and returned to the top of the absorption section of the column where the LEAN solvent enters the Absorber. The treated flue gas exiting the Absorber Condenser is vented to atmosphere.

Solvent Regeneration

The carbon dioxide-RICH CO_2BOL solvent leaves the bottom of the Absorber and is pumped by the RICH Solvent Pumps (P-106 A/B/C) to the solvent regeneration (CO_2 stripping) section of the plant. Here, the RICH solvent from the Absorber is first mixed with a non-polar "anti-solvent" liquid stream before being routed to the Solvent Cross Exchanger (E-107). The objective of mixing the "anti-solvent" stream at this point is to change the polarity of the carbon dioxide RICH CO_2BOL solvent (See Section 2.3 for details). This change in polarity destabilizes the chemically bound CO_2 so that full release of the CO_2 can take place at a lower temperature and with lower energy consumption in the Stripper.

The RICH CO_2BOL solvent / "anti-solvent" mixture is heated against the LEAN CO_2BOL solvent / "anti-solvent" mixture in the Solvent Cross Exchanger (E-107). The hot RICH CO_2BOL solvent / "anti-solvent" mixture then enters the Stripper below the wash section of the column. The RICH solvent stream with the anti-solvent flows down the Stripper counter-current to the stripping steam. The stripping steam provides energy for breaking the bond between the solvent and the CO_2 , thereby desorbing the CO_2 from the solvent. The CO_2 and remaining stripping steam travel upward in the column to the wash section of the Stripper. Here, condensed water from the

Overhead Accumulator (V-104) partially cools the gas and scrubs any entrained solvent and much of the vapor phase solvent from the overhead gas.

The resulting vapor from the top of the Stripper is cooled against cooling water in the Stripper Condenser (E-105), which condenses the majority of the water vapor carried in this stream. The two-phase mixture from the Condenser enters the Overhead Accumulator where the carbon dioxide and condensed water are separated. The low-pressure carbon dioxide product is sent from the Overhead Accumulator to the CO₂ Compressor (K-101). Condensed water in the Overhead Accumulator is pumped back to the Stripper by the Stripper Reflux Pumps (P-105 A/B). The majority of the condensate is returned to the Stripper as reflux while a smaller portion is sent back to the Absorber via the main LEAN solvent line.

The CO₂BOL solvent/"anti-solvent" mixture is collected at the bottom of the column and sent to the Reboiler (E-104 A-D). Heat input to the Reboiler is provided by condensing low pressure steam supplied from the power plant. Steam condensate from the Reboiler flows to the Reboiler Condensate Drum (V-105). Condensate from the drum is pumped by the Reboiler Condensate Pump (P-107 A/B) back to the power plant. A small portion of the steam condensate is used to desuperheat the incoming low pressure steam.

The LEAN CO_2BOL solvent/"anti-solvent" mixture leaving the Stripper is pumped by the LEAN Solvent Pumps to the Solvent Cross Exchanger where it provides heat to the RICH solvent. The cool LEAN solvent stream is then routed to the anti-solvent Coalescer (V-106) in which the LEAN CO_2BOL solvent is separated from the anti-solvent. The anti-solvent stream is mixed back with the RICH CO_2BOL solvent stream from the Absorber to complete the cycle. Meanwhile, the LEAN CO_2BOL solvent stream is routed back to the Absorber. To remove impurities from the circulating CO_2BOL solvent stream, a small fraction of the cooled LEAN solvent is sent to the LEAN Solvent Filters (F-102). The filtered solvent slipstream returns to the main LEAN solvent line where it is returned back to the Absorber.

CO₂ Compression

Following CO_2 recovery, the low-pressure CO_2 product from the Overhead Accumulator is sent to the CO_2 Compressor, a 6-stage integrally-geared machine with intercoolers and knock-out drums. The CO_2 product is extracted at an intermediate pressure and routed to the CO_2 Dehydration Package (PK-103) for water removal. The CO_2 is then returned to the CO_2 Compressor where it is compressed to the final product pressure of 2,215 psia and sent to plant battery limits.

The CO_2 compression power was estimated at 60,900 kW during the process evaluation for the recreated NETL Case 10 baseline and the CO_2BOL cases. This is substantially higher than the 48,790 from the NETL Case 10 value. The recreated Case 10 comparison was used in the LCOE evaluation.

Material and Energy Balances and Stream Tables

Aspen Plus® was used for the process simulations. Aspen Plus® is particularly well suited to generate the material and energy balances because it has a large number of built-in physical and chemical property models adaptable to the electrolyte chemistry occurring between the CO₂BOL

and CO_2 central to this system. Laboratory and literature data was incorporated directly into the models using the built-in regression system. Additionally, the impacts of physical properties such as viscosity are rigorously handled in the mass transfer calculations performed over small increments packing surface area of the gas-liquid contacting equipment (absorber and strippers) that are modeled here. These "rate-based" simulations are believed by the team, to be the best available for this purpose.

Fluor and Battelle have extensive experience in building and using simulations in Aspen Plus® for modeling carbon capture system, including in Fluor's case the commercial offering of carbon capture systems. The process flow diagrams and corresponding stream tables are shown as follows in **Figure 41**-Figure 43 and Table 15.

PK-102 BL-101 C-102 E-103A/B REFINCERATION FLANT BLONER ARXIORIES ARXIOGRAFIS INTERCOLLER F-101 DEC WATER FILTER P-102A/B/C DGS TRM COOLER PUNPS <u>C-102</u> **⊙** £-@ P-102A/B/C P-103A/B/C P-103A/B/c E-10/A/B/C E=101A/B/C PROCESS FLOW DIAGRAM CO₂BOLS PROCESS ABSORPTION ## 8% MPV PEV MVC FA APB APB | | BY -GK JAW BROOKS SAN HARRA PEN DITE BENCH S 1 N/16/18 HERUED FOR METERATION FLUOR. Battelle

Figure 41. Process Flow Diagram – Absorption System

Figure 42. Process Flow Diagram – Stripping System

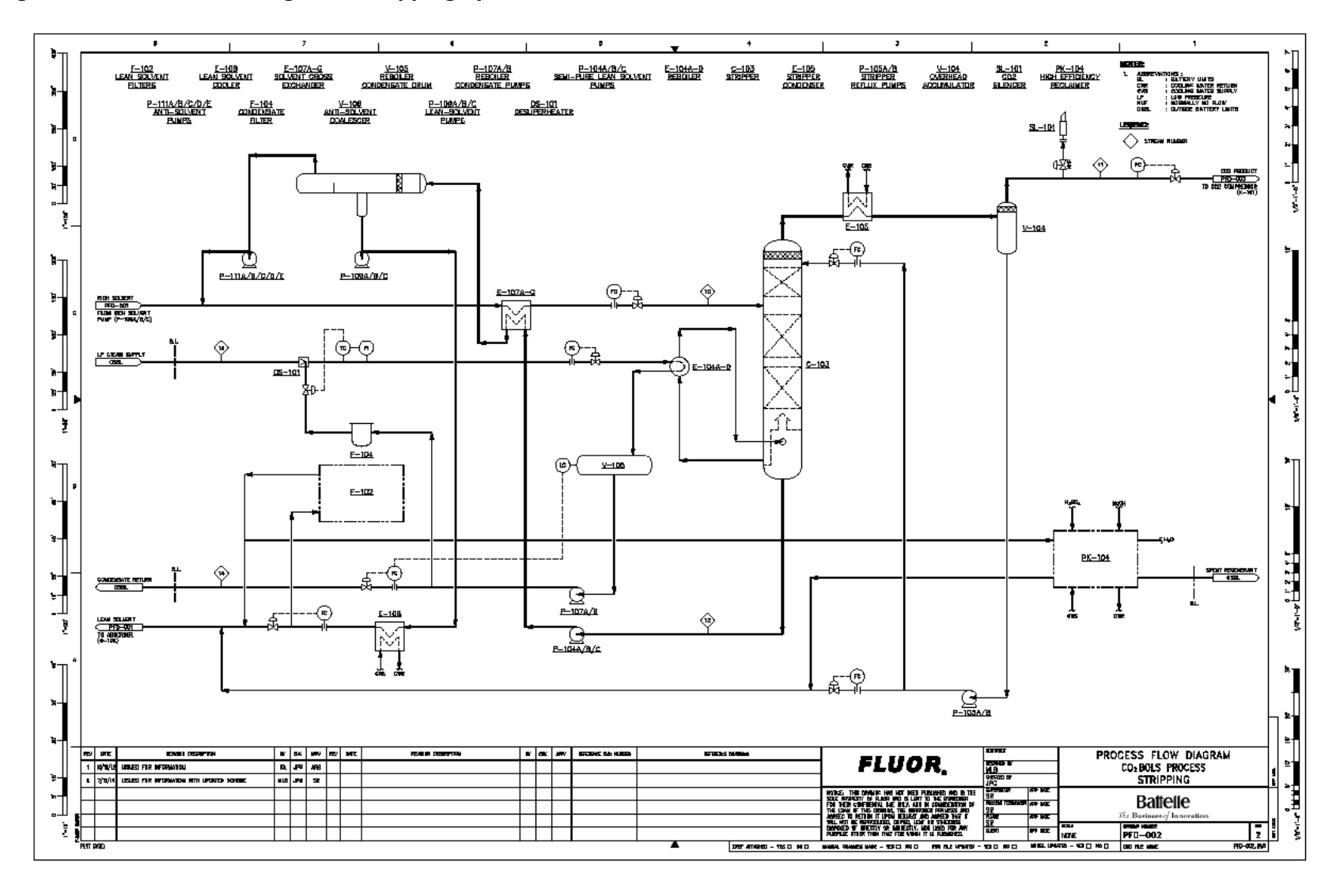


Figure 43. Process Flow Diagram – Compression System

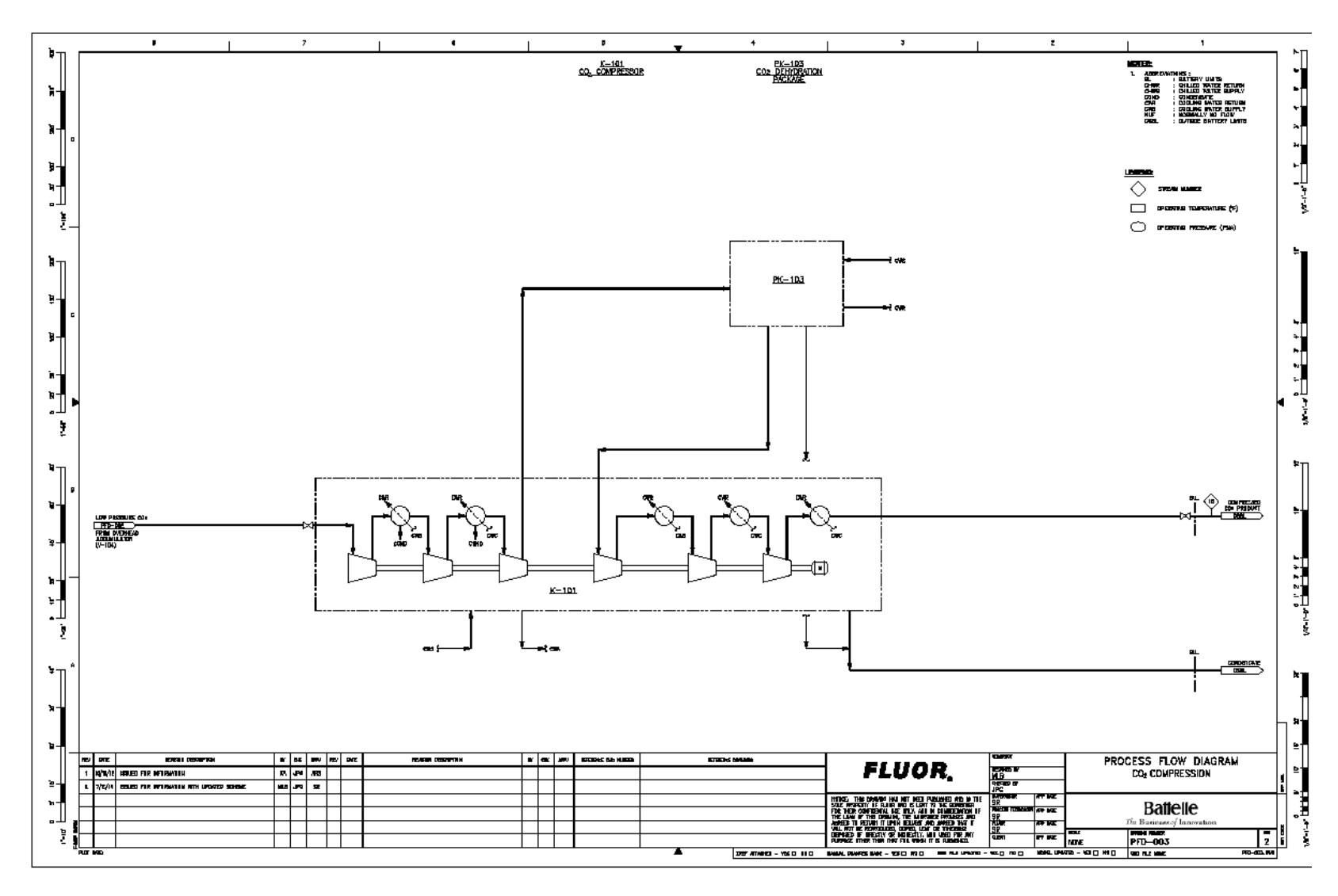


Table 15. Process Stream Tables (CO₂BOLs/PSAR case with 356 cP max viscosity)

Stream Descrip	tion	Post FGD Flue Gas	Treated Flue Gas from DCC	Excess Condensate from FG	Flue Gas to Absorber	Absorber Stack Vent to Atm	Lean Solvent to Absorber
Stream Number		1	2	3	4	5	6
Temperature (°F)		136	47	119	74	90	95
Pressure (psia)		14.9	14.5	50.0	16.7	14.9	50.0
<u>Components</u>	MW	<u>vol%</u>	<u>vol%</u>	<u>wt%</u>	<u>vol%</u>	vol%	<u>wt%</u>
H ₂ O	18.02	15.4%	1.1%	100.0%	1.1%	0.5%	4.1%
CO ₂	44.01	13.5%	15.8%	0.0%	15.8%	1.8%	1.9%
N_2	28.02	67.9%	79.4%	0.0%	79.4%	93.3%	0.0%
O_2	32.00	2.4%	2.8%	0.0%	2.8%	3.3%	0.0%
Ar	39.95	0.8%	0.9%	0.0%	0.9%	1.1%	0.0%
Solvent	171.24	0.0%	0.0%	0.0%	0.0%	0.0%	93.7%
Anti-solvent	226.45	0.0%	0.0%	0.0%	0.0%	20.8%	0.2%
Total Flow (lbmol/hr)		122,856	105,134	17,722	105,134	89,504	108,588
Total Flow (lb/hr)		3,541,660	3,222,350	319,310	3,222,350	2,552,741	13,207,343
Molecular Weight		28.8	30.7	18.0	30.7	28.5	121.6
Density (lb/ft ³)		0.07	0.08	61.73	0.09	0.07	64.60
Liquid Flow (gpm)	•	-	-	645	-	-	25491
Vapor Flow (ACFM)		877,164	656,052	-	600,050	586,449	-

Stream Descrip	tion	Absorber Intercooler Draw	Absorber Intercooler Return	Rich Solvent from Absorber	Rich Solvent to Stripper	Low-Press CO ₂ to Compressor	Lean Solvent from Stripper
Stream Number		7	8	9	10	11	12
Temperature (°F)		126	90	130	201	104	219
Pressure (psia)		16.3	50.0	16.5	24.5	24.3	27.0
<u>Components</u>	MW	wt%	wt%	wt%	wt%	vol%	wt%
H ₂ O	18.02	3.1%	3.1%	4.0%	1.2%	4.5%	1.2%
CO ₂	44.01	0.0%	0.0%	6.6%	1.9%	95.5%	0.6%
N_2	28.02	0.0%	0.0%	0.0%	0.0%	0.0%	0.0%
O_2	32.00	0.0%	0.0%	0.0%	0.0%	0.0%	0.0%
Ar	39.95	0.0%	0.0%	0.0%	0.0%	0.0%	0.0%
Solvent	171.24	96.7%	96.7%	89.2%	26.6%	0.0%	27.0%
Anti-solvent	226.45	0.3%	0.3%	0.2%	70.3%	0.0%	71.3%
Total Flow (lbmol/hr)		70,008	70,008	124,218	272,017	15,630	256,387
Total Flow (lb/hr)		9,508,088	9,508,088	13,877,038	47,204,862	669,695	46,535,167
Molecular Weight		135.8	111.7	173.5	42.8	181.5	225.5
Density (lb/ft ³)		63.1	63.8	62.9	48.6	0.2	48.5
Liquid Flow (gpm)		18,780	18,570	27,507	121,209	-	119,706
Vapor Flow (ACFM)		-	-	-	-	64,489	-

Stream Descrip	tion	Anti-solvent to Cross Exchanger	LP Steam Supply	LP Steam Condensate Return	CO ₂ Product
Stream Number		12A	13	14	15
Temperature (°F)		160	565	235	95
Pressure (psia)		71.1	73.5	65.0	2215.0
<u>Components</u>	MW	wt%	<u>vol%</u>	vol%	vol%
H ₂ O	18.02	0.0%	100.0%	100.0%	0.0%
CO ₂	44.01	0.0%	0.0%	0.0%	100.0%
N_2	28.02	0.0%	0.0%	0.0%	0.0%
O_2	32.00	0.0%	0.0%	0.0%	0.0%
Ar	39.95	0.0%	0.0%	0.0%	0.0%
Solvent	171.24	0.5%	0.0%	0.0%	0.0%
Anti-solvent	226.45	99.5%	0.0%	0.0%	0.0%
Total Flow (lbmol/hr)		147,798	36,500	36,500	14,930
Total Flow (lb/hr)		33,327,708	657,540	657,540	657,065
Molecular Weight		225.5	18.0	18.0	44.0
Density (lb/ft ³)		46		·	51
Liquid Flow (gpm)		89,888			Supercritical
Vapor Flow (ACFM)		-			Supercritical

Cost Estimates Basis

Equipment-factored capital cost estimates were prepared by Fluor for the CO₂BOLs/PSAR system assuming a maximum loaded RICH viscosity of 356 cP. The total processed CO₂ was 15,771 short tons per day, which corresponds to the rate from NETL Case 10. The assumed plant located was a generic site in Midwestern, United States. The capital cost estimate covers the Inside Battery Limit (ISBL) scope of work. This estimate is a class 5 type as defined in The Association for The Advancement of Cost Engineering (AACE) International Recommended Practice No. 18R-97. The estimate is based on a rough-sized equipment list. The purpose of this estimate is to provide a baseline Total Installed Cost (TIC) for comparisons to competing technologies. All costs are in U.S. dollars on an instantaneous mid-2007 basis, with no forward escalation.

The Direct Field Costs (DFC) were prepared factoring methods of equipment items by capacity. All major equipment pricing is derived from Fluor recent in-house pricing budgetary quotes from vendors. The capacity adjusted equipment costs are then multiplied by a factor for bulk materials and labor to produce the DFC. As indicated in the initial TEA projection report, the ensuing direct field cost is factored to include indirect field costs, home office costs, other costs and contingency to produce a Total Installed Cost (TIC) level. The TIC includes the following:

- Indirect field costs for construction management and heavy haul/heavy lift
- Home office costs (FEED and detail engineering),
- Other costs (such as vendor reps, spare parts, project insurance, etc.),
- Contingency

As with the initial feasibility study, the estimates are given using key assumptions and qualifications, such as:

- All costs are in U.S. dollars currency on an instantaneous 2007 basis, with no forward escalation.
 - Total Installed Cost estimates include the inside battery limits (ISBL) Process Unit only.
 - Average productivity is assumed to be 1.25 for the work location.
- The proposed plot area is assumed to be a clear and level site, with no underground obstructions.
- Field labor costs are based on working a 50-hour work week five 10 hour days. This assumes 40 hours of straight time pay plus 10 hours overtime incentive.
 - Minimal soundproofing is provided.
- An adequate supply of qualified craft labor and supervision are available within the local area of the project site, at the time of construction.
 - Two stand-alone process trains.
 - Piling is not required
 - Fireproofing not required

All costs in this section are contractor EPC costs, excluding Owner's costs. Standard Owner's costs include but are not limited to the following cost items:

- Client staff and expenses (including Project Management)
- Commissioning and start up
- Control Room and Distributed Control System

- Infrastructure
- Inlet ducting from the boiler stack to the CDCU battery limits
- Land cost / rights of access to the site
- Outside Battery Limit (OSBL) scope of work including power supply and distribution, steam and condensate systems, water systems, air and nitrogen systems
 - Owner's contingency / escalation
 - Permanent office and laboratory equipment
 - Permits (building / environmental)
 - Removal and proper disposal of any contaminated or hazardous materials
 - Sales and use taxes
 - Site clearing and demolition
 - Substation or major electrical equipment
 - Tie-in to existing utilities
 - Vendor representatives during and after start up

The Total Installed Cost is estimated to be \$1,103M in 2007 U.S. dollars, with an accuracy range of \pm - 40%. Note that the Total Installed Cost estimate from the initial TEA for CO₂BOLs/ PSAR was \$495M on the same basis. The lower estimate was based on an assumed maximum viscosity (RICH solvent) of 20 cP, where the current estimate is based on large equipment sizing to accommodate a RICH solvent corresponding to a maximum viscosity of 356 cP. Thus, it is clear that viscosity has very high impact on the cost of these systems.

LCOE Projections

Levelized Cost of Electricity (LCOE) estimates were made using the ASPEN simulation and equipment costing results. Table 16 and The LCOE data is shown below in Table 17. Breaking out the CO_2 capture plant costs between CO_2 removal system and CO_2 drying and compression, the higher costs of the CO_2 BOL case are a result of the CO_2 removal unit. CO_2 compression and drying capital costs were assumed to be the same for the NETL Case 10 and CO_2 BOL Case 2 and the 20cP theoretical target at \$91 /kWe. The CO_2 BOL Case 2 CO_2 removal system capital cost was priced as \$1,846 /kWe, which was three times the cost of the recreated Case 10 at \$702 /kWe. The higher costs for the CO_2 BOL case were associated with a larger absorber, stripper, and heat exchanger, in addition to the PSAR infrastructure such as the coalescing tank and piping. If the CO_2 BOL process could achieve its 20 cP target viscosity, the costs of the CO_2 BOL CO_2 removal system is projected to be \$707 \$/kWe, approaching the costs of the NETL Recreated Case 10.

Table 17 show the LCOE projections for fuel, variable and fixed costs.

In these tables, as labeled, the "MEA-Based Capture" columns represent the baseline established by NETL and as adjusted for higher CO₂ compression energy from PNNL's recreated Case 10. The CO₂BOLs Initial TEA shows the best-case CO₂BOLs performance cases with and without the PSAR modification based on equilibrium performance with a set 20 cP viscosity (used for equipment sizing). This is not a real case with the current solvent, but shows the benefit of obtaining a lower viscosity. (Research is currently underway through a new DOE program to develop a lower viscosity solvent.) The last two columns are based on the performance of the current solvent at two different RICH loadings from the absorber that correspond to the 356 and 578 centipoise viscosities shown.

Table 16. LCOE (fuel) projections for MEA Baselines, and CO₂BOLs/PSAR

2 2 2	No © Capture?	MEA-Base	d∎Capture®	artificial20cP	al@EA@2012)@@ @max@viscosity@ ed@	Predictions [®]	**Updated **Bwith**actual **sities**	?	?
Fuel@Costs@	NETLECase 1992	NETLECase 2102	Recreated Case 10 Case	No PSAR IIII	With PSAR?	With PSAR (356 Prich)	With PSAR (578 t P Prich)	?	Assumptions (list@below)
TOTAL STEAM TURBINE POWER, RWe 2	582,600፻	672,7002	672,7002	734,7002	760,8902	730,1572	739,7962] [12
AUXILIARYILOADISUMMARY,ikWe?	77	27	? P	27 2	77	27	77	lſ	7
☐ CoalaHandlingandaConveying ☐	450∄	540₪	540⊡	540₪	540₪	5402	540₪] [52
☐ Limestone ☐ Handling ☐ ☐ Prep ☐	950∄	1,3702	1,3702	1,3702	1,3702	1,3702	1,3702	ll	52
Pulverizers	2,9702	4,1802	4,180②	4,1802	4,1802	4,180₪	4,180₪	l í	52
	570⊡	800₪	8002	800₪	800₪	8002	800₪	l f	52
Primary@Air@Fans@	1,400⊡	1,9602	1,960₪	1,9602	1,960₪	1,960₪	1,960₪	1 [52
★ Forced Draft Fans ②	1,7802	2,5002	2,5002	2,5002	2,5002	2,500🛚	2,5002		52
☐ ☐ Induced Draft Fan ☐	7,5402	12,0802	12,0802	12,0802	12,0802	12,080⊡	12,0802		52
T T SCR2	50₪	70⊡	702	702	702	70⊡	702		52
⊞ Baghouse□	702	1002	1002	1002	1002	100₪	100₪	11	52
	3,1802	4,4702	4,470②	4,4702	4,470₪	4,470₪	4,4702	1 [52
Miscellaneous Balance of Plant 2	2,0002	2,0002	2,0002	2,0002	2,0002	2,0002	2,0002	1 1	52
Steam@urbine@Auxiliaries@	400⊡	4002	400₪	4002	4002	4002	4002	11	52
T T TT	77	2	13,0732	7,7032	7,7032	11,0902	11,0902	1 1	12
	77	7	5,5982	6,8362	6,8362	23,7782	22,4122	11	12
② ② ③ ③ ③ ③ ③ ② ② ② ② ③ ③ ③ ③ ③ ③ ③ ③ ③	77	2	77	13,0102	13,0102	13,0102	13,0102	1 1	12
III IIIIMiscellaneous Auxiliaries 2	77	7	7,7472	02	02	02	02	11	7
	77	22,4002	26,4182	27,5492	27,5492	47,8782	46,5122	11	12
	77	48,7902	60,9002	60,900⊡	60,9002	60,900⊡	60,9002	11	92
☐ ☐ Condensate Pumps ☐	890∄	7002	7002	7002	7002	7072	7102	11	12
☐ ☐ Circulating ☐ Water ☐ Pumps ☐	5,2502	11,1902	11,1902	11,1902	11,1902	11,190⊡	11,1902	11	52
	530∄	1,0202	1,0202	1,0202	1,0202	1,020⊡	1,0202	11	52
Cooling	2,7202	5,8202	5,8202	5,8202	5,8202	5,8202	5,8202	11	52
Transformeraloss2	1,8302	2,3502	2,3502	2,3502	2,3502	2,5562	2,5892	11	12
⊞ TOTALAUXILIARIES, ®kWe2	32,5802	122,7402	138,8682	139,9992	139,9992	160,5412	159,2112	11	22
NET®OWER,®kWe®	550,0202	549,9602	533,8322	594,701₺	620,8912	569,6162	580,5852	11	22
Net@Plant@Efficiency@[HHV)@	36.8%∄	26.2%2	25.4%2	28.3%2	29.5%2	27.1%2	27.6%2	11	22
Net@lant@Heat@Rate@Btu/kWh)	9,2772	13,0462	13,0462	14,1072	14,7292	13,5122	13,7722	1 1	2?
As-Received@coal@eed@kg/h)	198,3912	278,9562	278,9562	278,9562	278,9562	278,9562	278,9562	11	52
Thermal@nput,@kWt?	1,495,3792	2,102,6432	2,102,6432	2,102,643🛚	2,102,6432	2,102,6432	2,102,6432		52
Total Total	471,116₪	695,9542	695,9542	695,9542	695,9542	695,9542	695,9542		52
Percent©CO2©Captured②	0%2	90%2	90%2	90%2	90%2	90%∄	90%2		12
☐ Coaldincrease@perdNetdPowerd	0.0%᠌	40.6%᠌	44.9%2	30.0%᠌	24.6%2	35.8%⊡	33.2%☑		12
	\$62.22	\$87.42	\$87.42	\$87.42	\$87.42	\$87.4₺	\$87.42		52
	85%⊡	85%₫	85%2	85%∄	85%⊡	85%₪	85%2	1	52
☐ FuelaCosta(¢/kWe-hr) ☐	1.522	2.132	2.202	1.972	1.892	2.062	2.022	إ	2🛭

Assumptions:

- 1. From simulation (Aspen Plus)
- 2. Calculated from above parameters
- 3. From Aspen Economic Analyzer
- 4. Vendor quotes on major equipment
- 5. Same as NETL Case 10
- 6. Assume 22.6% of TPC
- 7. Based on Fluor Estimates
- 8. Same as Case 10 normalized to new net power
- 9. Based on revised predictions for Case 10

The LCOE data is shown below in Table 17. Breaking out the CO_2 capture plant costs between CO_2 removal system and CO_2 drying and compression, the higher costs of the CO_2 BOL case are a result of the CO_2 removal unit. CO_2 compression and drying capital costs were assumed to be the same for the NETL Case 10 and CO_2 BOL Case 2 and the 20cP theoretical target at \$91 /kWe. The CO_2 BOL Case 2 CO_2 removal system capital cost was priced as \$1,846 /kWe, which was three times the cost of the recreated Case 10 at \$702 /kWe. The higher costs for the CO_2 BOL case were associated with a larger absorber, stripper, and heat exchanger, in addition to the PSAR infrastructure such as the coalescing tank and piping. If the CO_2 BOL process could achieve its 20 cP target viscosity, the costs of the CO_2 BOL CO_2 removal system is projected to be \$707 \$/kWe, approaching the costs of the NETL Recreated Case 10.

Table 17. LCOE (capital & variable) projections for MEA Baselines, and ${\rm CO_2BOLs/PSAR}$

2 2	No@Capture?	MEA-Base	d © Capture2	CO2BOLs@initial@EA@2012)@@ artificial@OcP@max@iscosity@ used@		P@max@viscosity@ Predictions@@vith@actual@		? ?
Total@Capital@Costs@(\$/kWe)@	NETLECase 1992	NETLECase 2.02	Recreated Case 10	No₽SAR	With PSAR?	With@PSAR@@@ (356@cP@rich)@	With PSAR (578 of Parich) 2	Assumptions (list below)
Non-Carbon Capture Components: 2	77	27	27	7	77	7	77	77
	\$732	\$902	\$932	\$832	\$80₪	\$87₪	\$85₪	82
☑ ☑ Coal ☑ Sorbent Prep ☑ Feed ☑	\$342	\$432	\$442	\$402	\$382	\$42🛚	\$412	82
☑ ☐ Feedwater ☑ Misc. BoP ☑ ystems ②	\$1362	\$1812	\$1862	\$1672	\$1602	\$1742	\$1712	82
T PCBoiler2	\$4862	\$6172	\$6352	\$5702	\$5462	\$5952	\$5842	82
☑ Flue ☑Gas ☑Cleanup ☑	\$2462	\$3162	\$3262	\$2932	\$2802	\$3052	\$3002	82
☐ ☐ Combustion ☐ urbine/Accessories ☐	\$0₪	\$02	\$0₽	\$02	\$02	\$0᠌	\$02	82
☑ ☑ HRSG, Ducting ☑ Stack ☑	\$71🛭	\$76₪	\$782	\$70₪	\$672	\$73᠌	\$72ඕ	82
Steam Turbine Generator 2	\$2072	\$2342	\$2412	\$2162	\$2072	\$2262	\$2222	82
☐ ☐ Cooling ☐ Water ⑤ ystem ②	\$73⊡	\$119🛚	\$1222	\$1102	\$1052	\$1152	\$1132	82
☑ ☑ Ash/SpentSorbent3HandlingSys2	\$24🛚	\$292	\$302	\$272	\$252	\$282	\$272	82
② ② Accessory ③ Lectric ③ Plant ②	\$95₫	\$152🛚	\$1572	\$1412	\$1352	\$1472	\$1442	82
☑ ☑ Instrumentation ☑ Control ☑	\$392	\$472	\$482	\$432	\$412	\$45₪	\$442	82
☑ ImprovementsItoSite ☑	\$26ඕ	\$29ඕ	\$30⊡	\$27₪	\$25₪	\$28₪	\$27₪	82
■ Buildings ■ Structures □	\$1132	\$1142	\$1182	\$1062	\$1012	\$1112	\$1082	82
	77	27	\$7932	\$8332	\$7982	\$1,937🛚	Not@estimated@	3,4₺
	77	\$8052	\$7022	\$7422	\$7072	\$1,8462	77	77
② ② CO2©Compression ② ② ② ② ② ② ② ② ② ② ② ② ② ② ② ② ② ② ③ ② ③ ② ③ ② ③ ② ③ ② ③ ② ③ ② ③ ② ③ ② ③ ② ③ ② ③	77	\$912	\$912	\$912	\$912	\$912	\$912	77
☑ ☑ Owner's ☑ Costs ☑	\$3742	\$6672	\$6612	\$7992	\$7652	\$905.002	Not@stimated@	6,7₪
★ Total ** T	\$1,9972	\$3,6102	\$3,5632	\$3,5242	\$3,3762	\$4,8182	Not@stimated@	22
	0.1172	0.1242	0.1242	0.1242	0.1242	0.1242	0.1242	52
Capital Cost Cos	3.122	6.03🛚	5.95₪	5.882	5.642	8.042	Not@stimated@	22
2								

2 2 2	No@Capture?	MEA-Base	d © Capture2	CO2BOLs@initial@EA@2012)@@ artificial@OcP@nax@viscosity@ used@		x®viscosity® Predictions®®with®actual®		? ?	
Variable@Costs@\$k/yr)@	NETLECase®®	NETLECase 2102	Recreated? Case 20?	No PSAR IIII	With PSAR 2	With PSAR (356 Prich)	With PSAR (578 ot Parich) 2	1 1	Assumptions (list below)
Non-Capture System: 2	77	1	12	27	77	7	77	1	7
☑ ☑ Maintenance Material Cost ☑	\$8,7632	\$15,6442	\$14,9742	\$15,6442	\$15,6442	\$15,6442	\$15,6442		52
I Water Water 2	\$1,4252	\$2,7122	\$2,7122	\$2,7122	\$2,7122	\$2,7122	\$2,7122		52
III III MURRIWTIChemi	\$1,1032	\$2,1002	\$2,1002	\$2,1002	\$2,1002	\$2,1002	\$2,1002		52
☑ ☑ Limestone②	\$3,4962	\$5,0432	\$5,0432	\$5,0432	\$5,0432	\$5,0432	\$5,0432		52
	\$3,1362	\$4,4462	\$4,4462	\$4,4462	\$4,4462	\$4,4462	\$4,4462		52
I SCRICatalyst2	\$5932	\$8322	\$8322	\$8322	\$8322	\$8322	\$8322		52
☑ ☑ Flyash☑Disposal②	\$2,0502	\$2,8822	\$2,8822	\$2,8822	\$2,8822	\$2,8822	\$2,8822		52
Bottom Bottom	\$5122	\$7202	\$7202	\$720🛚	\$7202	\$720🛚	\$7202		52
	77	27	77	27	77	17	77		27
I Solvent2	\$0₪	\$1,1062	\$1,2692	\$4,8262	\$4,8262	\$4,8262	\$4,8262		72
III III NaOHI	\$0᠌	\$1,0622	\$4,3052	\$4,0712	\$4,0712	\$4,0712	\$4,0712		72
₽ ₽ H2SO42	\$0ඔ	\$3242	\$5392	\$496₽	\$4962	\$496₽	\$4962		72
Corrosion@nhibitor	\$0ඔ	\$7₪	\$72	\$0ඔ	\$0₽	\$0₪	\$0₪		72
☑ ☑ Activated ☑ ☐ Activated	\$0ඔ	\$6162	\$6172	\$6172	\$6172	\$617₪	\$6172		92
图 Total頃\$k/yr)②	\$21,0782	\$37,4962	\$40,4482	\$44,4132	\$44,4132	\$44,3912	\$44,3912		22
Wariable	0.512	0.922	1.02₺	1.002	0.962	1.052	1.03₪		2?
Fixed®Operating®Costs@\$k/yr)®	77	27	77	27	77	17	77		27
Operating Labor 2	\$5,5242	\$6,4452	\$6,4452	\$6,4452	\$6,4452	\$6,4452	\$6,4452		52
☑ ☑ Maintenance ☐ abor ☑	\$5,8422	\$10,4302	\$9,9832	\$10,4442	\$10,4442	\$10,4302	\$10,4302		52
☑ Administrative ☑ Support abor	\$2,8422	\$4,2192	\$4,2192	\$4,2192	\$4,2192	\$4,2192	\$4,2192		52
☑ ☑ Property②Taxes@and③Insurance②	\$17,8492	\$32,3672	\$32,3672	\$32,3672	\$32,3672	\$32,3672	\$32,3672		52
I Total □	\$32,0572	\$53,4602	\$53,0132	\$53,4752	\$53,4752	\$53,4602	\$53,4602		2🛭
☐ Fixed®Dperating®Cost®(¢/kWe-hr)®	0.782	1.31?	1.332	1.212	1.16₪	1.262	1.242	[?]	23

Table 18. LCOE (Summary) projections for MEA Baselines, and CO₂BOLs/PSAR

2 2 2	No © Capture?	MEA-Based@Capture@		CO2BOLs@dnitial@EA@2012)@2 artificial@OcP@nax@iscosity@ used@		Predictions	MJpdated2 BwithCactual2 sities2	?	?
Summary@f@Costs@¢/kWe-hr)@	NETLECase®®	NETLECase 2.02	Recreated Case 10	No ⊉ SAR ™	With PSAR?	With PSAR (356 Prich)	With PSAR (578 PPrich)	ΓI	Assumptions (list below)?
The Fuel Cost?	1.522	2.13🛽	2.202	1.972	1.89₪	2.06₪	2.022	l	2🛭
☑ Capital©cost②	3.12∄	6.032	5.95₪	5.882	5.642	8.042	Not@stimated@		22
☑ Variable©Cost②	0.512	0.922	1.02₪	1.002	0.96₪	1.05₪	1.03₺	77	2🛭
☐ Fixed®Dperating®Cost®	0.782	1.312	1.332	1.212	1.162	1.26₪	1.24ℤ	77	2?
Transp, Seques (Monitoring (TSM))	3	0.59₪	0.592	0.552	0.522	0.572	0.562	l	82
m Total?	5.942	10.972	11.092	10.612	10.172	12.982	Not@stimated@		2?
III Increase Iversus INO ICapture I	227	84.7% ℤ	<i>86.7%</i> ℤ	78.7% ²	71.1%2	119%2	Not@stimated@	li	2🛭

The LCOE summary in Table 18 shows each of the primary cost factors: Fuel, Capital, Variable, Fixed Operating, and Transportation, Sequestration & Monitoring (TSM). Additionally, the increase in total LCOE over the 'No Capture' case is shown. NETL Case 10 shows an 84.7% increase in LCOE over the 'No Capture' case. The 'Recreated Case 10' was 2.1% (absolute) higher in LCOE increase, primarily due to higher CO₂ compression energy estimate than stated in the NETL reference case. This higher compression energy was also used on each of the CO₂BOLs simulations.

The two CO₂BOLs cases from the initial TEA correspond to 'No PSAR' and 'With PSAR' (1:1 antisolvent to BOL). The fuel costs for these two cases are 1.97 and 1.89 ¢/kWe-h, respectively. The two updated higher viscosity CO₂BOLs (each with PSAR) cases show corresponding fuel costs of 2.06 and 2.02 ¢/kWe-h. The main reason for the increase fuel costs in the updated cases is due to the fact that the viscosity limitations imposed on the system (356 and 578 cP, respectively) forced lower RICH CO₂ loading levels that drove higher solvent recirculation rates. Note that the corresponding HHV efficiency for the power plant was 27.1% for the 356 cP CO₂BOLs/PSAR case, versus 29.5% for CO₂BOLs in the initial TEA projection (20 cP max assumption), and 25.4% for the 'Recreated Case 10.' This equates to a 15% reduction in parasitic load (compared to the recreated NETL Case 10 for MEA). The initial TEA projection for CO₂BOLs/PSAR (at 20 cP) corresponded to a 36% reduction in parasitic load.

The other LCOE costs elements between the initial and updated $CO_2BOLs/PSAR$ cases are similar, except for capital cost. Due to the extent of work required to gather equipment capital costing data for high viscosity fluids only the 356 cP CO_2BOLs case was populated with a capital cost estimate. Here, the normalized capital was 8.06 ¢/kWe-h, versus the earlier (20 cP) prediction of 5.67 ¢/kWe-h. Indeed, this increased cost element was the largest factor in the LCOE increase for CO_2BOLs going to 119% of the 'No Capture' case.

The LCOE estimate is much higher than the initial forecasts from the initial feasibility study, however both the fuel and capital costs increase would be reduced substantially if RICH solvent viscosities could be kept below 100 cP.

7. ESTIMATED USEFUL LIFE OF SOLVENT

Until a formal lifetime analysis has been completed, the estimated solvent life of CO_2BOLs will depend on thermal and chemical degradations. In this report, CO_2BOLs solvent replacement rate is based on calculated evaporative losses from the absorber plus the molar chemical/thermal loss rate as for MEA in Case 10. Projected degradation reactions of analogous compounds possessing similar reactivity with the CO_2BOL and its derivatives are highlighted. This section describes the projected degradation pathways of the CO_2BOL with respect to operating conditions and contaminants in flue gas.

Evaporative Losses

Based on the current cooling and wash configurations described in Section 6, we project attrition due to evaporation to be 0.7 ppb, which translates to 40 kg (0.04 MTA) of CO₂BOL per annum, compared to MEA's annual evaporative losses of 225 MTA. While CO₂BOL costs are higher than MEA, the reduced solvent makeup rates are estimated save money in the long run as

evaporative losses are orders of magnitude less. This low evaporative loses suggest CO₂BOL chemicals could meet emission requirements resulting in minimal environmental impact. Current costing projections of evaporative losses of (3) translate to \$1,400 per year in lost solvent.

Heat-Stable Salt (HSS) Formation

 CO_2BOLs contain a strong guanidine base that can react with acid gases to generate guanidinium salts of the respective acid source. Each acid gas (e.g. SO_x , NO_x , HCI) may consume stoichiometric quantities of the CO_2BOL resulting a solid that precipitates out of solution. The formation of each heat stable salt is dependent on relative kinetic rates, concentrations and temperatures of the reactants. The concentrations of these acid gasses in flue gas streams is in ppm quantities thus not all of the will react due to dilution factors. Until formal tests of CO_2BOL reactivity with HCI, SO_x and NO_x are completed, we predict the amount of HSS formation to be identical to that of MEA.

Since the CO_2BOL molecules are more costly than MEA, recovery of the CO_2BOL from HSS will be required. We propose the use of reclaimers, and recovery of the CO_2BOL by non-thermal means. We anticipate utilization of ion-exchange resins or caustic washes/extractions (KOH) will recover the CO_2BOL . The addition of ion exchange will result in minimal cost increase to the process and caustic waste streams that would need disposal. The anticipated heat-stable salt form each acid gas is outlined below.

Impact of SO_x

It is known that sulfur based acid gases SO_2 and SO_3 will react with water to form sulfurous acid and sulfuric acid respectively, which in turn react with the basic BOL to form the heat-stable guanidinium hydrogen sulfite (HSO₃) and guanidinium hydrogen sulfate (HSO₄) with the former shown in Figure 44. Under anhydrous conditions, SO_2 or SO_3 react with the BOL to for zwitterionic alkylsulfite (bottom of Figure 44) and alkylsulfate. High thermal regeneration temperature is required to strip these gasses from the BOL due to the high acidity of sulfurous and sulfuric acids relative to carbonic acid. Accumulation of sulfite and sulfate salts can be minimized by introducing a flue-gas desulfurization (FGD) unit to remove the SO_x in the front end of the absorber.

In presence of water

Figure 44. The proposed reactions of (3), SO₂ and H₂O

Zwitterionic alkylsulfite

Impact of NO_x

The nitrogen based acid gasses NO_x , that is NO (nitric oxide) and NO_2 react with water and/or oxygen according to the equations in Figure 45 to form nitric acid, which subsequently protonates the BOL to form that guanidium nitrate heat-stable salt. Removing NOx before contacting the flue gas with the BOL or passing LEAN solvent through SCR can minimize the salt formation. The CO_2BOL can be recovered from the heat stable salt by ion exchange or caustic (KOH) washing.

$$2 \text{ NO}_2 + \text{H}_2\text{O} \longrightarrow \text{HNO}_2 + \text{HNO}_3$$

$$3 \text{ HNO}_2 \longrightarrow \text{HNO}_3 + 2 \text{ NO} + \text{H}_2\text{O}$$

$$4 \text{ NO} + 3 \text{ O}_2 + 2 \text{ H}_2\text{O} \longrightarrow \text{4 HNO}_3$$

$$HO \longrightarrow \text{CH}_3 \longrightarrow \text{HNO}_3 \longrightarrow \text{HO}_3$$

$$H_3\text{C} \longrightarrow \text{NO}_3$$

$$H_3\text{C} \longrightarrow \text{NO}_3$$

$$H_3\text{C} \longrightarrow \text{HO}_3$$

Figure 45. The proposed reaction of (3) with NO_x and water

Impact of HCI

HCl will react with the base moiety of any CO_2BOL regardless of formulation to make a heat-stable hydrochloride salt at the same rate of MEA or other amine systems. Strong acid/base pairings of salts are often insoluble in CO_2BOLs and are projected to precipitate out of solution, especially in the LEAN solvent antisolvent mixture where the polarity is lowest. The team recommends reclamation of CO_2BOLs using stronger base washes such as (KOH) or using ion exchange resins.

Impact of Hg and Other Impurities

Impact of Hg

It is too early to definitively quantify the impacts of mercury on CO_2BOL performance, but the team projects minimal impact at this early stage of development. The elemental form of mercury is not anticipated to coordinate to CO_2BOL molecules, and is projected to exit through the stripper. Cationic mercury however, is expected to pass through the CO_2BOL , but there remains the remote possibility of chelation of the negatively charged alkylcarbonates of the CO_2BOL . If such a chelation were to be observed, the carbonate solution may solvate the mercury in solution that is, until the carbonate is decarboxylated in the stripper, where the mercury would be released. If chelation were observed, there may be a way to remove the solvated Mercury in a slipstream, this may be an area of recommended future studies. It should be noted that literature searches indicate Hg(II) has been routinely used catalytically in the synthesis of guanidines, indicating little precedence for negative interactions of mercury with BOL molecules.

Impact of As

Arsenic as with Mercury is not expected to significantly impact CO₂BOL lifetime and performance. Elemental arsenic would likely remain in solution where it could be filtered off by activated carbon. Arsenic may be chelated (albeit remotely) by alkylcarbonates in the CO₂BOL potentially offering Arsenic removal in a slipstream.

Mechanisms of Degradation of CO₂BOLs

There are many possible degradation routes of CO₂BOLs, ranging from thermal, hydrolysis, oxidation, nitration and heat stable salt formation. Each potential decomposition route was not formally evaluated due to budget and time restrictions. Instead, projections of potential degradation pathways are derived from analogous organic chemistry reactions of guanidines, amines and alcohols with flue gas constituents such as O₂, NO_x, and H₂O. Discussions of potential respective degradation mechanisms are outlined below.

Thermal degradation

Thermal degradation of this formulation is observed but is not considered a risk to the process. Vapor pressure and boiling point testing of (3) identified thermal degradation in the absence of O_2 and H_2O at temperatures at or above $200^{\circ}C$, far above the regeneration temperatures of the PSAR.

Hydrolysis

Guanidine bases are prone to base- or acid-catalyzed hydrolysis during thermal heating (commonly above 100°C). Hydrolysis is facilitated by the protonation (activation) of the guanidine nitrogen (Figure 46). Earlier generations CO₂BOLs were prone to this hydrolysis due to the lack of steric crowding of the central guanidine carbon. A water molecule could readily react with the guanidinium carbon resulting in C-O bond formation. After proton and electron transfers, the C=O bond formation cleaves the amine from the core, forming the precursor urea and the amino alcohol side chain. Both starting materials can be reclaimed and utilized for synthesis the BOL as outlined in Section 6. The current CO₂BOL (3) is designed to be less susceptible to this hydrolysis as the cyclic guanidine core sterically blocks water from freely reacting with the guanidine carbon. We also observed that the introduction of the PSAR chemistry reduces hydrolysis, as the temperature for regeneration is lower, the presence of a hydrophobic antisolvent reduces water accumulation in the solvent, and a non-polar antisolvent reduce the CO₂BOL solution's polarity thus destabilizing reactive intermediates needed in hydrolysis reactions. It should be noted that routine NMR sampling throughout the five months of continuous bench scale testing showed <5% of hydrolysis during testing.

Figure 46. Proposed Hydrolysis of CO₂BOL by Water at High Temperatures.

Oxidative degradation

 CO_2BOL molecules contain both nitrogen and alcohol atoms that may be sensitive to oxidation at high temperatures and O_2 concentrations. The relative rate and quantification of oxidative degradation was not performed due to time and budget constraints of the program. For this reason, the team projects oxidative degradation pathways and rates similar to tertiary alkanolamines like methyldiethanol amine (MDEA). Tertiary alkanolamines are more appropriately comparable to CO_2BOLs as both molecules contain alcohol groups, and nitrogen atoms in CO_2BOLs are more tertiary-like compared to the primary or secondary N-H groups in MEA or piperazine respectively. CO_2BOLs may be less susceptible to oxidative degradation than MEA considering MDEA is more stable than MEA.

Nitration

The nitration of CO₂BOLs can be considered problematic for two reasons, potential nitrosamine formation, or nitration to shock-sensitive organic salts. Nitration has yet to be proven in the laboratory, but nitration of alcohols and amines has been routinely presented in the literature, thus the team suggests nitration may occur (Figure 47). Here, we predict the nitration of the alcohol and/or the guanidine nitrogen in the molecule. It should be noted that this mechanism of nitration has not yet been observed and is speculation based on other literature reports of similar chemistries.¹³

Figure 47. Potential Nitration Mechanism for Alkanolguanidines

A literature search yielded no published accounts of nitration of guanidines under flue gas conditions, thus the probability of nitration remains unknown. Literature reports have studied nitration of amidines (similar in basicity as guanidines) specifically under acidic conditions. ¹³ Post-combustion gas streams contain many acid gasses which may decrease the pH of solution promoting this kind of chemistry, but the CO_2BOL formulation being highly basic and incompletely saturated with CO_2 are likely to minimize a similar nitration route.

Further, the rate of nitrosation of amidines may be kinetically slow. Nitration of amidines in the presence of glacial acetic acid results in rapid formation N-nitroso-product, but in buffered solutions of a pH of 3.9, the transformation is very slow. Similar nitration rates are predicted for

alkanolguanidines. If nitration were to occur, we project nitration any of the three nitrogens to form intermediates A or B that would potentially undergo a ring opening decomposition. Though decomposition pathway via nitration is highly unlikely given the basic conditions we will be operating in. Full characterization of either nitration product should be the focus of detailed studies due to the safety concerns of carcinogens or shock-sensitive materials in a workable process.

Corrosion potential of CO₂BOL formulation

Metals

The team originally projected reduced corrosion of CO_2BOLs to steels common in process infrastructure, which would suggest cheaper alloy steels might be used for process infrastructure. A study of the effects of DBU on corrosion of steel coupons in steam was performed in 2007 by Nasrazadani et al. ¹⁴ This study focused on the weight loss of AISI 1018 steel coupons exposed to steam (120 °C) in the presence of varied amine additives as a function of time. In their study, the presence of DBU was found to reduce the weight loss of steel in the coupons compared to coupons in the absence of amine additives. The conclusion of this study was that DBU was a corrosion inhibitor, and that of morphaline and DMA, DBU showed the lowest corrosion rate. This study implies that guanidine bases used in CO_2BOLs may exhibit similar corrosion retardation potential.

Informal corrosion studies of (3) were performed by visually inspecting the bench cart fittings, tubing and packing after the 5-months of continuous testing. Visual inspections of all Swagelok™ 316 stainless steel fittings, absorber and stripper tubing, packing were performed. No visually detected corrosion was observed in the cart after cleanup Figure 48. There may be potential metal leaching into the CO₂BOL solvent, but ICMS testing was not performed due to budget and time limitations. Thus, the team suggests more formal studies of corrosion potential of CO₂BOL formulations should be performed to determine if cheaper alloy steels might be used.



Figure 48. Visual inspection of bench cart hardware after cleanup

Plastics

Select coupons of plastics commonly used in lab-scale equipment were placed in the CO₂BOL and left to sit over a week. Plastics from left to right are: polypropylene (PP), nylon, polyester, chlorinated polyvinyl chloride (CPVC), polystyrene, acrylonitrile butadiene styrene (ABS), polyacrilonitrile (acrylic) and polyvinylchloride. Images of the various coupons in the BOL are shown

below in Figure 49. As the picture clearly shows, the first four plastics (PP, nylon, polyester and CPVC) showed high chemical tolerance for the BOL, while the remaining five plastics (polystyrene, ABS, acrylic and PVC) showed evidence of dissolution or decomposition in the BOL solution. Tygon™ tubing was also used on a gas manifold with the CO₂BOL formulation for distillations and synthesis. All Tygon™ tubing on the manifold showed significant blackening and became opaque like the PVC in the image below after a few days, however, the tubing still retained its plasticity and rigidity. While it is noted that plastics such as these are unlikely to be used in a power plant, we provide evidence of chemical tolerances for any others who wish to safely attempt bench scale testing of the BOL with common laboratory tubing or fittings.



Figure 49. Coupons of plastic materials placed in CO₂BOL at room temperature for 7 days.

8. CO₂BOL FORMULATION SYNTHESIS AND COSTING

CO₂BOL Synthesis Strategy

The BOL molecule (3) was synthesized using a single-step condensation reaction between a commercially available "Vilsmeier Salt" 2-chloro-1,3-dimethylimidazolinium chloride (2) with 1-amino-2-propanol (Figure 50). This simple condensation yields the desired CO₂BOL in 63% isolated yield. While simple and effective, the commercial Vilsmeier salt (2) is expensive, making scale-up cost prohibitive; thus it was decided to make our own Vilsmeir Salt from cost-effective 1,3-Dimethyl-2-imidazolidinone (1) using oxalyl chloride, which was found to be the most expensive reagent in the synthesis (Figure 51). A full synthetic procedure complete with reagent and intermediate characterization can be found in the literature.¹⁵

Cheaper alternatives such as phosgene may be used however. 16

Figure 50. One-Step Synthesis of Alkanolguanidine (3)

Figure 51. Synthesis of 2-chloro-1,3-dimethylimidazolinium chloride (2)

CO2BOL Material Costing

Projections of solvent cost were prepared with this recipe to make either 2-((1,3-dimethylimidazolidin-2-ylidene)amino)butan-1-ol or 2-((1,3-dimethylimidazolidin-2-ylidene)amino)propan-2-ol. All reagent pricing was gathered from on-line prices at Sigma-Aldrich's website. Projections of kilogram or liter volumes of reagents were based on Fluor's experience ordering custom chemicals in tonnage quantities. Costs for this synthesis are on the order of \$35 to \$70 per kilogram, due to the cost of the primary oxalyl chloride reagent. Therefore, less expensive synthesis procedures are required to build the guanidine base cores more cost-effectively. Alternatively, substituting the current base core with cheaper and non-toxic reagents such as phosphorous oxychloride (POCl₃), or thionyl chloride (SOCl₂) could be used approximately one fifth and one seventh the cost of oxalyl chloride respectively. These substitutions have the potential to lower the price of the CO₂BOL to <\$20/kg.

Also, a recent publication showcased a new promising method to make a Vilsmier salt using phthaloyl dichloride (Figure 52).¹⁹ In this process, the product Vilsmier salt precipitates out of solution and the phthalic anhydride byproduct remains in solution making product separation an easy filtration. In this process, phthalic anhydride is used to make phthaloyl dichloride via a zirconium-catalyzed reaction. This process is estimated to reduce the amount of stoichiometric byproducts compared to the synthesis strategy currently used (Figure 51).²⁰ This new synthesis strategy should be more economical, safe to handle, with high yields and purity of the Vilsmier salt (2).

Figure 52. Proposed more economical and less toxic synthesis of Vilsmeier salt 2.

Ultimately, first fill cost-projections were based on the assumed cost of \$35/kg as the team feels that this cost target is most likely at this stage of development. A first fill for a 550 MW net power plant would require an estimated 2,414,190 kilograms (2414 tons) of solvent, with an

estimated initial cost of \$84,496,650. Annual make up rates for CO_2BOLs assuming similar rate and amount of heat stable salt formation (HSS) to that of MEA, is calculated to be \$4,826,229 per annum.

9. EH&S ASSESSMENT

The initial feasibility study projected general anticipated health, safety or environmental impacts from CO₂BOL formulations. A simple comparison was made to aqueous ethanolamine in Table 19. It should be noted that this list of anticipated impacts is not considered comprehensive, and any risks may not be considered definitive or proven. We reproduce this table for sake of completeness for general assumptions for this class of solvent systems.

Table 19. Health and Safety and Environmental Impacts of CO₂BOL VS MEA

Risk Type	CO ₂ BOL Technology	Ethanolamine Technology
Acidification (promotion of acid rain)	The CO ₂ BOL is not sufficiently volatile to be a significant contributor to acid rain, but it is synthesized from ammonia and phosgene, release of which could cause some acid rain production.	Ethanolamines are not sufficiently volatile to be significant contributors to acid rain, but they are synthesized from ammonia, release of which could cause some acid rain production.
Bio-accumulation	No significant risk. Alkane antisolvents are very hydrophobic but are not persistent.	No significant risk.
Eutrophication	CO₂BOL and compounds from which it is made would contribute to eutrophication of surface waters if released.	Ethanolamines and compounds from which they are made would contribute to eutrophication of surface waters if released.
Energy usage/global warming	The CO ₂ BOL technology is expected to use less energy than the ethanolamine-based processes.	The CO ₂ BOL technology is expected to use less energy than the ethanolamine-based processes.
Human toxicity by ingestion	Unknown risk. Probably greater toxicity than ethanolamine due to greater $\log K_{ow}$ and fact that the CO_2BOL is not diluted by water.	Toxicity by ingestion is not a significant problem (LD50, oral, rat is 1720 mg/kg).
Human toxicity by inhalation	Unknown risk. Probably lower toxicity than ethanolamine due to the much lower vapor pressure.	U.S. permissible exposure limit for ethanolamine is 3 ppm.
Human carcinogenicity	Unknown risk.	Ethanolamine is not listed as a carcinogen.
Effect on skin/eyes	Unknown risk. Probably causes skin and eye burns on contact.	Ethanolamine causes skin and eye burns on contact.
Aquatic ecotoxicity	Unknown risk. Probably more ecotoxic than ethanolamine due to greater logK _{ow} .	Ethanolamine is not listed as a carcinogen.
Ozone depletion	No significant risk except from possible byproducts from use of phosgene during synthesis.	No significant risk anticipated.

Persistence No significant risk anticipated		No significant risk anticipated.		
Resource depletion	No significant risk anticipated. No significant risk anticipated.			
Smog formation	Lighter antisolvents (e.g. heptane) would contribute to smog formation if released.	No significant risk anticipated.		

The CO_2BOL solvent platform projects comparable environmental, health and safety viewpoint, are the expected energy savings compared to aqueous solutions of ethanolamine or its derivatives, however there remain a few unknowns with respect to aerosol formation or nitrosamines. Disadvantages of the CO_2BOL platform include potential for smog formation (depending on the choice of antisolvent) and potentially more ingestion by humans and possibly aquatic organisms. Other unknowns include possible exposure to the highly basic CO_2BOL by workers from contact as the CO_2BOL is basic enough that potential burning on skin or eye contact may occur.

Toxicology

The overall objective of this project was to test the toxicity of a new CO₂-absorbing compound and to compare its toxicity to that of two potential breakdown products, and to related compounds already in use and of known toxicity. The specific objectives were to describe the acute lethality of these compounds to fish and aquatic invertebrates and to compare the measured toxicities to those reported in the literature. This was a preliminary project, and did not include studies of chronic toxicity, rates of uptake, and depuration, bio-concentration factors, and metabolism of the parent compounds and of any products of hydrolysis or metabolism.

Compounds

The compounds tested included a novel CO_2 binding organic liquid ((1(1,3-dimethylimadasolidin-2-ylidine)amino)propan-2-ol (DMSIP)), two potential degradation products (DL-1-amino-2-propanol (CAS: 78-96-6; DLAP); 1,3-dimethyl-2-imidazolidinone (CAS: 80-73-9; DMI)) and ethanolamine (CAS: 141-43-5; EA), a compound with CO_2 binding characteristics that has been tested previously. The toxicity to daphnia (*Daphnia magna*) of all chemicals was tested because the daphnia test is relatively short (48 h), static (no solution renewal), and the test animals are quite small (< 1 mg), so that only limited amounts of test solution are needed (total of 150 mL per concentration). Tests with rainbow trout (*Oncorhynchus mykiss*) were longer (96 h), required much larger volumes of test solution (semi-static, 10 L/d for each concentration) and were limited by the availability of test chemicals. Hence, only EA, the positive control, was tested with trout to demonstrate the relative toxicity of these types of chemicals to the two species. A 48 h rangefinding test with only 2L/d of test solution provided a first estimate of the toxicity to trout of DMSIP.

Test Species

All animal holding and toxicity tests were conducted under Queen's Animal Care Protocol Hodson-2013-043. Neonate daphnia (≤ 24h old) and juvenile rainbow trout (0.5 to 1.0 g) were selected as test species representative of aquatic invertebrates and vertebrates. A culture of daphnia was obtained from Dr. P. Frost, Biology Department, Trent University. The abundance of

daphnia increased rapidly at room temperature (20-22 C) through natural reproduction, sustained by feeding with a culture of algae (*Selanastrum* sp) and dried yeast. Daphnia neonates were collected from beakers of 10 adults that had been separated from the general culture the previous day. Neonates were those daphnia that had been born overnight and were distinguished from adults by their much smaller size. Trout were purchased from Rainbow Springs Hatchery (Thamesville, ON) and held at 15°C in flowing water until tested. They were fed daily with a commercial trout chow at a rate of about 1.5% body wt per day until 48 h prior to testing, when feed was withheld. Because of animal care concerns about the testing of vertebrates, most tests were performed with daphnia and only limited numbers of trout were tested

Dilution Water

Water for all trout and daphnia culture was a municipal supply drawn by the City of Kingston from Lake Ontario, and filtered and chlorinated to a residual of about 1800 μ g/L. In the lab, the water was de-chlorinated by charcoal filtration and by the addition of about 1 mg/L of sodium bisulfite to reduce free chlorine concentrations to less than 10 μ g/L, a concentration safe for most aquatic species. The pH, hardness and alkalinity of Lake Ontario water is about 7.8 -8.0, 135 mg/L as CaCO₃, and 80 mg/L as CaCO₃, respectively

Toxicity tests

The acute toxicity of each compound was assessed following the guidance of Environment Canada protocols that describe the culture and testing of daphnia neonates (Environment Canada 1990)²² and of juvenile trout (Environment Canada 2007).²³ For each chemical and species, two tests were applied. The first was a range-finding test in which the exposure concentrations were broadly spaced, typically by one order of magnitude, and only two organisms were exposed to each concentration. Based on the highest concentration causing no mortality and the lowest concentration causing 100% mortality, a second test was run with a much narrower series of concentrations, each proportionally higher than the last. For example, a dilution ratio of 1.8 gave a test series of 10, 18, 32, 56, and 100 mg/L, based on a range-finding test with no mortality at 10 mg/L and 100% mortality at 100 mg/L.

All tests with daphnia were static (no solution renewal) 48 h exposures to dilutions of each chemical prepared from a single stock solution of the test chemical dissolved in de-ionized reverse-osmosis water. Tests with trout were static daily renewal assays in which most (>90%) of the test solution was replaced by solutions of test chemicals prepared daily by dilutions of a single stock solution.

For each test, the solutions were prepared in glass beakers (daphnia) or buckets lined with food-grade polyethylene bags (trout), after which the test animals were added to the solution. Each solution was examined carefully for dead animals at 1, 2, 4, 8, 24, and 48 h (daphnia) or 1, 2, 4, 8, and 24 h, and daily until 96 h (trout). Each trout that died was weighed to calculate the average weight of test fish and the biomass and loading rate of fish in each test solution, and to determine whether there was a relationship between the order of death (i.e., sensitivity) and fish size.

For the daphnia tests, there were 10 organisms per test solution, with three repeats run simultaneously, for a total of 30 animals per test concentration; the neonates for the three tests

were collected from three different parents. The test with ethanolamine was run three times, coincident with tests of the other compounds, and DMSIP was tested twice. Trout tests used only one replicate of 10 animals per test concentration.

Water chemistry

Ideally, LC50s should be calculated using the measured concentrations of test substances in test solutions. Consequently, samples were taken daily from the daphnia tests and provided to Dr. Tamer Andrea for analysis in the Jessop Lab. Unfortunately, the concentrations of the compounds that were toxic were below the limit of detection by the methods available to Dr. Andrea, so all LC50s are based on 'nominal' or applied concentrations. This also meant that there was no way of verifying whether the test compounds degraded when mixed with water, or decreased in concentration throughout the 24 to 48 hour periods between solution changeovers due to degradation, volatilization, accumulation by the test organisms, or absorption to the materials of the test chambers.

Statistics

At the end of the test, the numbers dying, numbers surviving and percent mortality were calculated. The 48 h median lethal concentrations (48 h LC50s) for daphnia and the 96 h LC50s for trout were calculated for each chemical from the percent mortality at each test concentration. Where there were one or more concentrations causing partial mortalities (i.e., more than 0 but less than 100% mortality), LC50s were calculated with a computer program written in BASIC using probit analysis, a moving average angle method, or the Trimmed Spearman-Karber method (Stephan 1989). Each method linearizes an S-shaped exposure-response curve by expressing mortality as a probability function and concentrations as logarithms. Each method has somewhat different requirements for the 'ideal' data set, and the data from these experiments were analyzed most consistently by the moving average angle method. Where exposure-response curves were steep (0% mortality at one concentration, 100% mortality at the next highest concentration) and 10 or more organisms were tested per concentration, the LC50 was interpolated as the geometric mean of the two test concentrations, with 95% confidence limits represented by the two test concentrations.

TOXICITY RESULTS and DISCUSSION

All compounds tested were lethal to daphnia neonates and to rainbow trout within 48h, with most mortality occurring in the first 24 h, with the exception of DLAP for which mortality to daphnia continued past 48 h and the test was extended to 96 h (Appendices 1-9). However, data collected beyond 48 h are not reliable due to the potential for death by starvation of daphnids, as indicated by increased control mortality after 48 h in the DLAP test. Based on added (nominal) concentrations, the novel compound DMSIP was intermediate in toxicity (average LC50 = 198 mg/L) between two of its possible breakdown products, DMI (about 4 times less toxic than DMSIP) and DLAP (about 2 times more toxic than DMSIP) (Table 20). The LC50 of EA, the reference compound, averaged 75 mg/L, about 2.6-fold more toxic than DMSIP. The standard deviation among replicates of EA tests of toxicity to daphnids was 24.2 mg/L, which gave a coefficient of variation of 32%. This variance was similar to that observed by Cowgill et al (1985)²⁵ for tests of the toxicity diethanolamine to daphnia.

The 96 h LC50 of DMSIP to trout was estimated from a range-finding test as 180 mg/L, the geometric mid-point between 100 mg/L (0% mortality) and 320 mg/L (100% mortality) (Table 20). This estimate suggests little difference in acute lethality of DMSIP between trout and daphnia. The 96 h LC50 of EA, the reference compound was estimated at 150 mg/L from a toxicity test in which the lowest concentration caused 70% mortality and all higher concentrations caused 100% mortality. If this estimate is reasonable, it suggests that daphnids are twice as sensitive to EA as trout.

Table 20. The median lethal concentration (LC50) and 95% confidence limits of the test chemicals for neonates of *Daphnia magna* and for juvenile rainbow trout. The LC50 was calculated by the moving average angle transformation (Stephan 1989).²⁴

	ı	1	
Test Chemical	CAS	LC50	95%
	Number	(mg/L)	confidence
			limits
			(mg/L)
Daphnia (48 h LC50) (N=30/test concentration)			
((1((1,3-dimethylimadasolidin-2-ylidine)amino)propan-2-ol (DMSIP)	-		
Trial 1		169	149-209
Trial 2		226	212-241
DL-1-amino-2-propanol (DLAP)	78-96-6	96	84-113
1,3-dimethyl-2-imidazolidinone (DMI)	80-73-9	847	763-977
Ethanolamine	141-43-5		
Trial 1		49	42-56
Trial 2		78	70-88
Trial 3		97	83-116
Rainbow trout (96 h LC50) (N=10/test concentration)			
((1((1,3-dimethylimadasolidin-2-ylidine)amino)propan-2-ol (DMSIP)	-	≈180	-
Ethanolamine	141-43-5	≈150	-

Overall, the compounds did not appear to be toxic, and would likely be classified as "low" to "moderately" toxic on the basis of the tested concentrations. While the results had variation among replicates of EA and DMSIP, the differences in toxicity among chemicals exceeded the differences among replicates, suggesting that these differences in compound toxicity were real.

Much of the variability in the daphnia data may be due to variations in the concentrations of test chemicals. There was a noticeable release of heat when the compounds were first mixed with water to prepare stock solutions for dilutions, suggesting that either the compounds were hydroscopic, or that chemical reactions were occurring that changed the structure of the test compound (e.g., hydrolysis). For trout tests with a daily renewal of test solutions, stock solutions of EA or DMSIP in de-ionized water were prepared once and diluted on subsequent days. This created the potential for declining concentrations in stock solutions over the course of each test. Overall, the potential reactivity of the test chemicals in water generated uncertainty about the actual concentrations of compounds that were in test solutions. Without measurements of the chemicals in water and stock solutions, it is unknown whether the organisms reacted to the original compounds or to some degradation product, and whether the extent of mortality reflected the initial concentrations, or some integral of declining concentrations over the period of the test.

There were also issues related to the high viscosity of compounds that were liquid. Viscosity slowed the mixing of test compounds in water, and mixing may have been incomplete if compounds with a specific gravity greater than 1.0 sank and created gradients of concentration within the test chambers. In the fish tests of EA, it appeared that the smallest fish died first, which was particularly evident at the highest test concentration. Because small fish often hide on the bottom to avoid larger, more dominant fish, they may have encountered higher concentrations of test chemicals than the larger fish. The kinetics of uptake of compounds by fish is usually slower in larger fish because their metabolic demand per gram of fish decreases with increasing size and percent muscle mass. If the difference in fish size was sufficiently large to have affected kinetics, the larger fish would have accumulated the compounds more slowly and survived longer. If concentrations of the test compounds declined over time, this longer survival may allow larger fish to avoid lethality at test concentrations close to the threshold of toxicity.

The toxicities measured for DLAP and EA can be compared to those reported for other aquatic species, although the database is not large. The toxicity of DLAP to fish ranged by more than 10-fold, and even lowest concentrations toxic to goldfish are more than twice those toxic to daphnia. The toxicity of DLAP to fish appeared to be pH sensitive, with greater toxicity at higher pH (9.9 vs 7.0; Bridié et al 1979). For EA, reported LC50s to three species of freshwater fish ranged from 150 to 375 mg/L in freshwater (Geiger et al 1990; Mayer et al 1986; Juhnke and Liidemann 1978), 27,28,29 while the range for marine invertebrates and algae was 18-43 mg/L (Lebralat et al 2008; 2010). The apparently greater sensitivity of daphnia and marine invertebrates to these compounds may be related to an inherent characteristic of invertebrate physiology, the young age of the test organisms (usually newly hatched larvae), or to differences between marine and freshwater chemistry. Without further systematic testing, and the standardization of exposure methods, life stage exposed, test duration, etc., the actual source of variations among species and studies cannot be identified. Nevertheless, the test results from the present study appear to be in the same range as the published data.

While the test data for the test compounds suggest a relatively low risk of toxicity to aquatic species, they should be used primarily as a guidepost for a more complete evaluation. The potential degradation of compounds in water during the preparation and testing of solutions suggests that toxicity was likely under-estimated. Without a sensitive and reliable assay for measuring concentrations in water, the true toxicity remains unknown. The ultimate measure of

toxicity will be tests supported by chemical analyses of test solutions to define exposure concentrations and to identify the extent and rate of degradation and appearance of new products.

As indicated in the introduction, these tests assessed acute lethality only. The potential long-term effects of an acute exposure (delayed effects) or the effects of a chronic exposure (over weeks or months) in situations where there is chronic release of chemicals to the environment were not considered. There are also no data available for plants (phytoplankton), and no information about environmental distribution, persistence, and fate.

10.PROJECT OUTPUT

This project has produced multiple documents, manuscripts and conference presentations. The program delivered 10 quarterly reports to NETL, chronologically detailing program advances, budget, deliverables and milestones. The program additionally delivered an initial feasibility document for the go-no go decision in October of 2013. Additionally, this final report was also delivered as required by the FOA.

The project has recorded a significant amount of data, leading to publication in perreviewed journals. Currently, two manuscripts have been published and two more are being drafted for publication after this report is submitted. The synthesis and characterization of (3) used in this study was published in *RSC-Advances*, while the VLE data and thermodynamic modeling of the CO₂BOL/PSAR process was published in *Energy and Environmental Science*. The kinetic measurements are currently being drafted for publication in *Industrial and Engineering Chemical Research*, while the bench scale testing results and analysis will be drafted for *Energy and Environmental Science*.

The project team also presented 11 talks at national and international conferences with 4 of them invited talks. The project team presented in annual meetings for both the American Chemical Society (ACS), The American Institute of Chemical Engineers (AIChE) and the Green House Gas Technologies biennial conferences. The team also presented talks for the Pittsburgh Coal Conference and the NETL annual showcase.

11. REFERENCES

- Jessop, P. G.; Heldebrant, D. J.; Li, X. W.; Eckert, C. A.; Liotta, C. L., Green chemistry - Reversible nonpolar-to-polar solvent. *Nature* 2005, 436, (7054), 1102-1102.
- 2. Heldebrant, D. J.; Koech, P. K.; Rainbolt, J.; yonker, C. R.; Ang, T.; Liang, C.; Jessop, P. G., Reversible Zwitterionic Liquids, The Reaction of Alkanol Guanidines, Alkanol Amidines and Diamines with CO₂. *Green Chem.* **2010**, 12, 713-721.
- 3. Heldebrant, D. J.; Koech, P. K.; Rainbolt, J. E.; Zheng, F.; Smurthwaite, T.; Oss, M.; Leito, I., Performance of Single-Component CO₂-Binding Organic Liquids (CO₂BOLs) For Post Combustion CO₂ Capture *Chem. Eng. J.* **2010**, 171(3), 15, 794-800.

- 4. Phan, L.; Chiu, D.; Heldebrant, D. J.; Huttenhower, H.; John, E.; Li, X. W.; Pollet, P.; Wang, R. Y.; Eckert, C., A.; Liotta, C. L.; Jessop, P. G., Switchable solvents consisting of amidine/alcohol or guanidine/alcohol mixtures. *Ind. Eng. Chem. Res.* **2008**, 47, (3), 539-545.
- 5. P. M. Mathias, K. Afshar, F. Zheng, M. D. Bearden, C. J. Freeman, T. Andrea, P. K. Koech, I. Kutnyakov, A. Zwoster, A. R. Smith, P. G. Jessop, O. Ghaffari Nik, D. J. Heldebrant, "Improving the Regeneration of CO₂-Binding Organic Liquids with a Polarity Change." *Energy Environ. Sci.*, 2013, 6, 2233.
- 6. Dugas, R.E. "Carbon Dioxide Absorption, Desorption, and Diffusion in Aqueous Piperazine and Monoethanolamine." Ph.D. Dissertaion (2009)
- 7. Gui, X., Tang, Z., Fei, W. J. Chem. Eng. Data, **2011**, 56 (5), pp 2420–2429
- 8. Wilcox, J.,* Rochana, P., Kirchofer, A., Glatz, G., and He, J. *Energy Environ. Sci.*, 2014,7, 1769-1785
- 9. Versteeg, G.F., Van Duck, L.A.J., Van Swaaij, W.P.M., Chem. Eng. Comm., 1996, 1, 113-158)
- 10. (Onda, K., Takeuchi, H. and Okumoto, Y., Mass transfer coefficients between gas and liquid phases in packed columns, J. Chem. Eng. Jap., 1968, 1, 56-62.
- 11. "Cost and Performance Baseline for Fossil Energy Plants, Volume 1: Bituminous Coal and Natural Gas to Electricity," Revision 2, **2010**, DOE/NETL-2010/1397.
- 12. Lepaumier, H.; Picq, D.; Carrette, P.-L. *Ind.* "New Amines for CO₂ Capture. II. Oxidative Degradation Mechanisms." *Eng. Chem. Res.* **2009**, *48*, 9068
- 13. Loeppky, R. N.; Yu, L. "Nitrosamines, N-nitrosoamides, and diazonium ions from tri-n-substituted amidines." *Tetrahdron Lett.* **1990**, *31*, 3263.
- 14. (Corrosion science 49, (2007) 3024-3039)
- 15. RSC Adv., 2013, 3, 566-572.
- 16. Harres-Pawlis, S.; Florke, U.; Henkel, G. "Tuning of Copper(I)—Dioxygen Reactivity by Bis(guanidine) Ligands." *Eur. J. Inorg. Chem.* **2005**, *19*, 3815.
- 17. Mylari, B. L.; Withbroe, G. J.; Beebe, D. A.; Brackett, N. S.; Conn, E. L.; Coutcher, J. B.; Outes, P. J.; Zembrowski, W. *Bioorg. Med. Chem.* **2003**, *11*, 4179.
- 18. Metallinos, C.; Xu, S. Org. Lett. 2010, 12, 76.
- 19. Kimura, Y.; Matsuura, D.; Hanawa, T.; Kobayashi, Y. *Tetrahedron Lett.* **2012**, *53*, 1116.
- 20. Kimura, Y.; Takao, Y.; Sugiyama, T.; Hanawa, T.; Ito, H. *U.S. Patent* 2011, 0178336 Δ1
- 21. T. Arthur, J. Harjani, P. G. Jessop, and P. V. Hodson "Effects-Driven Chemical Design: The Acute Toxicity of Switchable Surfactants to Rainbow Trout can be Predicted from Octanol-Water Partition Coefficients", Green Chem., (2012) 14, 357-362
- 22.Environment Canada. 1990. Biological Test Method: Reference Method for Determining Acute Lethality of Effluents to *Daphnia magna*, Environment Canada Ottawa. Eps 1/Rm/14
- 23.Environment Canada. 2007. Biological Test Method: Acute Lethality Test Using Rainbow Trout., Method Development and Applications Section (MDAS), Biological Methods Division, Environment Canada, Ottawa, ON. EPS 1/RM/9

- 24.Stephan CE. 1989. Software to calculate LC50 values with confidence intervals using probit, moving averages, and Spearman- Karber procedures. U.S. Environmental Protection Agency, Duluth, MN.
- 25.Cowgill, U.M., Takahashi, I.T., and Applegath, S.L. 1985. A comparison of the effect of four benchmark chemicals on Daphnia magna and *Ceriodaphnia dubia-affinis* tested at two different temperatures. Environ Toxicol Chem 4: 415-422.
- 26. Bridié, A.L., Wolff, C.J.M., and Winter, M. 1979. The acute toxicity of some petrochemicals to goldfish. Water Research 13(7): 623-626.
- 27. Geiger, D.L., Brooke, L.T., and Call, D.J. 1990. Acute Toxicities of Organic Chemicals to Fathead Minnows (Pimephales promelas), Volume 5., Center for Lake Superior Environmental Studies, University of Wisconsin, Superior, WI.
- 28. Mayer, F.L., Jr., and M.R. Ellersieck. . 1986. Manual of Acute Toxicity: Interpretation and Data Base for 410 Chemicals and 66 Species of Freshwater Animals. , U.S.Dep.Interior, Fish Wildl.Serv., Washington, DC.
- 29. Juhnke, I., and Liidemann, D. 1978. Ergebnisse der Untersuchung von 200 chemischen Verbindungen auf akute Fischtoxizit~it mit dem Goldorfentest. Z Wasser Abwasser-Forschung 11: 161-164.